CNWRA® 2008-001

INFILTRATION TABULATOR FOR YUCCA MOUNTAIN: BASES AND CONFIRMATION

Prepared for

U.S. Nuclear Regulatory Commission
Contract NRC–02–07–006

Prepared by

Stuart Stothoff

Center for Nuclear Waste Regulatory Analyses
San Antonio, Texas

August 2008

CONTENTS

CONTENTS (continued)

FIGURES

FIGURES (continued)

FIGURES (continued)

TABLES

ACKNOWLEDGMENTS

This report was prepared to document work performed by the Center for Nuclear Waste Regulatory Analyses (CNWRA®) for the U.S. Nuclear Regulatory Commission (NRC). The initial work was conducted under Contract Nos. NRC–02–97–009 and NRC–02–02–012. The final report was completed under Contract No. NRC–02–07–006. The activities reported here were performed on behalf of the NRC Office of Nuclear Material Safety and Safeguards, Division of High-Level Waste Repository Safety. The report is an independent product of CNWRA and does not necessarily reflect the views or regulatory position of NRC.

The author wishes to particularly acknowledge the invaluable contributions of R. Fedors, who developed the overland flow module in the Infiltration Tabulator for Yucca Mountain, tested the code, and provided an excellent sounding board for aspects of the models implemented in the code. The author also wishes to acknowledge important insights into interrelationships among soil, vegetation, rocks, and infiltration provided during field expeditions and related discussions with R. Fedors, D. Or, D. Groeneveld, D. Woolhiser, and O. Chadwick.

The author wishes to thank C. Dinwiddie and S. Painter for thorough technical reviews and useful insights, L. Mulverhill for editorial expertise, W. Patrick for programmatic review, and J. Simpson, N. Naukam, and B. Street for their administrative support.

QUALITY OF DATA, ANALYSES, AND CODE DEVELOPMENT

DATA: All CNWRA-generated data contained in this report meet quality assurance requirements described in the Geosciences and Engineering Division Quality Assurance Manual. Sources of other data should be consulted for determining the level of quality of those data.

ANALYSES AND CODES: ArcView GIS® 3.3 (Environmental Systems Research Institute, 2002), ArcGIS® 9.0 (Environmental Systems Research Institute, 2004), and EarthVision® 7.5 (Dynamic Graphics, Inc., 2002), were used to display results for this report and are controlled in accordance with CNWRA software procedure Technical Operating Procedure (TOP)–018, Development and Control of Scientific and Engineering Software.

KINEROS2 Versions 1.09 and 1.12 (Smith, et al., 1995) are validated in accordance with CNWRA software procedure TOP–018. Results from KINEROS2 Versions 1.09 and 1.12 simulations were used to develop abstractions presented in this report.

Microsoft® Excel® 2000 Version 9.0.3821 SR-1 (Microsoft Corporation, 2002) and MATLAB® Version 7.1.0.246 (The MathWorks, Inc., 2005) were used to generate results for this report and are considered uncontrolled software in accordance with CNWRA software procedure TOP–018.

REFERENCES:

Dynamic Graphics, Inc. “User’s Guide 7.5.” Alameda, California: Dynamic Graphics, Inc. 2002.

Environmental Systems Research Institute. “What is ArcGIS?” Redlands, California: Environmental Systems Research Institute. 2004.

———. “ArcView GIS 3.3.” Redlands, California: Environmental Systems Research Institute. 2002.

Microsoft Corporation. “Excel.” Redland, Washington: Microsoft Corporation. 2002.

Smith, R.E., D.C. Goodrich, D.A. Woolhiser, and C.L. Unkrich. “KINEROS—A KINematic Runoff and EROSion Model.” *Computer Models of Watershed Hydrology*. V.P. Singh, ed. Highlands Ranch, Colorado: Water Resources Publications. pp. 697–732. 1995.

The MathWorks, Inc. “MATLAB.” Version 7.1.0.246. Natick, Massachusetts: The MathWorks, Inc. 2005.

EXECUTIVE SUMMARY

The Infiltration Tabulator for Yucca Mountain (ITYM)[1] program estimates the net amount of water infiltrating from the ground surface into shallow bedrock at Yucca Mountain as a function of climate. ITYM was developed for the U.S. Nuclear Regulatory Commission (NRC) in the mid to late 1990s to provide estimates of mean annual infiltration (MAI)[2] to the NRC's Total-system Performance Assessment (TPA) code NRC staff used in its evaluation of the potential repository at Yucca Mountain, Nevada, and to provide an independent tool for assessing estimates of MAI that the U.S. Department of Energy (DOE) may provide. ITYM was developed specifically to consider the potential effects of terrain and climate at Yucca Mountain, Nevada, under present and potential future conditions.

This document is the third report in a series assessing the role of climate change on infiltration at Yucca Mountain. The first report (Stothoff and Musgrove, 2006) reviewed literature from outside of the Yucca Mountain program related to infiltration under climates analogous to climates that may occur at Yucca Mountain. The second report (Stothoff and Walter, 2007) constructed potential future climate sequences based on orbital mechanics and paleoclimatic inferences, and used ITYM to estimate million-year-average net infiltration at Yucca Mountain given the climatic sequences. This third report documents the ITYM mathematical model and input parameters used by Stothoff and Walter (2007), including confirmatory analyses of the parameters.

The version of ITYM used by Stothoff and Walter (2007) is the same version of ITYM that is distributed with the TPA Version 5.1a code (CNWRA and NRC, 2007). ITYM was originally developed as a module within TPA Version 3.0 (Manteufel, et al., 1997), and was recast as a standalone preprocessor code for TPA Version 4.0 (Mohanty, et al., 2000). Appendix H of the TPA Version 4.0 code documentation (Mohanty, et al., 2000) provides a user guide for ITYM. Hydraulic and climatic input parameter values have remained unchanged since TPA Version 4.0, except for an enhancement in 2003 to include the effects of overland flow on infiltration. ITYM was also enhanced in 2006 to provide additional output information.

ITYM performs Monte Carlo analyses of MAI for a set of grid cells, providing the mean and standard deviation of net infiltration for each grid cell for a set of reference climatic states characterized by mean annual precipitation (MAP)[3] and mean annual temperature (MAT).[4] The input grid is referenced to a standard U.S. Geological Survey digital elevation model that describes the site topography with a grid resolution of 30 m [98 ft].

ITYM uses three abstracted representations of MAI as a function of soil thickness, climate, and soil and bedrock hydraulic properties. The abstractions consider (i) deep soil, (ii) shallow soil

---

[1] Infiltration Tabulator for Yucca Mountain is used frequently throughout this summary; consequently, the abbreviation ITYM will be used.

[2] Mean annual infiltration for Yucca Mountain is used frequently throughout this summary; consequently, the abbreviation MAI will be used.

[3] Mean annual precipitation is used frequently throughout this summary; consequently, the abbreviation MAP will be used.

[4] Mean annual temperature is used frequently throughout this summary; consequently, the abbreviation MAT will be used.

overlying a medium with coarser pores (i.e., a capillary barrier), and (iii) shallow soil overlying a medium with finer pores (i.e., a capillary attractor). Unsaturated hydraulic properties are described using the van Genuchten (1980) model. These abstractions are based on approximately 500 detailed one-dimensional simulations of bare-soil infiltration using various combinations of the input properties. The simulations used 10 years of hourly meteorological records from the National Weather Service station located at nearby Desert Rock, Nevada. The abstracted representations enable bare-soil MAI to be estimated for any combination of input properties likely in a grid cell; two additional abstractions modify these estimates to account for plants and overland flow. The heuristic abstraction for plant transpiration reduces estimated bare-soil infiltration rates, with the amount of reduction increasing with soil thickness. An abstraction developed from two-dimensional overland-flow simulations locally increases infiltration by increasing effective MAP.

Each grid cell uses site-specific information describing soil and bedrock hydraulic properties, soil cover thickness, and climatic properties. Where systematic spatial variability is easily described mathematically, the distribution is generated internally to the program (e.g., elevation-dependent inputs such as MAP and MAT); otherwise, external files provide a direct or indirect property description for each cell. External models provide direct estimates of the spatial distribution of soil thickness, mean annual wind speed, and the clear-sky incident shortwave radiation as a function of ground orientation. External files indirectly provide properties in the form of soil and bedrock unit identifiers for each grid cell, which are used to look up tabulated properties and their associated variability and uncertainty.

ITYM considers both variability in and uncertainty about the input parameters in order to formally estimate the expected value of MAI as a function of expected MAP and temperature. Parameter variability is accommodated by Monte Carlo sampling of the input parameters. Parameter uncertainty is accommodated by Monte Carlo sampling of the statistical parameters describing the input-parameter distributions.

This report describes the ITYM input parameters developed in the late 1990s, which were used for TPA Versions 4.0 through 5.1a. These parameters are drawn from a variety of input sources. MAP and MAT relationships are derived from Cooperative Observer Program weather station observations from Nevada and bordering states (National Climatic Data Center, 1997). The mean annual vapor density relationship is derived from observations at Desert Rock, Nevada (National Climatic Data Center, 1994), and stations in the Kawich Range (McKinley and Oliver, 1994). The mean annual wind speed distribution is based on Yucca Mountain meteorological observations (TRW Environmental Safety Systems, Inc., 1998). Incident radiation is estimated from Solar and Meteorological Surface Observation Network observations (National Climatic Data Center, 1961–1990). Soil and bedrock hydraulic properties are taken from the U.S. Geological Survey infiltration model (Flint, et al., 1996), which in turn is based on field and laboratory measurements. Fracture hydraulic properties are partially taken from the U.S. Geological Survey infiltration model (Flint, et al., 1996), partially from U.S. Geological Survey laboratory measurements (U.S. Geological Survey, 1997), and partially from staff understanding based on field visits. Finally, soil thickness across the site is estimated using an independently derived mass balance model, with input parameters obtained from the literature and calibrated with field observations.

With the passage of time, additional site information has become available, and previously available information has been examined in further detail. This report provides independent confirmatory analyses to place some of the ITYM input properties in context.

Confirmatory information related to climate (MAP, MAT, and vapor density) suggests that climatic trends across the Yucca Mountain site have a systematic effect on estimated infiltration. This systematic effect is small relative to the effect of soil and bedrock properties, however. Confirmatory analysis during the preparation of this report identified a mistyped value in the ITYM input file that reduces mean annual vapor density by approximately an order of magnitude. The mistyped value would be expected to increase evaporation rates by approximately 37 to 46 percent, thereby reducing bare-soil infiltration. The mistyped value has been used for all analyses using ITYM to date, but is not expected to strongly affect ITYM infiltration estimates, because the ITYM plant uptake abstraction uses parameters that, in effect, compensate for higher evaporation with reduced transpiration. Stothoff and Walter (2007) compared ITYM estimates (which are based on the mistyped value) to available site and regional observations and concluded that the ITYM estimates were consistent with observations.

Confirmatory analyses examining soil hydraulic properties suggest that soil hydraulic conductivity and van Genuchten capillary pressure most strongly affect infiltration. Soil texture appears to be relatively uniform in the shallow soils across the potential repository footprint, consistent with surficial deposit maps attributing an eolian source to most shallow soils (Lundstrom, et al., 1996, 1995, 1994; Lundstrom and Taylor, 1995), so the soil hydraulic properties also should be relatively uniform spatially. Hydraulic conductivity measurements and estimates were performed for the DOE infiltration model (Flint, et al., 1996; Bechtel SAIC Company, LLC, 2004), but retention measurements were not (because the DOE model does not use retention properties to estimate infiltration); thus the capillary pressure parameter is more uncertain than the hydraulic conductivity parameter. The confirmatory analyses suggest that the capillary pressure parameter is by far the largest soil-property contributor to infiltration uncertainty in the ITYM model; this source of infiltration uncertainty may be reducible with relatively few measurements, because the soil is relatively uniform across the site.

ITYM considers four bedrock pathways for infiltration: (i) the bedrock matrix, (ii) soil fillings in fractures, (iii) carbonate fillings in fractures, and (iv) unfilled portions of fractures. Confirmatory analyses suggest that only nonwelded or moderately welded tuff units have a sufficiently permeable bedrock matrix to permit significant bare-soil infiltration (i.e., without considering plant uptake) through the bedrock matrix pathway. Within the potential repository footprint, the Tiva Canyon formation moderately welded caprock on Yucca Crest and some ridgetops are the primary moderately welded tuff exposures, with minor exposures of nonwelded tuff on the west flank of Yucca Mountain and in washes in the northern portion of the footprint.

The analyses suggest that the soil-fill pathway is usually the dominant fracture pathway for infiltration, with fracture volume fraction, fracture conductivity, and fracture van Genuchten capillary pressure all strongly affecting bare-soil infiltration. Both volume fraction and van Genuchten capillary pressure are considered highly uncertain. The abstraction for the unfilled-fracture pathway estimates significant infiltration under present-day climatic conditions only where soil is extremely thin {less than approximately 10 to 15 cm [4 to 6 in]}.

Confirmatory analyses examined bedrock matrix and fracture properties such as hydraulic conductivity and fracture volume fraction by independent analysis of core-sample measurements. Estimated matrix properties for hydrogeologic units were similar to the properties used in ITYM analyses, and would yield similar estimates for MAI. The confirmatory analyses suggest that the upper lithophysal unit of the Tiva Canyon formation and the middle nonlithophysal unit of the Topopah Spring formation may be better represented with

hydrogeologic units that have smaller saturated hydraulic conductivity. Only a small area within the potential repository footprint would be affected by the alternative representation.

Field evidence from the infiltration experiment at Alcove 1, which took place in a Tiva Canyon caprock unit, is consistent with the properties ITYM uses to describe the caprock fractures. This confirmation is particularly important because the caprock dominates infiltration in the ITYM model. Another confirmatory analysis examined the fracture volume fraction estimates for welded units underlying the caprock, using pavement surveys and detailed line surveys from the Exploratory Studies Facility. This analysis supports the use of larger fracture volume fractions in the upper lithophysal and middle nonlithophysal units of the Tiva Canyon formation. The increased values imply that these units may contribute significantly to net infiltration, particularly on north-facing slopes, but are not sufficiently large to change the conclusion that the caprock units dominate infiltration. The confirmatory analyses suggest that using the revised estimates would increase net infiltration within the potential repository footprint by less than a factor of two, which is considered small relative to the overall uncertainty in net infiltration.

In summary, the confirmatory analyses suggest that the ITYM infiltration estimates may change in detail when information obtained in the last 10 years is included and when alternate interpretations of existing data are considered, but general trends and estimates are not expected to change dramatically. The confirmatory analyses suggest that conclusions and decisions drawn from the existing ITYM infiltration estimates would also be supported by a revised input set using the more-recent information. The analyses further suggest that measurements of the soil retention properties in the shallow soils above the potential repository may be the most easily obtained information to reduce ITYM estimates of infiltration uncertainty.

References

Bechtel SAIC Company, LLC. "Simulation of Net Infiltration for Present-Day and Potential Future Climates." MDL–NBS–HS–000023. Rev. 00. Las Vegas, Nevada: Bechtel SAIC Company, LLC. 2004.

CNWRA and NRC. "Total-system Performance Assessment (TPA) Version 5.1a Code." San Antonio, Texas: CNWRA. 2007.

Flint, A.L., J.A. Hevesi, and L.E. Flint. "Conceptual and Numerical Model of Infiltration for the Yucca Mountain Area, Nevada." Milestone 3GUI623M. Las Vegas, Nevada: DOE. 1996.

Lundstrom, S.C. and E.M. Taylor. "Preliminary Surficial Deposits Map of the Southern Half of the Topopah Spring NW 7.5-Minute Quadrangle." U.S. Geological Survey Open-File Report 95-134. Scale 1:12,000. 1995.

Lundstrom, S.C., S.A. Mahan, and J.B. Paces. "Preliminary Surficial Deposits Map of the Northwest Quarter of the Busted Butte 7.5-Minute Quadrangle." U.S. Geological Survey Open-File Report 95-133. Scale 1:12,000. 1996.

Lundstrom, S.C., J.W. Whitney, J.B. Paces, S.A. Mahan, and K.R. Ludwig. "Preliminary Surficial Deposits Map of the Southern Half of the Busted Butte 7.5-Minute Quadrangle." U.S. Geological Survey Open-File Report 95-131. Scale 1:12,000. 1995.

Lundstrom, S.C., J.R. Wesling, E.M. Taylor, and J.B. Paces. "Preliminary Surficial Deposits Map of the Northeast Quarter of the Busted Butte 7.5-Minute Quadrangle." U.S. Geological Survey Open-File Report 94-341. Scale 1:12,000. 1994.

Manteufel, R.D., R.G. Baca, S. Mohanty, M.S. Jarzemba, R.W. Janetzke, C.B. Connor, G.A. Cragnolino, A.H. Chowdhury, T.J. McCartin, and T. Ahn. "Total-system Performance Assessment (TPA) Version 3.0 Code: Module Descriptions and User's Guide." San Antonio, Texas: CNWRA. 1997.

McKinley, P. and T. Oliver. "Meteorological, Stream-Discharge, and Water-Quality Data for 1986 through 1991 from Two Small Basins in Central Nevada." U.S. Geological Survey Open-File Report 93-651. 1994.

Mohanty, S., T.J. McCartin, and D.W. Esh. "Total-system Performance Assessment (TPA) Version 4.0 Code: Module Descriptions and User's Guide." San Antonio, Texas: CNWRA. 2000.

National Climatic Data Center. "Cooperative Summary of the Day Western United States." Asheville, North Carolina: National Oceanic and Atmospheric Administration. 1997.

———. "WBAN Hourly Surface Observations (1984 to 1994)." Asheville, North Carolina: National Oceanic and Atmospheric Administration. 1994.

———. "Solar and Meteorological Surface Observational Network 1961–1990 (Western Region)." CD-ROM. Asheville, North Carolina: National Oceanic and Atmospheric Administration. 1961–1990. <http://ols.nndc.noaa.gov/plolstore/plsql/olstore.prodspecific?prodnum=C00066-CDR-S0001>

Stothoff, S. and M. Musgrove. "Literature Review and Analysis: Climate and Infiltration." CNWRA 07-002. San Antonio, Texas: CNWRA. 2006.

Stothoff, S. and G. Walter. "Long-Term-Average Infiltration at Yucca Mountain, Nevada: Million-Year Estimates." CNWRA 07-003. San Antonio, Texas: CNWRA. 2007.

TRW Environmental Safety Systems, Inc. "Yucca Mountain Site Description." B00000000–01717–5700–00019. Rev. 00. Las Vegas, Nevada: TRW Environmental Safety Systems, Inc. 1998.

U.S. Geological Survey. "Updated Fracture/Fault Properties for the Fast Pathways Model." Data Package GS950708312211.003. LSN # DEN000200373. 1997. <http://lsnnet.gov/home.aspx?pg=advsearch>

van Genuchten, M.Th. "A Closed-Form Equation for Predicting the Hydraulic Conductivity of Unsaturated Soils." *Soil Science Society of America Journal*. Vol. 44. pp. 892–898. 1980.

1 INTRODUCTION

Yucca Mountain, Nevada, has been studied for more than 20 years as a potential location for geologic disposal of high-level waste. Yucca Mountain is located approximately 160 km [100 mi] northwest of Las Vegas, Nevada, in an area with little rainfall and hot summers. The potential repository would be located in the thick unsaturated zone roughly 250 m [825 ft] above the current water table, with 250 to 450 m [825 to 1,480 ft] of unsaturated rock overlying the repository horizon. Performance assessments of the potential repository indicate that water fluxes contacting waste can strongly influence repository performance (NRC, 2004). The importance of water fluxes on performance is evidenced by the significance of waste package longevity and the distribution and magnitude of seepage fluxes into drifts. Because net infiltration is the ultimate source of water at depth, the amount and distribution of net infiltration above the repository footprint is anticipated to strongly influence potential repository performance.

This report is part of a series of net infiltration reports under present and potential future climates at Yucca Mountain. The first report in the series, a literature review and analysis by Stothoff and Musgrove (2006), provided a global and regional context for estimates of net infiltration at Yucca Mountain. The second report (Stothoff and Walter, 2007) synthesized several lines of climatic evidence to estimate future climatic sequences and used the Infiltration Tabulator for Yucca Mountain (ITYM)[1] code to estimate bounds on million-year-average net infiltration for these climatic sequences. The third report (this document) provides the technical basis for the ITYM code and associated inputs that were used by Stothoff and Walter (2007).

The literature review and analysis by Stothoff and Musgrove (2006) considered worldwide natural analog sites with climatic conditions similar to previous stages of the glacial cycle at Yucca Mountain to augment direct observational evidence from the Yucca Mountain vicinity. The literature review concluded that site-specific conditions strongly influence recharge. The studies from outside the American West are difficult to directly apply to Yucca Mountain because the scatter in recharge estimates is even wider than the scatter in estimates of present-day net infiltration at Yucca Mountain. Literature from locations in the American West, while more useful, was found to require careful interpretation. One study of 16 hydrologic basins in east-central Nevada provided sufficient information to derive a relationship between mean annual precipitation (MAP)[2] and mean annual recharge for upland areas analogous to Yucca Mountain. Extrapolating this newly derived site-scale relationship to mean annual infiltration (MAI)[3] values typical of Yucca Mountain under present-day conditions yields estimates of MAI of 2.5 to 6.3 mm/yr [0.098 to 0.25 in/yr].

Stothoff and Walter (2007) built on the analysis by Stothoff and Musgrove (2006) to estimate bounds on million-year-average areal-average net infiltration at Yucca Mountain. Stothoff and Walter (2007) assumed that global climate, local climate, and vadose-zone processes are the

---

[1] Infiltration Tabulator for Yucca Mountain is used frequently throughout this chapter; consequently, the abbreviation ITYM will be used.

[2] Mean annual precipitation is used frequently throughout this chapter; consequently, the abbreviation MAP will be used.

[3] Mean annual infiltration is used frequently throughout this chapter; consequently, the abbreviation MAI will be used.

three major factors affecting net infiltration at Yucca Mountain. Global climate, driven by predictable changes in the Earth's orbital mechanics and characterized by continental ice volume, plays a dominant role in determining the local climate at Yucca Mountain by affecting the movement and nature of atmospheric air masses. Local climate at Yucca Mountain, responding to the air masses moving over Yucca Mountain and characterized by MAP and mean annual temperature, directly affects the water balance above the potential repository footprint by mediating water supply to and loss from the vadose zone. Vadose-zone processes, which respond to local climate and depend on soil and bedrock hydraulic properties, vegetation, and overland flow, also directly affect the water balance above the potential repository by determining what fraction of infiltration pulses overcomes evapotranspiration and moves deep within Yucca Mountain. Stothoff and Walter (2007) used the ITYM model to characterize vadose-zone processes. Using the estimated future climatic sequence developed by Sharpe (2003) and Bechtel SAIC Company, LLC (2004a), Stothoff and Walter (2007) estimated a mean and standard deviation of 41 and 32 mm/yr [1.6 and 1.3 in/yr], respectively, for million-year-average net infiltration averaged over a rectangle circumscribing the potential repository footprint. For the same rectangle, Stothoff and Walter (2007) estimated a mean and standard deviation of 41 and 33 mm/yr [1.6 and 1.3 in/yr], respectively, using an independently estimated set of potential future climatic sequences. Thus, estimates for million-year-average net infiltration were nearly identical when using the different approximations for future climates.

The ITYM code was originally developed with two purposes: (i) encapsulate understandings of infiltration-affecting processes at the Yucca Mountain site and the effects of parameter uncertainty and (ii) provide a preprocessor module to the U.S. Nuclear Regulatory Commission's (NRC) Total-system Performance Assessment (TPA) code. ITYM was originally developed as a module within TPA Version 3.0 (Manteufel, et al., 1997) and was recast as a standalone preprocessor code for TPA Version 4.0 (Mohanty, et al., 2000). Appendix H of the TPA Version 4.0 code documentation (Mohanty, et al., 2000) provides a user guide for ITYM. Hydraulic and climatic input parameter values have remained unchanged since TPA Version 4.0, except for an enhancement in 2003 to include the effects of overland flow on infiltration. ITYM was slightly modified in 2006, providing the output estimates in a different format, because the abstraction in TPA Version 5.1 is modified from earlier abstractions (Leslie, et al., 2007).

The present document provides an expanded technical basis for the ITYM code and discusses in detail the input parameters that were used by Stothoff and Walter (2007). The TPA Version 5.1 code (CNWRA and NRC, 2007) uses the same version of the ITYM code as a preprocessor and uses the same input parameters.

1.1 Site Characteristics

Numerous authors (e.g., TRW Environmental Safety Systems, Inc., 1998) describe the Yucca Mountain site in detail. Following is a brief overview of site characteristics that particularly influence net infiltration estimates at Yucca Mountain. Sections 5–7 of this report describe the site in greater detail and relate the site characteristics to net infiltration.

Yucca Mountain is a cuesta, or gently sloping planar landform terminated by a steep face, with tuff beds dipping to the east with a slope angle of 10 to 15°. Exposed bedrock is almost exclusively moderately to densely welded tuff. Less than 5 percent of the area above the potential repository footprint has nonwelded tuff units exposed (on the west flank of Yucca Mountain and the extreme north of the footprint). The west flank of Yucca Mountain is steep, with slopes of up to 50°, and the channels are correspondingly steep with little branching.

East of Yucca Crest, numerous washes deeply dissect the ridge, with the channels exhibiting a dendritic pattern. The eastern washes are V shaped with quite uniform hillslopes, incised up to 200 m [660 ft], and sideslope angles are limited to approximately 30° with much shallower channel slopes. Channels are separated by approximately 400 m [1,300 ft], so there are at least 10 washes within the potential repository footprint.

MAP in the study area is between 150 and 200 mm/yr [5.9 and 7.9 in/yr], with significant seasonal and interannual variability. The summer rainfall period maximum is in August, and the winter rainfall period includes the months of October through April (French, 1983). Summer precipitation often occurs as high-intensity thunderstorms, while winter rainfalls are generally of longer duration and lower intensity. Overland-flow events are infrequent and tend to be of short duration—on the order of hours to days. Potential evapotranspiration is an order of magnitude greater than MAP (Shevenell, 1996).

Present-day soil on the ridgetops and sideslopes is generally less than 50 cm [1.6 ft] deep and almost exclusively composed of a spatially uniform sandy loam matrix mixed with bedrock fragments, with fine-fraction characteristics consistent with an eolian source. Bedrock-fragment volume fraction depends strongly on location. Alluvial deposits in washes are gravelly to very gravelly sandy loams. It is not uncommon for channels to expose rock above the repository footprint, but alluvial deposits become increasingly thick downstream. Remnant alluvial terraces exist in some washes (e.g., Split Wash), which have been incised up to 20 m [66 ft].

1.2 Infiltration Modeling Approaches

A watershed model is often used to estimate net infiltration at the landscape scale, and the U.S. Department of Energy (DOE) has adopted this approach at Yucca Mountain. For example, Bechtel SAIC Company, LLC (2004b) uses the INFIL model to estimate net infiltration at Yucca Mountain over periods of 50 to 100 years using daily timesteps. Watershed models at the scale of Yucca Mountain may consider more than 100,000 grid cells, and each simulation represents a large computational effort.

ITYM was developed in the mid to late 1990s, balancing several factors in the development process. The U.S. Nuclear Regulatory Commission (NRC) wanted to use a physically based model to provide estimates of net infiltration to the TPA simulator under present and potential future climates, which places a premium on computational efficiency. NRC also wanted to have an independent capability for assessing assumptions and uncertainties related to net infiltration at Yucca Mountain, which places a premium on inclusiveness and the capability of generating many realizations. Finally, site-specific information was only sparsely available at the time that ITYM was under development, which places a premium on the capability of readily updating estimates as additional information becomes available. These demands led to an approach for estimating net infiltration at Yucca Mountain that is rather different from the classical watershed-model approach, even though the same or similar information is used in both models.

ITYM relies on abstracted responses of MAI to environmental conditions at a local scale to estimate MAI at that scale. These abstractions were created based on approximately 500 vertical one-dimensional bare-soil simulations using a fine grid, relevant soil physics and atmospheric boundary layer models, and a 10-year record of meteorological observations with an hourly resolution. Unsaturated hydraulic properties are described using the van Genuchten (1980) parameterization. Each simulation considered a different combination of hydraulic and

climatic input parameters. The BREATH code (Stothoff, 1995) was used to run the simulations used to develop the ITYM abstractions.

The bare-soil abstractions at the heart of the ITYM model consider either deep soil or shallow soil overlying bedrock. ITYM independently estimates MAI for several pathways for infiltration, including the bedrock matrix, unfilled fractures, soil-filled fractures, and carbonate-filled fractures. These pathways compete for infiltrating water because each of the pathways features a different capillary behavior at the interface between soil and bedrock. ITYM abstracts the competition between pathways by estimating MAI using the pathway with largest estimated MAI.

The largest-pathway bare-soil abstraction represents the sensitivity of net infiltration to hydraulic and climatic parameters, but further abstractions are required to consider overland flow (i.e., run-on and runoff) and plant transpiration.

Overland flow is abstracted as an effective increase in mean annual precipitation, using a regression equation developed from the results of external event-based simulations at the watershed scale. Additional effective precipitation is estimated with contributing upslope area and upslope soil volume as the predictive variables. The KINematic Runoff and EROSion (KINEROS) model (Woolhiser, et al., 1990) provides estimated responses to several observed precipitation events for a number of hillslope positions; these responses provide the basis for the regression equation for run-on. The BREATH model allows excess infiltration to runoff during simulations, but run-on was not considered.

A heuristic post-processing approach unique to ITYM accounts for reduction of MAI due to plant transpiration. Post-processing occurs after overland flow is considered. The idea is that the plant community will eventually scavenge essentially all near-surface water given enough soil water storage capacity, but shallow soil does not have sufficient storage to prevent all wetting pulses from reaching the bedrock or fracture system and passing out of the rooting zone before the plants have an opportunity to completely remove the infiltrated water. Soil water is a limiting factor for plant communities in arid and semiarid climates (except in areas where the water table is high), therefore there is strong competition for soil water and the species that can most advantageously obtain this resource have a competitive edge. The strong competition for soil water may drive plant community dynamics, but results in efficient uptake of available water regardless of the specific composition of the community. The heuristic model avoids detailed characterization of plants and plant communities because an efficient mix of plants is expected regardless of anticipated climate. The model assumes that (i) plants scavenge a fraction of the estimated bare-soil MAI, (ii) the scavenged fraction increases with increasing water storage capacity, and (iii) a single relationship between water storage capacity and scavenging efficiency describes plant communities over the range of climates expected at Yucca Mountain.

1.3 Input Parameters

Using the ITYM abstractions, MAI can be estimated rapidly on a fine grid over the repository footprint given inputs of environmental parameters. Numerous realizations of input parameters can be and often are assessed for a typical climatic condition. For example, Stothoff and Walter (2007) calculated 2,000 realizations of decadal-average MAI for each of 16 climatic conditions on a grid of 300 × 200 cells in approximately 2 days on a standard 3 GHz workstation. These realizations can consider both actual parameter variability and uncertainty in estimates of the statistical parameters governing the variability and can consider correlations between

parameters. Thus, both parameter variability and parameter uncertainty are formally incorporated into performance assessment.

ITYM uses 5 sampled climatic parameters (i.e., mean annual averages of precipitation, temperature, vapor density, wind speed, and cloud cover), 6 sampled soil parameters (intrinsic permeability, van Genuchten pressure, porosity, soil thickness, and soil and rock-fragment volume fractions), 19 sampled bedrock parameters (intrinsic permeability, van Genuchten capillary pressure and van Genuchten *m*, and porosity for each of 4 media, plus the volume fraction of 3 of the media), and 6 sampled vegetation parameters to describe scavenging efficiency. The larger of the two sampled soil volume fractions (i.e., the larger of soil and rock-fragment fractions) is discarded to satisfy the constraint that the volume fractions must sum to 1. ITYM uses climatic parameters established from regional observations with long record periods, and distributes systematically varying climatic parameters to the site using ground elevation. ITYM uses unit-specific hydraulic parameters derived from available site observations, in some cases supplemented with outside information, and describes the soil and bedrock units using surficial deposit maps and stratigraphic maps in order to distribute the hydraulic parameters to each grid cell. ITYM uses an estimated soil thickness map derived from an external preprocessor model to estimate systematic variation of soil thickness across the site. Upslope contributing area is derived from ground elevation, and upslope soil volume is derived from ground elevation and the soil thickness map.

This document provides the bases and rationale for the parameter values used in the ITYM input set in its roles as (i) a preprocessor for the TPA code and (ii) an estimator for long-term-average areal-average net infiltration. ITYM was developed in the mid to late 1990s, and all of the climatic and hydraulic parameter values were estimated in the late 1990s (except for the overland flow submodel, which was developed in 2003). In some cases, limited information was available during development of the parameters, and additional information and analyses have become available in the intervening years. This more-recent information is used to place the input parameter values in context.

1.4 Document Outline

Section 2 describes the overall computational approach employed for ITYM, including the Monte Carlo approach to estimating uncertainty. Section 3 describes the one-dimensional BREATH simulations used to develop abstractions for ITYM, and Section 4 describes the abstractions. Finally, Sections 5, 6, and 7, respectively, describe the climatic, hydraulic-property, and soil-thickness parameters provided in the standard ITYM input file and provide confirmatory analyses to place the parameter values in context. The standard input file was used to provide estimates of MAI to the TPA Version 5.1 code. Stothoff and Walter (2007) used the default MAI estimates provided for TPA Version 5.1 to estimate long-term net infiltration at Yucca Mountain.

2 COMPUTATIONAL SCHEME

The Infiltration Tabulator for Yucca Mountain (ITYM)[1] model provides an intermediate step between (i) detailed deterministic numerical mass and energy balance calculations performed on spatial scales of centimeters to meters at hourly time scales and (ii) estimates of the statistics of multi-watershed-average mean annual infiltration (MAI)[2] on millennial time scales. ITYM estimates the statistical distribution of MAI at the horizontal scale of ones to tens of meters, for several climate states, by combining statistical descriptions for the input parameters with response functions for decadal-average MAI given the input parameters. Approximately 500 detailed numerical simulations performed with the BREATH code (Stothoff, 1995) were used to develop the response functions. External processing of the ITYM output yields averages that are representative of larger space and time scales (e.g., Stothoff and Walter, 2007; CNWRA and NRC, 2007). This section describes the overall computational scheme used for ITYM simulations; subsequent sections describe the model and model inputs in greater detail.

2.1 Sampling Algorithm Overview

The ITYM model performs Monte Carlo sampling to estimate statistics of MAI on each grid cell in a rectangular grid. The underlying parameters are considered uncertain and may be spatially variable across the grid. The sampling procedure is repeated for each combination of several nominal values of mean annual precipitation (MAP)[3] and mean annual temperature (MAT)[4] at a specified reference elevation. For example, nominal values of MAP may be 100, 200, 400, and 800 mm/yr [3.9, 7.9, 15.8, and 31.5 in/yr], and nominal values of MAT may be 0, 7.33, 14.7, and 22 °C [32, 45.1, 58.4, and 71.6 °F]—all at an elevation of 1,400 m [4,600 ft]. The sampling procedure is repeated for all 16 combinations of MAP and MAT to build up separate MAI estimates for each climate. Each combination of MAP and MAT may have hundreds or thousands of realizations of MAI for each grid cell.

The Monte Carlo sampling process considers several categories of input parameters: (i) soil-class hydraulic properties, (ii) bedrock-class hydraulic properties, (iii) climatic properties, (iv) soil thickness, and (v) plant uptake properties. The sampling process considers correlations between properties within each category. For example, each soil class has several correlated hydraulic properties (intrinsic permeability, van Genuchten hydraulic parameters, and porosity) that are sampled simultaneously, and typically two soil classes (e.g., fine matrix and rock fragments) coexist in each grid cell. The statistical properties of mean, standard deviation, and correlation coefficients are uncertain for each property and are considered independent normally distributed parameters. Each class in each category is sampled separately, first

---

[1] Infiltration Tabulator for Yucca Mountain is used frequently throughout this chapter; consequently, the abbreviation ITYM will be used.

[2] Mean annual infiltration is used frequently throughout this chapter; consequently, the abbreviation MAI will be used.

[3] Mean annual precipitation is used frequently throughout this chapter; consequently, the abbreviation MAP will be used.

[4] Mean annual temperature is used frequently throughout this chapter; consequently, the abbreviation MAT will be used.

independently sampling the uncertain statistical parameters and then simultaneously sampling the correlated input parameters.

The sampling process accounts for two concepts: (i) spatial variability of the property and (ii) uncertainty about the values of the property. For example, consider a lithological unit. The unit will have a certain level of spatial heterogeneity, with different parameter values at different locations, but the physics governing the formation of the unit dictates that the properties will tend to fall within some band about the mean value. The mean value and the variation about the mean are inherently uncertain unless every location is measured. ITYM keeps these two concepts distinct in the sampling process; Section 6.3 describes the effective variability obtained by merging the two concepts.

A formal representation of the spatial variability of material properties would yield distinct values for each material property in each grid cell and require that the spatial correlation structure be described for all material properties. This implies that each MAI realization would require separately sampled values for each material property in each grid cell. If material-property variability has a negligibly small effect on lateral hydrologic interactions between adjacent grid cells, however, this level of detail has negligible effect on estimates of MAI and material properties in each grid cell can be considered independently.

Material property variability would affect lateral subsurface flow directly, by inducing lateral flow through capillary forces, or indirectly, by modifying the rates of lateral flow induced by gravity. Lateral flow induced by variability in capillary properties would induce lateral flow tending to systematically move towards porous media with a finer texture. Such systematic lateral flow would tend to increase MAI in finer materials and decrease MAI in coarser materials. The abstractions developed in Section 4 suggest that transfer of water from a grid cell with coarse material to a grid cell with fine material (or more generally, from a high-MAI cell to a low-MAI cell) would slightly reduce combined MAI for both cells because the increase in MAI for the fine material would not be as large as the decrease in MAI for the coarse material, therefore neglecting lateral flow induced by capillary forces would tend to overestimate MAI. Lateral flow induced by capillary forces would not induce bias in spatial patterns, however, because systematic textural patterns are accounted for using the soil maps. Capillary-force-induced redistribution is expected to have a negligible effect on MAI estimates, because large contrasts in capillary properties are required to induce lateral flows that are significant at the scale of ITYM grid blocks, whereas variations in soil and bedrock properties at Yucca Mountain appear to be fairly uniform spatially at the grid-cell scale.

Indirect effects that modify rates of either lateral subsurface transfer or overland flow between cells, such as local variability in hydraulic properties or soil depth, are not anticipated to induce systematic effects on MAI because there is no systematic effect that preferentially moves water from high-MAI cells to low-MAI cells or vice versa.

These considerations indicate that overall MAI may be slightly overestimated by neglecting the details of local variability in soil or bedrock hydraulic properties, but neglecting such details would not be expected to introduce spatial bias in MAI. Accordingly, ITYM simply samples material properties once per realization for each soil and bedrock class and assigns the properties to all grid cells containing the class.

Once the sampling process is completed for a realization, soil and bedrock classes are merged into soil and bedrock units. ITYM allows each unit to include several classes; the input file used by Stothoff and Walter (2007) and Total-system Performance Assessment (TPA) Version 5.1

describes all soil units with two soil classes (fine soil matrix and rock fragments) and all bedrock units with four classes (a matrix class, an unfilled fracture class, a soil-filled fracture class, and a carbonate-filled fracture class).

The relative proportion of each class (i.e., the volume fraction of the class) is uncertain. By definition, the volume fraction for all classes must sum to one; thus the volume fractions for each class are dependent upon all other classes. The sampling procedure discards the largest volume fraction among all of the classes, calculating a new value with the constraint. The volume fraction for both fine-matrix and rock-fragment classes are sampled for each realization of a soil unit, because either class may have a larger volume fraction during sampling. The volume fraction for the matrix class is not sampled for bedrock units and is always calculated using the volume fraction constraint, because the volume fraction for fractures is never larger than the volume fraction for the matrix.

Once all sampling and merging is complete for a realization, MAI is estimated for each grid cell, using abstractions described in Section 4 and the set of input parameters for that cell. First, the input parameters are obtained by lookup according to soil and bedrock unit or are independently obtained by scaling the values in spatially distributed input files (e.g., soil thickness is provided as a spatially distributed input file, and a single sampled parameter is used to uniformly scale each soil thickness value). Second, four separate bare-soil MAI estimates are made, one for each bedrock class, to represent different potentially dominant pathways. Third, the largest of the four bare-soil MAI pathway estimates is used to describe the entire grid cell, based on the rationale that the pathways compete for infiltrating water and each pathway has significantly different capillary properties. A pathway with coarse capillary properties (e.g., the unfilled-fracture pathway) requires relatively saturated conditions to activate, which may be rarely achieved if a pathway with finer capillary properties (e.g., the bedrock matrix) is sufficiently permeable to be the dominant pathway. Note that the material properties used for ITYM simulations typically produce a dominant pathway that has much larger estimated MAI than the other pathways (usually either the soil-filled fractures or the bedrock matrix), and estimates of grid cell MAI are not sensitive to the aggregation procedure in such cases. Finally, the bare-soil MAI estimate for the grid cell is adjusted to account for the effects of transpiration.

Once MAI is estimated for each grid cell, ensemble MAI statistics are updated. The mean and standard deviation of both MAI and $\log_{10}$(MAI) are tracked for each grid cell. At the end of the simulation, all four sets of statistics can be output in files that ITYM calls DTBL files, which conceptually consist of a table of so-called DEM files—one DEM file for each climate combination. ITYM uses the term “DEM file” to refer to a file with the same format as the 30-m [98-ft] digital elevation model files distributed by the U.S. Geological Survey (USGS).[5] Coarser DTBL grids can be obtained by averaging the statistics over N^2 grid cells, where N is a positive integer. Simulations for TPA Version 5.1 coarsened with N = 4, whereas Stothoff and Walter (2007) did not coarsen the results (i.e., used N = 1).

The original rectangular grid describing ground surface elevation was derived from a 30-m [98-ft] USGS digital elevation model. All input parameters are required for each grid cell. Some parameters are directly specified in a DEM file; for example, bedrock unit and soil unit

[5] U.S. Geological Survey is used frequently throughout this chapter; consequently, the abbreviation USGS will be used.

classifications are provided as DEM files. Bedrock and soil hydraulic properties are sampled by the corresponding bedrock and soil unit for each Monte Carlo realization, and all grid cells for that unit are provided the same property set. Soil thickness is provided as a DEM file. Climatic properties are provided as functional relationships of elevation or are derived from additional DEM files.

The TPA code has used ITYM to provide input files since TPA Version 4.0 (Mohanty, et al., 2000). The TPA code calculates repository performance using subarea-average deep percolation fluxes. The UZFLOW module of the TPA code estimates subarea-average deep percolation flux for each user-defined subarea. Typically, hundreds or thousands of ITYM grid cells lie with each subarea. The subarea averages vary over time based on a time history of MAP and MAT at the same reference elevation considered by ITYM. For computational efficiency, UZFLOW averages the DTBL files at the onset of a TPA simulation to provide tables describing the statistics of subarea-average MAI for each combination of nominal MAP and MAT considered by ITYM.

The TPA code considers both uncertainty in future climate and uncertainty in MAI given a particular climate. The TPA code considers uncertainty in future climate by using sampled parameters to adjust the magnitude of MAP and MAT in the future climate sequence. The TPA code considers uncertainty in MAI given a particular climate by using sampled parameters to create a realization of the tables describing subarea average MAI for each combination of nominal MAP and MAT considered by ITYM. The time sequence of future subarea-average MAI is estimated for a TPA realization using table lookup.

2.2 Abstractions

It is computationally demanding to perform uncertainty analyses using numerical simulators, and this was even more the case in the mid-1990s when ITYM was developed. For example, a BREATH simulation is at the scale of a single grid cell, and BREATH simulations discussed in Section 3 typically required between several hours and several weeks to complete, depending on parameter combinations. Stothoff and Walter (2007) used a grid with 59,600 cells, 16 climate combinations, and 2,000 realizations per climate combination, equivalent to 1.9×10^9 BREATH simulations. Although computer speed and numerical algorithms have improved greatly since ITYM was developed, it would not be feasible to consider a similar analysis using direct numerical simulation at the same spatial and temporal resolution that was used for the BREATH simulations. In comparison, total ITYM computational time was approximately 2 days on a standard workstation for the Stothoff and Walter (2007) analysis.

ITYM replaces individual grid-cell simulations with abstracted relationships for MAI given relevant input parameters. This procedure has several advantages: (i) abstracted relationships have trivial computational cost; (ii) abstracted relationships can be developed with relatively few simulations, then refined as additional simulations are performed; (iii) abstracted relationships provide insight into the input parameters controlling MAI; and (iv) additional fine-scale simulations are not required as information regarding input parameters evolves. The primary disadvantage of the abstraction procedure is that the abstraction may only approximately capture the full set of simulation results.

The abstractions in ITYM are derived from approximately 500 one-dimensional BREATH simulations of mass and energy transport in near-surface porous media. These simulations are discussed in Section 3. The one-dimensional simulations do not consider plant uptake or lateral redistribution and assume that just one pathway into the bedrock is available for flow

(e.g., unfilled fractures, soil-filled fractures, carbonate-filled fractures, or bedrock matrix). Section 4 describes (i) how the simulations are abstracted into relationships for bare-soil, (ii) how plant uptake is abstracted as an adjustment reducing bare-soil MAI, and (iii) how overland flow is abstracted as an increase to MAP.

2.3 Uncertain Parameters

All of the inputs required to estimate MAI are uncertain and are usually spatially or temporally variable. Often an input parameter is correlated to one or more other inputs.

Correlated properties are generated through the lag-0/lag-1 expression by Matalas (1967), simplified to the lag-0 expression

$$\delta = B\varepsilon \tag{2-1}$$

$$BB^T = C \tag{2-2}$$

where δ is a vector of random deviations from zero, ε is a vector of random impulses drawn from a normal distribution with zero mean and unit variance, and the C matrix is the covariance matrix for the variables.

The B matrix in Eq. (2-1) is the Cholesky decomposition of the covariance matrix C. Following a procedure suggested by Bras and Rodriguez-Iturbe (1993), the B matrix can be obtained from C by defining two matrices P and E such that

$$CP = PE \tag{2-3}$$

$$P^T P = PP^T = I \tag{2-4}$$

where E is a diagonal matrix of eigenvalues for C and I is the identity matrix. The B matrix can be decomposed through yielding

$$C = PEP^{-1} = BB^T \tag{2-5}$$

yielding

$$B = PE^{-1/2} \tag{2-6}$$

Realizations are recovered from the vector of deviations, by taking into account the mean

$$v = m + \delta \tag{2-7}$$

where v is the vector of variables and m is the corresponding mean value. Truncated distributions are obtained by discarding and resampling if a realization has one or more variables falling outside a specified bounding range. A realization of C is built by

- Sampling for the variances (diagonal elements in C) to calculate the standard deviation
- Sampling for each pairwise correlation coefficient

- Multiplying each pairwise correlation coefficient by the corresponding standard deviations

The covariance matrix for three variables, for example, is defined by

$$C = \begin{bmatrix} s_1^2 & r_{12}s_1s_2 & r_{13}s_1s_3 \\ r_{12}s_1s_2 & s_2^2 & r_{23}s_2s_3 \\ r_{13}s_1s_3 & r_{23}s_2s_3 & s_3^2 \end{bmatrix} \quad (2\text{-}8)$$

where each s_i is a sampled standard deviation and each r_{ij} is a sampled correlation coefficient. It is assumed that uncertainties in the means, variances, and pairwise correlation coefficients are independent and thus are sampled from their respective distributions.

2.4 Spatially Distributed Parameters

Yucca Mountain is spatially heterogeneous in surface elevation and soil and bedrock characteristics. Consequently, input parameters used in the abstractions also differ from location to location.

ITYM describes spatial variability of an input parameter in several ways:

- The parameter is derived from the surface-elevation grid using regression relationships [e.g., MAT, mean annual vapor density (MAV)].[6]
- The parameter is derived from the surface-elevation grid using regression relationships and is modified by additional DEM files (e.g., MAP).
- The parameter is derived from the surface-elevation grid with the aid of additional input [e.g., mean annual shortwave radiation (MASW)].[7]
- The parameter is described separately for each grid cell using a separate DEM file [e.g., soil thickness, mean annual wind speed (MAW)].[8]
- The parameter is indexed to a soil class, soil units are considered a mixture of one or more soil classes, and the soil unit for each cell is described with a DEM file (e.g., soil permeability).

---

[6] Mean annual vapor density is used frequently throughout this chapter; consequently, the abbreviation MAV will be used.

[7] Mean annual shortwave radiation is used frequently throughout this chapter; consequently, the abbreviation MASW will be used.

[8] Mean annual wind speed is used frequently throughout this chapter; consequently, the abbreviation MAW will be used.

- The parameter is indexed to a bedrock class, bedrock units are considered a mixture of one or more bedrock classes, and the bedrock class for each cell is described with a DEM file (e.g., bedrock permeability, fracture porosity).

Site-specific climatic inputs are described in Section 5. Most climatic parameters are described as elevation dependent, such as MAP, MAT, and MAV; orientation dependent, such as MASW; or independent of location, such as mean annual longwave radiation (MALW).[9] The abstraction for overland flow modifies the elevation-dependent description for MAP based on upslope soil volume and contributing area. Elevation-dependent parameters are described using uncertain regression relationships that are sampled for each realization. Orientation-dependent MASW uses an external table describing shortwave radiation outside the Earth's atmosphere for given ground orientations and interpolates actual cell orientation within the table to determine cell-dependent values. Uncertainty in both MASW and MALW is accounted for by sampling mean annual cloud cover (MACC),[10] which is the largest uncertainty affecting both parameters. Spatial patterns for MAW are too complex to describe with a simple formula; thus a representative spatial distribution is provided as a DEM file. Uncertainty in MAW is accounted for with a single multiplier factor that is sampled once per realization and used to uniformly scale each value of the representative MAW distribution.

Site-specific hydraulic properties are described in Section 6. Hydraulic parameters are generally tied to a soil or bedrock class and are considered to be spatially uniform within each class. The spatially uniform parameter values are considered uncertain. Soil and bedrock units are provided as index maps, with a separate DEM file for soil and bedrock units derived from the U.S. Department of Energy Geographical Information System coverages of site maps. Soil units typically consist of two separate soil classes: a fine {i.e., <2 mm [0.08 in]} matrix and embedded rock fragments. Each soil unit can have different soil classes; the volume fraction for each soil class is an uncertain parameter for each soil unit and is sampled for each realization. Bedrock units typically consist of four separate bedrock classes: (i) bedrock matrix, (ii) unfilled fractures, (iii) soil-filled fractures, and (iv) carbonate-filled fractures. Typically, each bedrock unit uses a different bedrock matrix class, but the same fracture classes are used for each bedrock unit. The volume fraction for each bedrock class is an uncertain parameter for each bedrock unit. The largest volume fraction is adjusted after sampling for each unit to ensure that the volume fractions for both soil and bedrock sum to unity.

Soil thickness varies systematically across Yucca Mountain, reflecting the interplay between dust deposition, bedrock entrainment, and lateral redistribution due to overland flow and creep. An external numerical mass balance model estimates soil thickness across the site using the same elevation DEM file used by ITYM. The soil thickness model is described in Section 7.

A representative soil thickness distribution resulting from the external analysis is provided as a DEM file. Uncertainty in soil thickness is accounted for with a single multiplier factor that is sampled once per realization and used to uniformly scale each value of the representative soil thickness distribution.

---

[9] Mean annual longwave radiation is used frequently throughout this chapter; consequently, the abbreviation MALW will be used.

[10] Mean annual cloud cover is used frequently throughout this chapter; consequently, the abbreviation MACC will be used.

3 SHALLOW-INFILTRATION SIMULATIONS

The Infiltration Tabulator for Yucca Mountain (ITYM)[1] simulator calculates spatially distributed estimates of mean annual infiltration (MAI)[2] across Yucca Mountain. To estimate MAI, ITYM: (i) samples soil, bedrock, and climatic properties for each grid cell; (ii) estimates bare-soil MAI for each combination of cell-specific properties; and (iii) adjusts bare-soil MAI to account for plant uptake. ITYM does not perform detailed simulations to estimate bare-soil MAI, instead relying on a response surface abstracted from approximately 500 detailed numerical one-dimensional column simulations. Section 3 describes the detailed simulations that are abstracted into the response surface, and Section 4 describes the abstraction process and mathematical form of the response surface.

3.1 Simulation Procedure

The BREATH simulator used in the study considers the coupled flow of moisture and energy in a porous medium, as described in detail by Stothoff (1995). The sensitivity of net long-term infiltration estimates to hydraulic properties, using BREATH, was considered by Stothoff (1997). Following the procedures in Stothoff (1997), two types of simulations are considered: (i) semi-infinite columns of alluvium and (ii) columns of shallow colluvium overlying a semi-infinite fracture or bedrock continuum. At the bottom of the column, the gradients of saturation and temperature are assumed to be zero, allowing gravity drainage of water and advective losses of energy. In all cases, the semi-infinite behavior is approximated by using columns deep enough that the bottom boundary conditions have minimal impact on the estimated net infiltration values. A domain of 30 m [98 ft] in depth is assumed sufficient to achieve this goal for the hydraulic and thermal properties considered.

All simulations are driven using the same sequence of 10 years of hourly meteorologic conditions, based on hourly readings from the Desert Rock, Nevada, National Weather Service meteorologic station located approximately 46 km [29 mi] to the east of Yucca Mountain (National Climatic Data Center, 1994). Procedures for converting the National Weather Service readings into BREATH meteorological inputs are discussed by Stothoff (1997). The meteorological record runs from March 1, 1983, through February 28, 1993; the sequence was the longest available for this station at the onset of the study with all the meteorologic inputs measured at hourly intervals. The sequence is repeated until the effects of the initial conditions are eliminated. Centuries are required to eliminate initial conditions in deep-alluvium, low-MAI cases, but the initial conditions dissipated in the first cycle for all of the fracture-continuum simulations. The response surface is based on the last decade of the simulations. One decade may be too short of a time period to capture the full range of precipitation events in a statistically robust way; however, this is sufficiently long to gain considerable insight into the changes in behavior that might be expected with different hydraulic properties and climatic regimes.

Individual simulations use a modified Desert Rock sequence to approximate the effects of climatic change by scaling (all input factors except for air temperature) or shifting (air temperature) all hourly readings. This procedure approximates all changes in precipitation

---

[1] Infiltration Tabulator for Yucca Mountain is used frequently throughout this chapter; consequently, the abbreviation ITYM will be used.

[2] Mean annual infiltration is used frequently throughout this chapter; consequently, the abbreviation MAI will be used.

patterns by modifying rainfall intensity, without changing either the precipitation frequency or the season in which precipitation falls.

Precipitation in excess of infiltration is assumed to runoff without ponding, and neither overland nor subsurface lateral flow is considered in the column simulations. ITYM considers overland flow by locally increasing the value of mean annual precipitation (MAP)[3] provided to each grid cell, as described in Section 4.6, but does not consider lateral subsurface flow. Incorporating lateral subsurface flow in ITYM would likely decrease MAI at the top of slopes, increase MAI at the bottom of slopes, and have little effect on midslope regions.

The meteorological sequence input to BREATH is based on hourly meteorological observations. Adaptive timestepping is used to ensure mass balance, with a maximum timestep of 1 hour. During rainfall events, a single hour may take several hundred timesteps. The input sequence is smoothed to a monthly moving average during periods dominated by evaporation to reduce computational effort. A series of tests suggests that MAI estimates are not greatly affected (i.e., within approximately 10 percent) if the smoothing process is applied more than 24 hours from a precipitation event.

3.2 Semi-Infinite Soil

Two homogeneous alluvium columns are used to illustrate the impact of climatic factors on MAI in deep alluvium. A high-permeability {intrinsic permeability $k = 10^{-5}$ cm^2 [1.6×10^{-6} in^2]} and medium-permeability {$k = 10^{-8}$ cm^2 [1.6×10^{-9} in^2]} alluvium are considered, both with porosity = 0.3, van Genuchten m = 0.2, and van Genuchten P_o = 1 kPa [0.0099 atm]. The 30-m [98-ft] column is discretized with 51 nodes, with a top element of 2 cm [0.8 in] and each successive element increasing in length by 10 percent. Much higher net infiltration occurs for the medium-permeability alluvium than for the high-permeability alluvium due to reduced evaporation. Stothoff (1997) found that, for a similar semi-infinite column with all parameters held constant (aside from k), as k decreases from 10^{-5} cm^2 to 10^{-10} cm^2 [1.6×10^{-6} to 1.6×10^{-11} in^2], MAI increases to a peak value with k at roughly 10^{-8} cm^2 [1.6×10^{-9} in^2], then drops precipitously to essentially zero with k at 10^{-10} cm^2. However, Stothoff (1997) noted that when k is larger than 10^{-10} cm^2, MAI tends to decrease with decreasing k when other hydraulic properties also vary with k according to their correlation with k.

The basecase simulation for each alluvium uses the Desert Rock meteorological record, as was the case for all simulations presented by Stothoff (1997). Additional simulations were run for each column, with each simulation having one of the meteorologic inputs systematically perturbed from the basecase value, to identify first-order sensitivities to inputs. A similar procedure was followed by Stothoff (1997) to examine the effect of hydraulic properties on MAI.

The long-term net infiltration rate resulting from each simulation is plotted in Figure 3-1, where the perturbation for most weather parameters is obtained by uniformly scaling each hourly value for the parameter. The scale factor is indicated next to the symbol (e.g., “x 1.5” next to a symbol indicates that the scale factor is 1.5). Temperatures, however, are perturbed by adding a

[3] Mean annual precipitation is used frequently throughout this chapter; consequently, the abbreviation MAP will be used.

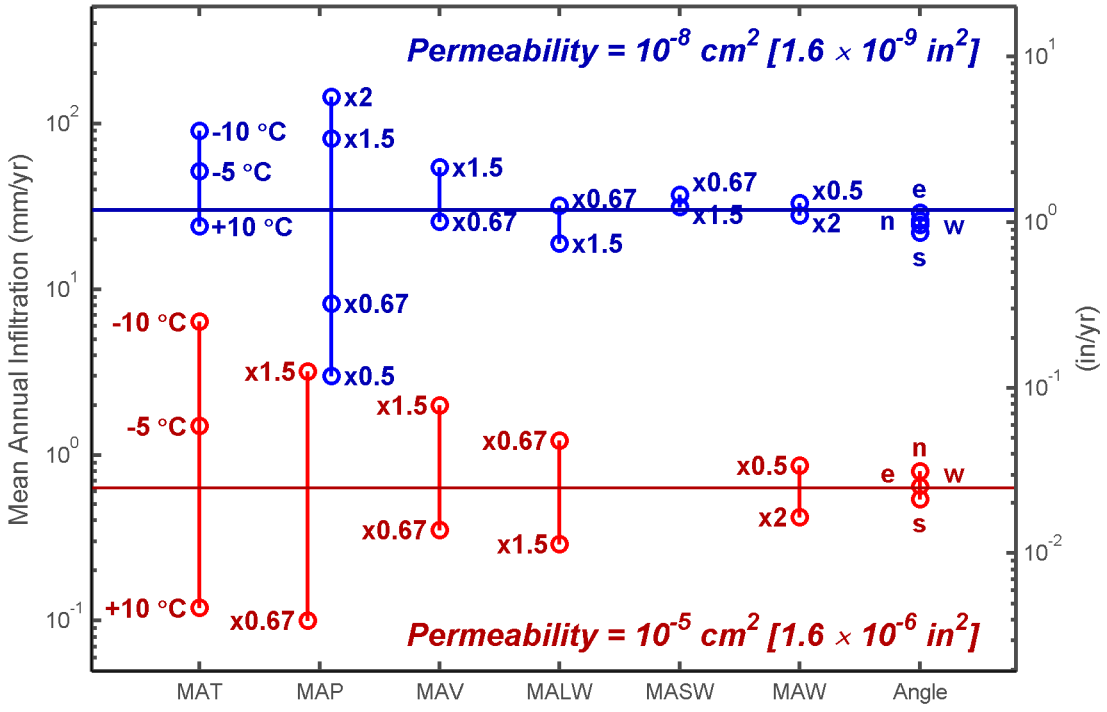

Figure 3-1. Mean Annual Infiltration in Reference Bare-Soil Simulations With Deep Soil, Varying Reference Meteorological Factors. Annotation Denotes Perturbation Value (for MAT), Scale Factor (for MAP, MAV, MALW, MASW, and MAW), or Direction of 30° Rotation (for Angle). [°F = (9/5)°C + 32]

constant value to all hourly temperature values (the perturbations are indicated by a plus or minus). Simulations with incident solar radiation arising from a ground rotation of 30° east, west, north, and south are denoted "Angle" in Figure 3-1. Relative changes in MAI for the same perturbation in the meteorologic input parameter are roughly twice as great in the low-MAI (high-permeability) column than in the high-MAI (medium-permeability) column.

Figure 3-2 shows MAI as a function of the mean annual moisture content below the wetting-pulse perturbation depth for the same set of simulations. Conditions at depth are almost steady state in these simulations, so that the direct link between flux and saturation provided by the relative permeability function provides the strong correlation between MAI and moisture content seen in Figure 3-2. Most points arise from simulations that modify evaporation-affecting parameters. The remaining points, from modified-precipitation simulations, align with the evaporation-affecting results. Interestingly, multiplying MAI by $k^{0.55}$ and dividing each moisture content by the corresponding basecase moisture content yields curves that are aligned. Note that scaling by $k^{0.5}$ is appropriate for a diffusion-dominated system. In contrast, simulations

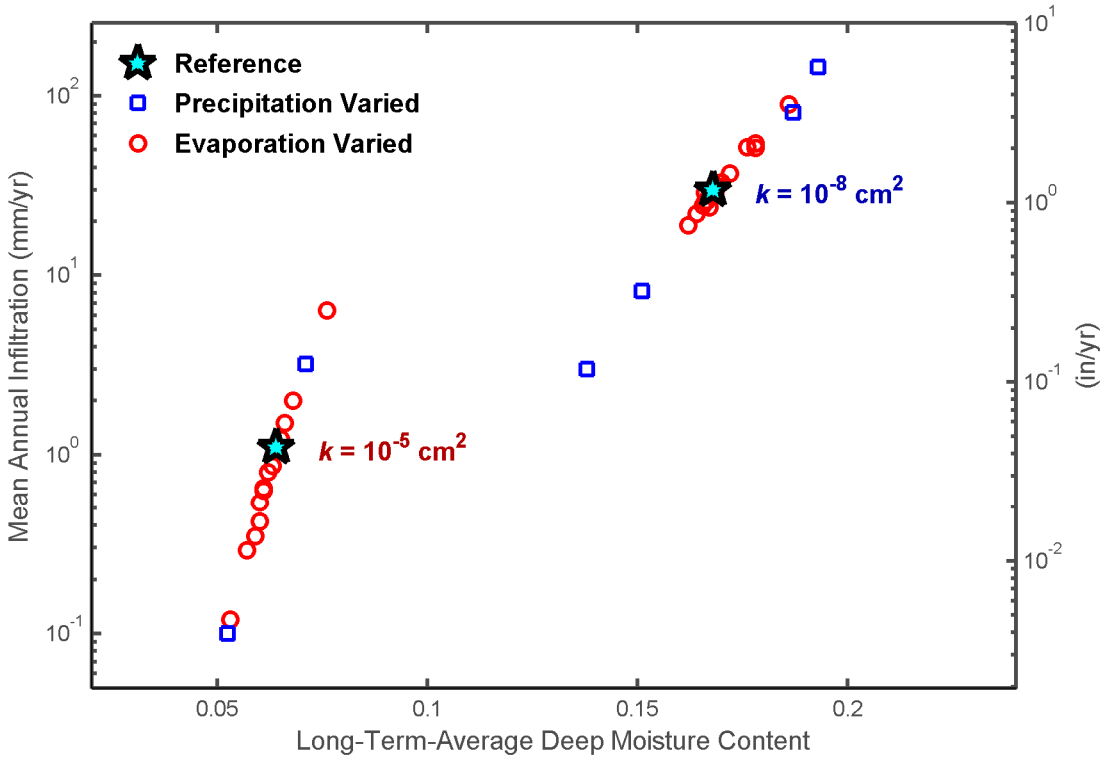

Figure 3-2. Relationship Between Bare-Soil Mean Annual Infiltration and Long-Term-Average Deep Moisture Content in Deep Alluvium Due to Systematic Change in Meteorological Parameters

considering a shallow layer overlying a deeper layer (described in Section 3.3) have different slopes for modified-precipitation and modified-evaporation simulations.

Meteorological factors have less effect on MAI in deep alluvium than do the hydraulic properties examined by Stothoff (1997); hence identifying the hydraulic properties of alluvium is overall more significant to identifying MAI in deep alluvium at Yucca Mountain. Nevertheless, systematic trends in the meteorologic variables (i.e., due to elevation variation or climatic change) can yield systematic variation in MAI. Elevation variation at Yucca Mountain results in small but systematic variability in MAP, MAT, and MAV, while slope aspect effects (e.g., north-facing slopes versus south-facing slopes) result in systematic variability in mean annual incoming radiation through variability in incident shortwave radiation. A somewhat different pattern of systematic MAW variation occurs, because of differing protection from prevailing winds and differing air-drainage patterns; surface roughness also changes from location to location due to variation in vegetation and soil composition, with a similar effect. Significant variation in both MAP and MAT should occur due to climatic change, with perhaps some change in MAV and cloud cover (with concomitant impact on incoming radiation) as well. Of these factors, MAP and MAT would appear to have the most significant influences on the spatial distribution of MAI—a point that is demonstrated in Section 5.

3.3 Shallow Soil Over Fractured Bedrock

The fractures at the top of the bedrock at Yucca Mountain are typically unfilled, filled with soil, or filled with carbonate or silicaceous material. Stothoff (1997) examined the response of distributed bare-soil MAI to increasing thickness of soil above an unfilled fracture continuum with negligible flow in the rock matrix. Stothoff (1997) found that for the basecase soil examined herein, bare-soil MAI dropped sharply with increasing cover, decreasing to zero with only a fraction of a meter of cover and staying at zero for soil depths up to almost 10 m [33 ft]. However, once the soil cover reached 10 m [33 ft], the medium was essentially semi-infinite and MAI reached approximately 1 percent of MAP (depending on soil properties). The increase in soil depth was accompanied by a monotonic increase in mean annual moisture content at the soil/fracture interface, reaching essentially saturated conditions with 10 m [33 ft] of cover. The strongly nonmonotonic behavior for bare-soil MAI through unfilled fractures is explained by the capillary barrier represented by the unfilled fracture; the soil immediately above the fracture must be essentially saturated before the fracture begins to flow. Saturation occurs through wetting pulses (shallow case) or near-perched conditions (deep case). The presence of shrubs or other plants would allow water scavenging at depth; thus, MAI would be reduced and essentially saturated conditions in the deep case (if saturation even occurred) would require considerably greater cover thickness.

Simulations not reported by Stothoff (1997) were run using hydraulic properties for the fracture continuum that are more representative of soils or carbonates. Note that the assumption of a fracture continuum in a one-dimensional context tacitly implies that lateral redistribution in the soil is sufficiently rapid to not limit exchange between the soil and the fracture system. Elements at the ground surface were about 1 mm [0.04 in] in length, with a minimum of 20 soil elements and 30 fracture elements. These simulations assume that the fracture filling is semi-infinite {at least 30 m [98 ft] thick}, although the fracture fillings may exist for a few meters or less in most locations. A capillary barrier may exist between fracture fill material and the unfilled part of a fracture, but the strength of the capillary barrier is not known for the typical situation where the fill material gradually peters out within a fracture. No simulations were performed to examine the effect of a finite-length filling.

Simulations with carbonate-filled fractures are more problematic than unfilled fractures, as there are few data on filling properties; simply obtaining samples from the fractures is difficult, particularly for the more fragile samples (which would be expected to have relatively large permeabilities). Data package GS950708312211.003, prepared by the U.S. Geological Survey (1997), reports 15 measurements of fracture-fill materials from Yucca Mountain, with 4 measurements parallel to and 11 measurements perpendicular to the fracture. All four parallel measurements have saturated hydraulic conductivity values in the range of 8×10^{-7} to 3×10^{-6} m/s [10^{3} to 3.7×10^{3} in/yr], while 10 of the perpendicular measurements range from less than 10^{-13} to 5×10^{-8} m/s [1.2×10^{-4} to 62 in/yr] and one is about 10^{-6} m/s [1,200 in/yr]. The samples may represent a mixture of carbonate and silicate fillings, and the relatively sparse data set may not be representative of the site as a whole. Accordingly, simulations labeled as carbonate filled may not use properties representative of actual fillings.

Carbonate and silicate fracture fillings are likely to exhibit anisotropy if deposition occurs due to evaporation as water moves along fracture surfaces. The along-fracture conductivity may be significantly greater than the across-fracture conductivity in such cases. Flint, et al. (1996a) used a hydraulic conductivity of 5×10^{-7} m/s [620 in/yr] {$k = 5.1 \times 10^{-10}$ cm^2 [7.9×10^{-11} in^2]} for carbonates, but do not report retention properties. The simulations presented by Stothoff (1997) suggest that bare-soil alluvium with this permeability is in the transition zone between exhibiting

significant MAI and having no net infiltration. Baumhardt and Lascano (1993) and Hennessy, et al. (1983) suggest that calcite has a texture of a fine soil. In the simulations reported herein, carbonate retention properties were assumed to be similar to those of clays. Sensitivity of simulation results to the carbonate retention properties is quite small.

Figure 3-3 illustrates the response of bare-soil MAI to different soil cover thicknesses for four sets of simulations, with the basecase hydraulic properties for the simulations reported in Table 3-1. The semi-infinite soil and soil/unfilled-fracture cases were presented by Stothoff (1997). The third set represents a soil-filled fracture, while the fourth set represents a carbonate-filled fracture. The covering-soil hydraulic properties are identical in all four sets.

The response to increases in cover thickness is quite different for the unfilled-fracture set than the two sets with fracture fillings; interestingly, however, the soil- and carbonate-filled sets are quite similar despite having somewhat different hydraulic properties. The unfilled-fracture set has large MAI with very shallow cover, but MAI decreases rapidly as the soil cover increases to only a few tens of centimeters. Stothoff (1997) found that this behavior was essentially insensitive to the unfilled-fracture hydraulic properties. The filled-fracture sets have a much gentler decrease in MAI as the soil cover increases. It is expected that bare-soil MAI for the semi-infinite case would be achieved for a soil depth of about 10 m [33 ft] regardless of the filling material. These simulations suggest that there may be a minimum MAI for some intermediate soil depth.

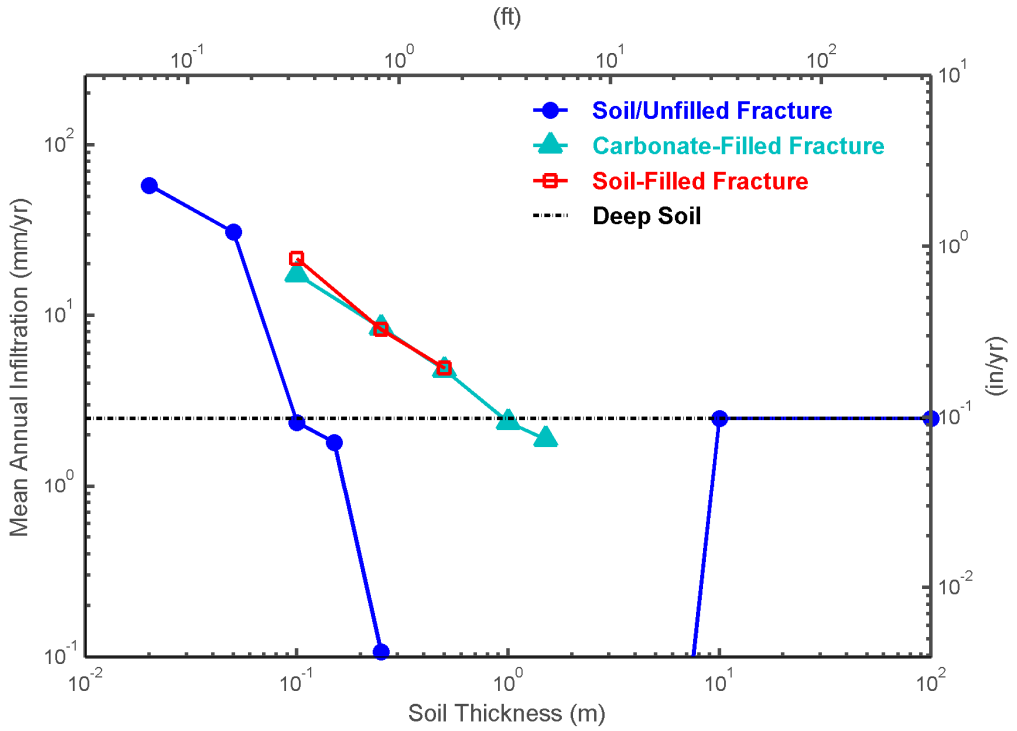

Figure 3-3. Mean Annual Infiltration in Reference Bare-Soil Simulations With Soil Overlying Unfilled, Soil-Filled, and Carbonate-Filled Fractures. Bare-Soil Mean Annual Infiltration for a Semi-Infinite Column With the Same Soil Properties Is Shown for Reference.

Table 3-1. Hydraulic Properties Used To Assess Infiltration Sensitivity. Note That Only One Property Is Perturbed for Each Simulation.					
Case	**Intrinsic Permeability k (cm^2)**	**Saturated Hydraulic Conductivity K_{sat} (mm/yr)**	**van Genuchten m**	**van Genuchten Pressure P_o (kPa)**	**Porosity ε**
Soil Cover					
Low perturbation	10^{-9}	3.1×10^{4}	0.1	1	0.2
Basecase	10^{-8}	3.1×10^{5}	0.2	2	0.3
High perturbation	10^{-7}	3.1×10^{6}	0.3	5	0.5
Unfilled Fracture					
Low perturbation	1.15×10^{-4}	3.6×10^{9}	0.6	9.8×10^{-4}	10^{-4}
Basecase	1.15×10^{-2}	3.6×10^{11}	0.7	9.8×10^{-3}	10^{-3}
High perturbation	1.15	3.6×10^{13}	0.8	9.8×10^{-2}	10^{-2}
Carbonate−Filled Fracture					
Low perturbation	1.15×10^{-11}	3.6×10^{2}	0.4	—	10^{-5}
Basecase	1.15×10^{-10}	3.6×10^{3}	0.5	10	10^{-4}
High perturbation	1.15×10^{-9}	3.6×10^{4}	0.6	100	—
cal3	5.7×10^{-10}	1.8×10^{4}	0.5	10	10^{-4}
Soil−Filled Fracture					
Low perturbation	—	—	—	—	10^{-4}
Basecase	10^{-8}	3.1×10^{5}	0.2	2	10^{-3}
High perturbation	—	—	—	—	10^{-2}
Bedrock					
tcshar	1.6×10^{-9}	4.9×10^{4}	0.237	330	0.235
tccap	3.2×10^{-12}	99	0.301	200	0.105
tcul	9.1×10^{-15}	0.28	0.31	340	0.108
tslnl	1.7×10^{-13}	5.3	0.236	315	0.141
mw7	1.15×10^{-10}	3.6×10^{3}	0.48	120	0.283
mw8	1.15×10^{-11}	3.6×10^{2}	0.435	150	0.226

Unfilled-fracture and filled-fracture simulations exhibit a fundamentally different behavior stemming from the different fracture air-entry pressures. Air-entry pressure is much smaller in unfilled fractures than in the soil, so that as modeled, the fractures represent a capillary barrier to the downward percolation of water in the overlying soil (even though the fractures are extremely permeable) and drainage into the fracture requires essentially saturated conditions in the soil. Note that the simulations do not consider small-scale heterogeneity, which may allow less-saturated soil to supply water to unfilled fractures. Filled fractures have air-entry pressures no less than in the soil, so that although a filled fracture would have a much smaller saturated hydraulic conductivity than if it were unfilled, the filling material is not a capillary barrier. Indeed, carbonate fillings may preferentially attract water, consistent with observations for caliche by Baumhardt and Lascano (1993) and Hennessy, et al. (1983). These two situations are handled with different abstractions in Section 4. ITYM considers a weighted average of filled and unfilled fracture flow pathways when calculating net infiltration in each grid cell, as described in Section 6.

3.3.1 Sensitivity to Hydraulic Properties

Figure 3-4 illustrates typical responses of MAI to different soil and fracture-filling hydraulic properties by varying one property between runs and holding constant all other inputs. The basecase simulation set represents the bare-soil over carbonate-filled fracture simulation set shown in Figure 3-3. One pair of simulation sets has saturated hydraulic conductivity (K_{sat}) of the soil one order of magnitude greater and lesser than the basecase, while the other similarly varies the carbonate K_{sat}. Less permeable fracture fillings reduce MAI, in accord with intuition. The counterintuitive decrease in MAI with increasing soil K_{sat} in Figure 3-4 is consistent with the findings of Stothoff (1997), who demonstrated that evaporation is more effective (limiting MAI) if K_{sat} increases without concurrent changes in the retention properties. If the retention properties change concurrently with K_{sat}, however, MAI increases with increasing soil K_{sat}.

The way that soil properties influence MAI is fundamentally different from the way fracture properties influence MAI. A change in soil properties affects the slope of the response of MAI with soil thickness, while a change in filling properties only offsets the response curve. Changing the soil hydraulic properties affects the number and magnitude of wetting pulses reaching the soil/fracture interface; changing the fracture hydraulic properties only affects the rate at which wetting pulses enter the fracture and escape evaporation.

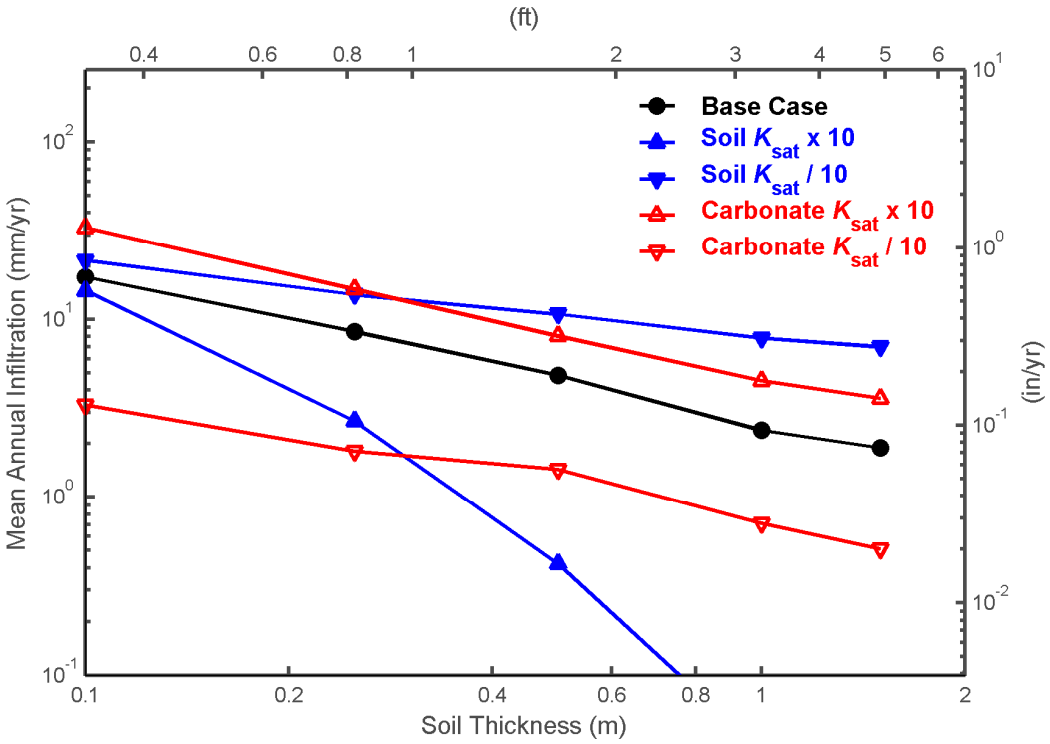

Figure 3-4. Mean Annual Infiltration in Reference Bare-Soil Simulations With Soil Overlying Carbonate-Filled Fractures, Varying Soil and Carbonate Saturated Hydraulic Conductivity

3.3.2 Sensitivity to Climate

Figure 3-5 illustrates the response of bare-soil MAI to various climatic factors for two systems with 2 and 15 cm [0.8 and 5.9 in] of soil over an unfilled fracture continuum. The same procedure was followed to produce Figure 3-1. The basecase unfilled fracture and soil cover hydraulic properties in Table 3-1 are used. Fracture properties considered here are based on the range of parameters reported by Schenker, et al. (1995) and are representative of both the Tiva Canyon and the Topopah Spring densely welded tuffs. Stothoff (1997) found that the fracture properties do not materially affect simulated infiltration rates as long as there are a few unfilled fractures.

The response to each of the climatic factors is investigated in the same way as in Section 3.2. As with the deep-alluvium case, changes in MAP and MAT have the largest influence on MAI, while shortwave radiation has minimal impact. Wind speed, vapor density, and longwave radiation have moderately small effects. There is significantly increased sensitivity to climatic change as the soil thickness increases. For example, north-facing and south-facing slopes have essentially identical values of bare-soil MAI for the shallow soil, while for the deeper soil, north-facing slopes have about 2.5 times larger MAI than south-facing slopes. These results suggest that the depth of soil can have a far more significant impact on MAI than most of the climatic inputs and can amplify the effect of climatic inputs.

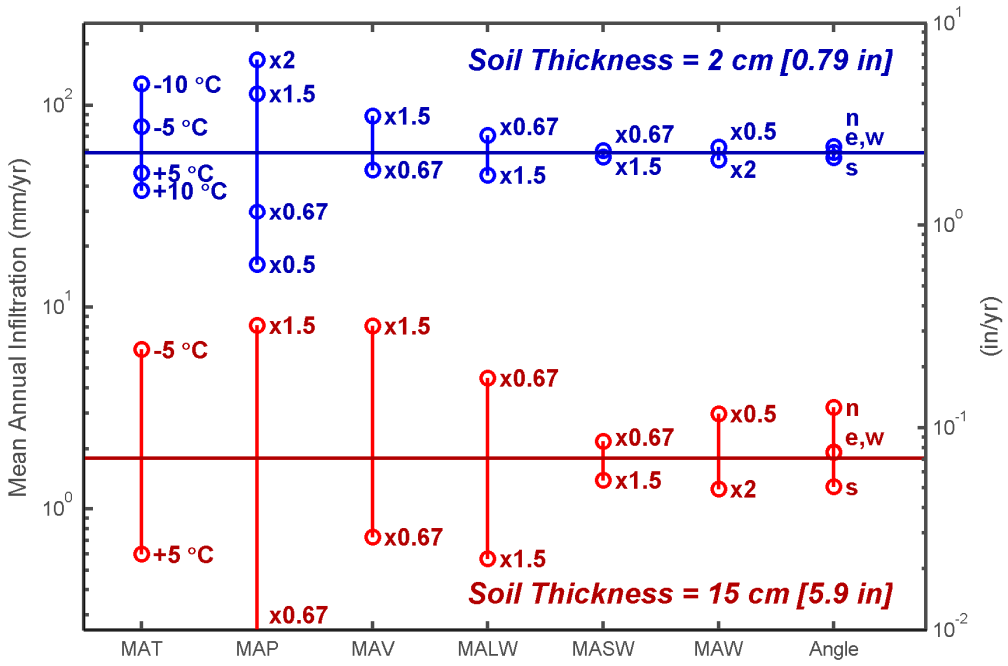

Figure 3-5. Mean Annual Infiltration in Reference Bare-Soil Simulations With 2 and 15 cm [0.79 and 5.9 in] Soil Overlying Unfilled Fractures, Varying Reference Meteorological Factors

Figure 3-6 demonstrates the response of MAI to MAP and MAT (the most significant meteorologic inputs identified in Figure 3-5) for the soil-over-carbonate system using the basecase soil cover and carbonate hydraulic properties described by case cal3 in Table 3-1. In these simulations, MAI responds exponentially to multiples of MAP and increments in MAT. There is also an increased sensitivity to changes as the soil thickness increases. A similar behavior occurs for the set with soil over a soil-filled fracture.

3.4 Shallow Soil Over Intact Bedrock

Several simulations illustrate how bare-soil MAI responds in the absence of fractures. Simulations were performed with bedrock representative of densely welded tuffs (Tiva Canyon upper lithophysal, tcul; Topopah Spring lower nonlithophysal, tslnl), moderately welded tuffs (Tiva Canyon caprock, tccap), and nonwelded tuffs (Tiva Canyon shardy base, tcshar), with hydraulic properties reported in Table 3-1. Bedrock properties are based on values Flint, et al. (1996b) reported, with samples TPC52s, PW19s, and BT26Hs used to provide retention properties. Two non- to moderately welded tuffs (mw7, mw8) were also used with representative properties. Bare-soil MAI under nominal climatic conditions is shown in Figure 3-7.

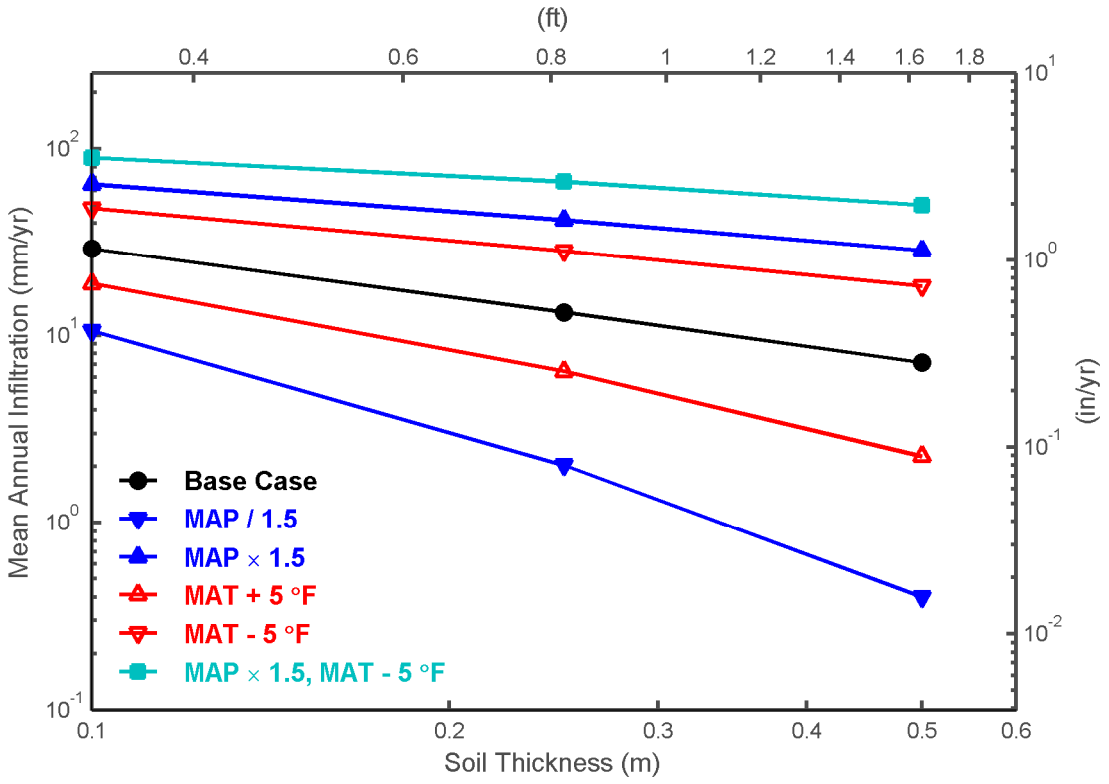

Figure 3-6. Mean Annual Infiltration in Reference Bare-Soil Simulations With Soil Overlying Carbonate-Filled Fractures, Varying Mean Annual Precipitation and Temperature

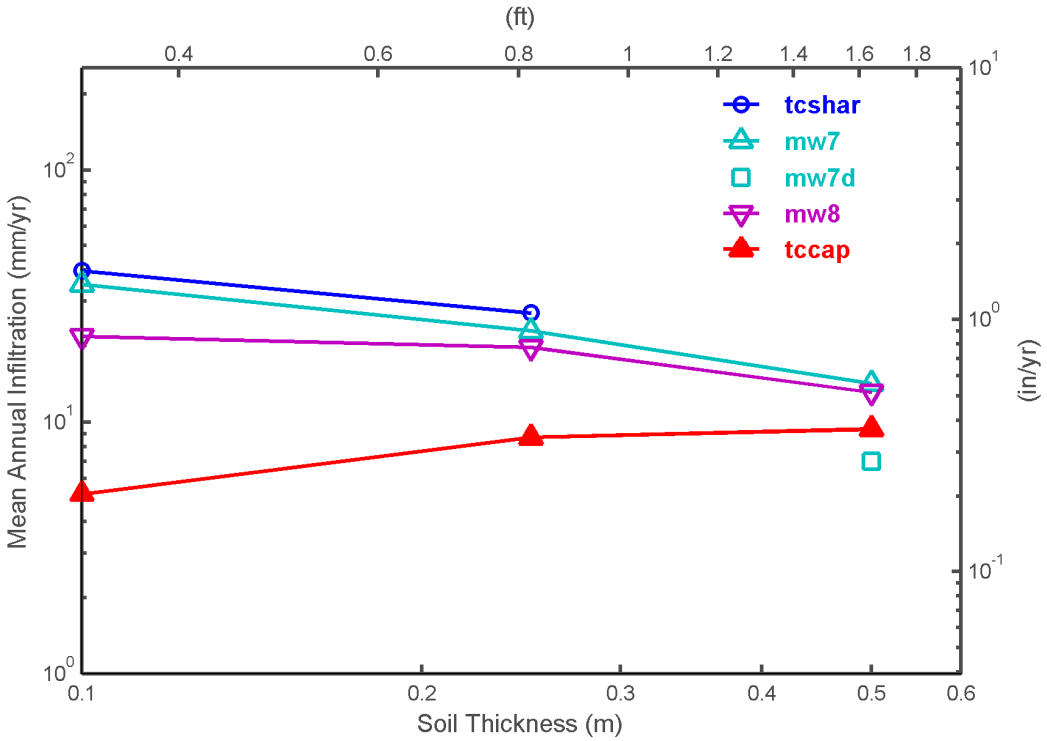

Figure 3-7. Mean Annual Infiltration in Reference Bare-Soil Simulations With Soil Overlying Unfractured Tuff Bedrock, Varying the Tuff Hydraulic Properties. Note That Using Daily Meteorological Inputs (mw7d) Can Result in Systematically Lower Mean Annual Infiltration Estimates Relative to Hourly Inputs (mw7).

Stothoff (1997) found that bare-soil MAI was negligible when the permeability of semi-infinite alluvium was less than 10^{-10} cm^2 [1.6×10^{-11} in^2]. If true of tuffs as well, only the semi-infinite tcshar tuffs might be permeable enough to exhibit significant bare-soil MAI. The densely welded tuffs (not shown) indeed exhibited little to no infiltration {<10^{-3} mm/yr [<4×10^{-5} in/yr] for tcul and <1 mm/yr [<0.04 in/yr] for tslnl} even with soil cover, but the more permeable tuffs exhibited significant infiltration. The caprock tuff is the only tuff with significant infiltration that has extensive exposure at Yucca Mountain.

It is interesting that bare-soil MAI increases with increasing soil depth for very shallow soils over the less permeable bedrock tuffs, in contrast to the case when unfilled fractures are considered. Significant MAI apparently requires extended contact time for moisture to enter the bedrock in these lower permeability tuffs; without soil cover, precipitation simply runs off. Non- to moderately welded tuffs (with K_{sat} greater than the asymptotic deep-soil infiltration rate) would presumably reach the asymptotic deep-soil rate shown in Figure 3-3 as soil depth increases, whereas densely welded tuffs with K_{sat} lower than the asymptotic rate would presumably reach a deep-soil rate of approximately their K_{sat} value.

An additional simulation, labeled mw7d, is also shown in Figure 3-7. The mw7d simulation is identical to the corresponding mw7 simulation, except that the hourly meteorologic readings are used for case mw7 and daily meteorologic readings are used for case mw7d. Averaging meteorologic readings to a day or longer reduces MAI, with additional simulations (not shown)

suggesting that this effect is larger for low-MAI situations. Most of this effect arises from underestimating the depth of wetting-pulse penetration during and immediately after precipitation (thus over predicting evaporation during this period), because daily-averaged flux rates are smaller than hourly rates. Further, atmospheric relative humidity tends to be higher on days with precipitation, lowering potential evaporation and allowing deeper penetration of wetting fronts. Based on several simulations with different averaging strategies, the averaging effect is largely removed by using hourly meteorologic values in the days before, during, and after precipitation. Simulations varying the duration of the averaging period outside of this precipitation window, up to 1 month, showed little influence on MAI.

4 SHALLOW-INFILTRATION ABSTRACTIONS

A response function is a mathematical formula relating mean annual infiltration (MAI)[1] to relevant input parameter values. The response functions developed in Section 4 are based on the detailed simulations discussed in Section 3. For a deep system, two major regions of response are identified depending on whether the soil permeability is above or below a critical value related to the typical storm intensity. For a two-layer system, the response also depends on whether the underlying system forms a capillary barrier.

Three types of response function abstractions for bare-soil MAI are presented. The first type is for semi-infinite soil {i.e., greater than approximately 10 m [33 ft] in depth with underlying bedrock or bedrock fractures having sufficient permeability to accommodate the soil-derived fluxes}. If the permeability is too small, MAI is approximately zero. The second type is for shallow soil above a medium providing a neutral to strong capillary barrier (e.g., soil-filled and unfilled fractures). The third type is for shallow soil above a permeable medium providing a neutral to strong capillary attractor (e.g., soil- or carbonate-filled fractures and non- to moderately welded tuffs). The second and third abstractions are almost identical in form, only differing by the representation of the dependence of MAI on soil thickness.

The three response function abstractions differ primarily in their treatment of soil thickness and the hydraulic properties of the underlying medium. The first abstraction does not consider soil thickness or the underlying medium. The second abstraction is strongly affected by soil thickness, but the properties of the underlying medium have little effect on estimated MAI. The third abstraction is moderately affected by soil thickness, and the properties of the underlying medium have a significant effect on estimated MAI. The first and second abstractions monotonically respond to changing inputs, while the third abstraction may feature a critical soil thickness that provides maximal MAI.

The third abstraction was developed using perturbation to only the inputs having large influences on MAI, so that coefficients associated with other parameters cannot be determined. Undetermined coefficients are estimated by scaling the equivalent coefficients from the other abstractions.

Coefficients in the abstractions were determined using a Microsoft® Excel® 97 SR-1 spreadsheet containing all simulation results. The Excel solver uses a generalized reduced gradient nonlinear optimization algorithm, minimizing an objective function of the form

$$\frac{1}{N^{1/2}}\left[\sum_{i}^{N}(Y_{si}-Y_{ai})^2\right]^{1/2} \tag{4-1}$$

where Y_{si} and Y_{ai} are the $\log_{10}$ simulation and abstraction predictions, respectively, for N simulations. The solver used a precision of 10^{-6}, tolerance of 10^{-3}, and convergence criterion of 10^{-4} and was generally restarted once to reduce the objective function further. Several sets of initial values were considered, with the results from the set with the smallest objective function reported here.

---

[1] Mean annual infiltration is used frequently throughout this chapter; consequently, the abbreviation MAI will be used.

4.1 Response Functions

The wide variation in MAI is most appropriately described in log space. Four general types of functions are used to describe the response of $\log_{10}$(MAI) to any particular input: (i) power-law function, P(x); (ii) logarithmic, L(x); (iii) limited logarithmic, $L_1(x)$; and (iv) V-shaped logarithmic, $L_2(x)$. Inputs that cause logarithmic change in $\log_{10}$(MAI) for one parameter range but little change for another range are described using the limited logarithmic function. Inputs that cause logarithmic change in $\log_{10}$(MAI) for two parameter ranges, but with different slopes, are described using the V-shaped logarithmic function. The V-shaped function is only used to describe the depth dependence when capillary-attractor lower layers are used.

The four shape functions are defined by

$$\mathrm{P}(x) = \left(\frac{x}{x_0}\right)^a - 1 \tag{4-2}$$

$$\mathrm{L}(x) = \log_{10}\left(\frac{x}{x_0}\right) \tag{4-3}$$

$$\mathrm{L}_1(x) = \log_{10}\left[1 + \left(\frac{x}{x_0}\right)^a\right] \tag{4-4}$$

$$\mathrm{L}_2(x) = \log_{10}\left[1 + \left(\frac{x}{x_0}\right)^a + \left(\frac{x}{x_0}\right)^b\right] \tag{4-5}$$

where x is the variable of interest, x_0 is a normalizing value for the variable of interest, and a and b are constants with opposite sign.

After rearranging and simplifying, the relationship describing the response of bare-soil MAI to input parameters can be described generically as

$$H = \log_{10}\left(\frac{\mathrm{MAI}}{\mathrm{MAP}}\right) = A_1(S,F,W) + A_2(S,F,W)H \tag{4-6}$$

where mean annual precipitation is MAP,[2] S, F, and W represent shape functions for soil (top layer), fracture (bottom layer), and weather inputs, respectively; and A_1 and A_2 represent combinations of these shape functions. The relationship can be rearranged as follows

[2] Mean annual precipitation is used frequently throughout this chapter; consequently, the abbreviation MAP will be used.

$$H = \frac{A_1}{1 - A_2} \tag{4-7}$$

As a practical matter, certain combinations of inputs yield A_1 and A_2 such that H is incorrectly greater than 0 (i.e., MAI > MAP). In such cases, if $A_2 < 1$ (generally for very wet and cool conditions), then H is set to 0; otherwise, H is set to a minimum cutoff value.

4.2 Deep Alluvium

The response of bare-soil MAI in deep alluvium is abstracted into two simple formulae accounting for soil properties and meteorological inputs for two permeability ranges. The generally used formula provides a serviceable representation for bare-soil MAI in deep alluvial materials coarser than a loam or sandy loam texture. The other formula, applied when permeability is smaller than a threshold value, simply states that fine-textured media (e.g., the fine extreme of soils and bare unfractured bedrock) have essentially zero MAI.

Stothoff (1997) demonstrated that there are two distinct behaviors for MAI in deep alluvium, depending on the value for permeability. In low-permeability media {intrinsic permeability k is $<10^{-10}$ cm^2 [1.6×10^{-11} in^2]}, MAI is essentially zero. In the low-permeability range, significant numbers of wetting events have rainfall rates too large for the ground to accept, runoff often occurs, and evaporation is able to reclaim the small amount of MAP that enters the ground. In high-permeability media {$k > 10^{-8}$ cm^2 [1.6×10^{-9} in^2]}, there is a trend toward decreasing MAI with increasing permeability (holding other hydraulic properties constant). All precipitation is accepted into the ground; however, evaporation becomes more effective with increasing permeability, leaving less moisture for net infiltration.

The intrinsic permeability range of 10^{-8} through 10^{-10} cm^2 [1.6×10^{-9} to 1.6×10^{-11} in^2] is transitional from the behavior of high- to low-permeability media, and MAI appears to be strongly medium dependent. The permeability yielding greatest MAI is in the transition zone between the two limiting permeability behavior zones; most events are accepted by the medium, but some of the largest storms generate runoff. There is an extremely rapid drop off in MAI as permeability decreases from the largest-MAI permeability; simulated MAI may change several orders of magnitude with a change of less than one order of magnitude in permeability. No attempt is made to characterize the response of MAI in this zone. Section 6.1 suggests that deep-soil permeability at Yucca Mountain generally lies in the high-permeability range (Figure 6-3).

Characterizing the response of MAI to parameters of a low-permeability medium is quite straightforward. At the Yucca Mountain site, any imbibing water is removed by evaporation, so that MAI is zero when soil or bare-bedrock permeability is below a cutoff permeability {approximately 10^{-9} to 10^{-10} cm^2 [1.6×10^{-10} to 1.6×10^{-11} in^2]}. The formula for low-permeability media is simply

$$\text{MAI} \approx 0 \tag{4-8}$$

for permeability less than 10^{-10} cm^2 [1.6×10^{-11} in^2]. Based on this formula extrapolated from semi-infinite soil column simulations, no exposed unfractured bedrock at Yucca Mountain would be expected to have significant MAI.

High-permeability media provide quantifiable trends in the behavior of MAI, and this behavior is abstracted as

$$\mathrm{H} = \log_{10}\left(\frac{\mathrm{MAI}}{\mathrm{MAP}}\right) = \alpha_0 + \mathrm{S}(1+\alpha_s \mathrm{H}) + \mathrm{W}(1+\alpha_w \mathrm{H}) \tag{4-9}$$

where the α parameters account for the increased sensitivity for smaller values of MAI. The relationship can be rearranged as follows

$$A_1 = \alpha_0 + S + W \tag{4-10}$$

$$A_2 = \alpha_s S + \alpha_w W \tag{4-11}$$

$$S = s_1 \mathrm{L}(k) + s_2 \mathrm{P}(m) + s_3 \mathrm{P}(P_o) + s_4 \mathrm{P}(\varepsilon) \tag{4-12}$$

$$W = w_1 \mathrm{L}(\mathrm{MAP}) + w_2 \mathrm{P}(\mathrm{MAT}) + w_3 \mathrm{P}(\mathrm{MAV}) + w_4 \mathrm{L}(\mathrm{MAW}) + w_5 \mathrm{L}(\mathrm{MAR}) \tag{4-13}$$

where k is intrinsic permeability, m is van Genuchten m = 1 - 1/n (n is van Genuchten n), P_o is the reciprocal of van Genuchten α in pressure units, ε is porosity, mean annual temperature is MAT[3], mean annual vapor density is MAV[4], and mean annual wind speed is MAW.[5] The remaining values are constants determined through least-squares minimization. Incoming radiation is calculated by summing longwave and net shortwave radiation (albedo is assumed to be 0.33).

The results from a total of 65 simulations of deep alluvium, all with permeability at least 10^{-8} cm^2, were used to determine the 12 fitting constants. All exponents were derived by inspecting scatter plots of actual and abstracted simulation results, varying the exponent used for the abstracted results until the points were well aligned. The coefficients in the abstraction are presented in Table 4-1.

The only counterintuitive behavior in the abstraction is for permeability, with decreasing MAI for increasing permeability. As discussed before, permeability is correlated to both van Genuchten m and P_o in such a way that MAI generally is larger for more permeable soils. Otherwise, MAI increases as precipitation increases and decreases as evaporation is enhanced.

---

[3] Mean annual temperature is used frequently throughout this chapter; consequently, the abbreviation MAT will be used.

[4] Mean annual vapor density is used frequently throughout this chapter; consequently, the abbreviation MAV will be used.

[5] Mean annual wind speed is used frequently throughout this chapter; consequently, the abbreviation MAW will be used.

Table 4-1. Coefficients for Response of Deep-Alluvium Bare-Soil Mean Annual Infiltration to Hydraulic and Meteorological Inputs. The Objective Function Is 0.0162 Using 65 Values. Exponents Are All Estimated Visually.				
Parameter	**Function**	**Reference Value**	**Coefficient**	**Exponent***
α_0			–1.3509	
α_s			0.0370	
α_w			–1.3000	
Soil Properties				
k	L†	10^{-8} cm^2	–0.5835	
m	P‡	0.2	0.6730	2
P_o	P	2 kPa	1.6127	–0.5
ε	P	0.3	–1.0126	1
Meteorological Inputs				
MAP (mean annual precipitation)	L	162.8 mm/yr	0.8389	
MAT (mean annual temperature)	P	290.31 K	–4.9504	1
MAV (mean annual vapor density)	P	4.842×10^{-6} g/cm^3	0.1122	2
MAR (mean annual radiation)	L	483.3 W/m^2	–0.4570	
MAW (mean annual wind speed)	L	4.18 m/s	–0.1261	
*Estimated by inspection †L = function defined by Eq. (4-3) ‡P = function defined by Eq. (4-4)				

4.3 Soil/Capillary-Barrier System

The soil/capillary-barrier system has a neutral to strong capillary barrier at the soil/fracture interface. The underlying medium is typically an unfilled fracture continuum, which requires saturation at the interface to initiate fracture flow. A soil-filled fracture represents a neutral endpoint for the abstraction. The abstraction is determined for bare-soil MAI when soil thicknesses are less than 50 cm [20 in], although as a practical matter the abstraction can be used up to at least 5 m [16 ft] with the understanding that any MAI value below some cutoff {e.g., 0.01 mm/yr [4×10^{-4} in/yr]} is essentially zero. Responses for soil thicknesses greater than 5 m [16 ft] begin to transition to the semi-infinite soil responses. As with the deep system, normalized MAI is used in the abstraction. Normalized MAI is dominated by soil moisture holding capacity above the soil/bedrock interface. There is a tendency for increasing sensitivity as MAI decreases. The relationship describing the response of bare-soil MAI to the input parameters is

$$H = log_{10}\left(\frac{MAI}{MAP}\right) = \alpha_0 + F(1+\alpha_f H) + S(1+\alpha_{s2} H) + W(1+\alpha_{w2} H) + \left[\alpha_1 + S(1+\alpha_s H) + W(1+\alpha_w H)\right] L_1(B_b) \quad (4\text{-}14)$$

The relationship can be rearranged as follows

$$A_1 = \alpha_0 + F + S + W + (\alpha_1 + S + W)\mathrm{L}_1(B_b) \tag{4-15}$$

$$A_2 = \alpha_f F + \alpha_{s2} S + \alpha_{w2} W + (\alpha_s S + \alpha_w W)\mathrm{L}_1(B_b) \tag{4-16}$$

$$\mathrm{S} = \mathrm{s}_1 \mathrm{L}_1(\mathrm{k}_\mathrm{s}) + \mathrm{s}_2 \left(\frac{\mathrm{m}_\mathrm{s} - \mathrm{m}_{\mathrm{s}0}}{\mathrm{m}_{\mathrm{s}0}} \right)^2 + \mathrm{s}_3 \mathrm{L}(\mathrm{P}_{\mathrm{os}}) \tag{4-17}$$

$$F = f_1 \mathrm{L}_1(k_f) + f_2 \mathrm{P}(m_f) + f_3 \mathrm{L}(P_{of}) + f_4 \mathrm{L}_1(\varepsilon_f) \tag{4-18}$$

$$W = w_1 \mathrm{L}(\mathrm{MAP}) + w_2 \mathrm{P}(\mathrm{MAT}) + w_3 \mathrm{P}(\mathrm{MAV}) + w_4 \mathrm{L}(\mathrm{MAW}) + w_5 \mathrm{L}(\mathrm{MAR}) \tag{4-19}$$

$$B_b = \varepsilon_s b \tag{4-20}$$

where *s* and *f* subscripts represent soil and fracture, respectively, and B_b is the soil moisture holding capacity (pore space times soil thickness). The *b* subscript on B_b stands for a capillary barrier.

The constants in the response function determined by nonlinear least-square minimization are presented in Table 4-2. The mean of the squared deviates was 0.0145, using the results from 207 simulations that include simulations with unfilled and soil-filled fractures. Soil depths considered ranged from 2 through 50 cm [0.8 through 20 in]. Additional simulations with MAI less than 0.02 mm/yr [8×10^{-4} in/yr] were considered inaccurate for estimation in log space and discarded.

Figure 4-1 illustrates representative matches between simulation results and abstraction predictions. Responses to different soil and fracture hydraulic properties are shown in Figure 4-1(a,b), while responses to different meteorological inputs are shown in Figure 4-1(c). The response of MAI to the input parameters is captured adequately, with matches at worst within roughly a factor of two. The abstraction tends to have a flatter decrease in MAI with increasing soil thickness than do the simulation results. The reliability of the simulation predictions decreases as the soil thickness increases, due to the dependence of MAI on the few wetting pulses large enough to initiate fracture flow. An improved fit to the unfilled-fracture results shown in Figure 4-1 can be achieved if the soil-filled-fracture simulations are not used; however, the range of parameters for which a robust abstraction is obtained is severely limited.

The response of MAI to the soil van Genuchten *m* parameter differs from the deep-soil case, in the sense that changing the parameter from the basecase results in larger values of MAI regardless of whether the parameter is increased or decreased. The effect may be artificial. The functional representation capturing this effect has little effect on predictions if *m* is in the range considered in simulations (0.1 to 0.3), but has a large effect outside the range.

Table 4-2. Coefficients for Response of Bare-Soil Mean Annual Infiltration to Hydraulic and Meteorologic Inputs for Soil Over an Unfilled or Soil-Filled Fracture Continuum. The Objective Function Is 0.0145 Using 207 Values.

Parameter	Function	Reference Value	Coefficient	Exponent
α_0	—	—	0.0611	—
α_1	—	—	–0.0415	—
α_s	—	—	–0.4049	—
α_f	—	—	–4.5757	—
α_w	—	—	–0.1769	—
α_{s2}	—	—	2.5714	—
α_{w2}	—	—	–2.2809	—
B_b	L_1*	1.0053 cm	—	3.9509
Soil Properties				
k_s	L_1	4.951×10^{-11} cm^2	–0.894	0.0705
m_s	$[(m_s - m_{s0})/m_{s0}]^2$	0.203	1.1438†	2‡
P_{os}	L§	2 kPa‡	–0.9476	—
Fracture Properties				
k_f	L_1	2.718×10^{-9} cm^2	4.337	–2.2429
m_f	P‖	0.4‡	0.1437	–0.2143
P_{of}	L	1 kPa‡	0.0096	—
ε_f	L_1	0.1884	–0.4054	–0.0205
Meteorological Inputs				
MAP (mean annual precipitation)	L	162.8 mm/yr‡	0.3367	—
MAT (mean annual temperature)	P	290.31 K‡	–2.9743	1‡
MAV (mean annual vapor density)	P	4.84×10^{-6} g/cm^3‡	0.0608	2‡
MAR (mean annual radiation)	L	483.3 W/m^2‡	–0.0609	—
MAW (mean annual wind speed)	L	4.18 m/s‡	–0.1581	—

*L_1 = function defined by Eq. (4-4)
†Use 0 for m outside the range 0.1 through 0.3
‡Estimated by inspection
§L = function defined by Eq. (4-3)
‖P = function defined by Eq. (4-4)

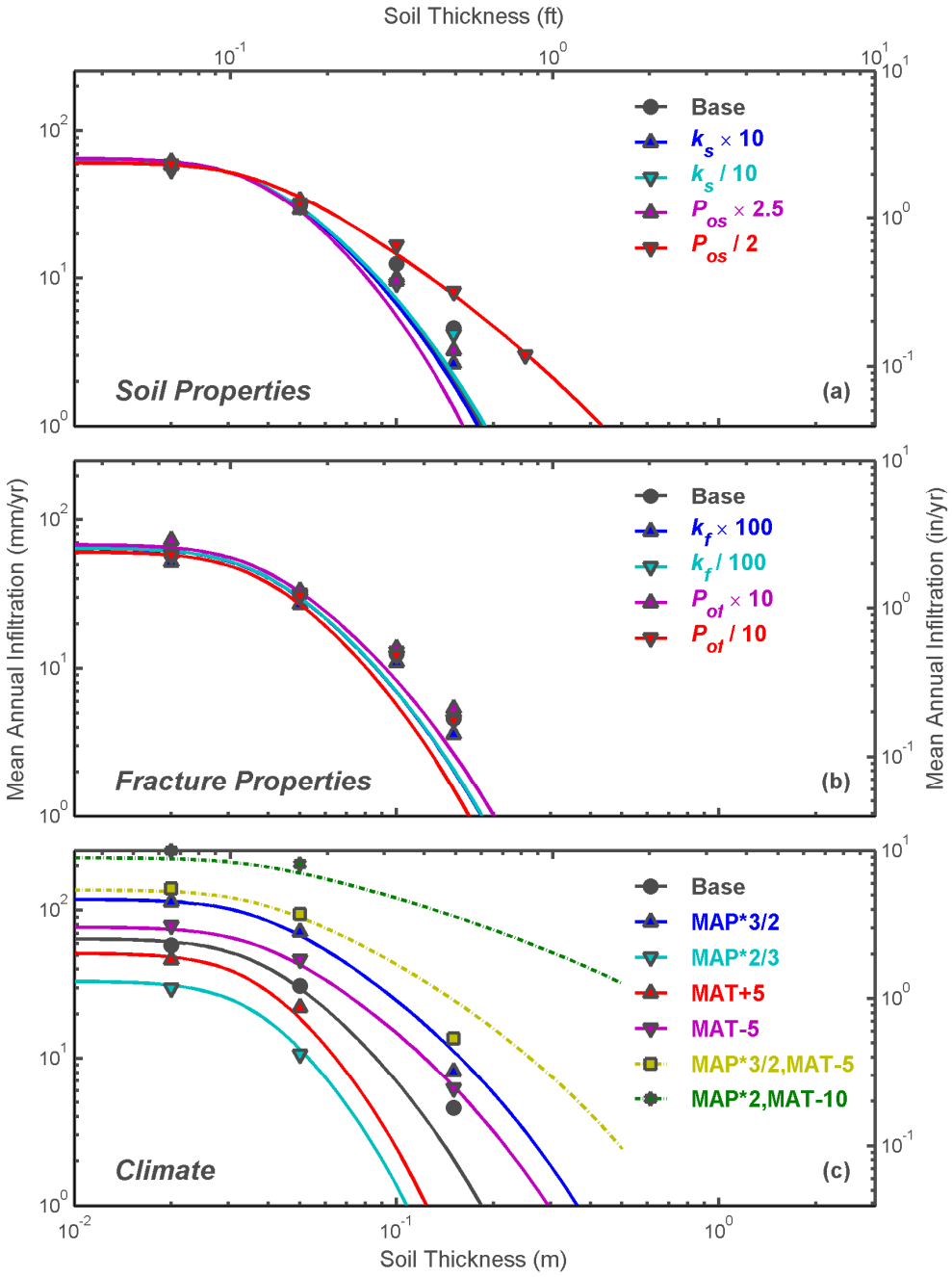

Figure 4-1. Abstraction for Mean Annual Infiltration Compared to Reference Bare-Soil Simulations for Soil Overlying Unfilled Fractures. (a) Soil Hydraulic Properties, (b) Fracture Hydraulic Properties, and (c) Climate Are Varied. Lines Represent the Abstraction and Symbols Represent Simulation Results.

The van Genuchten *m* parameter for the overlying soil is not used in the Infiltration Tabulator for Yucca Mountain (ITYM)[6] simulator, because MAI is quite insensitive to *m* in the range of 0.1 to 0.3 and may have spurious behavior outside this range. The parameter is part of the input data set in case future work refines the abstraction.

4.4 Soil/Capillary-Attractor System

The soil/capillary-attractor system features a neutral to strong capillary attraction at the soil/fracture interface, in direct contrast to the soil/capillary-barrier system. In the case of capillary attraction, water is preferentially drawn into the fractures and retained against evaporation. Even though the permeability of unfilled fractures may be far larger than for filled fractures, the filled-fracture properties are more conducive to retaining imbibed water.

The two shallow-soil abstractions are identical in form except for the relationship between MAI and soil moisture holding capacity. In the capillary-barrier system, B_b is only a function of soil moisture holding capacity, and $\log_{10}$(MAI) monotonically changes with B_b. In the capillary-attractor system, however, the underlying medium may have sufficiently small permeability that a small amount of soil cover is required to promote infiltration. In this lower permeability system, B_a (the subscript stands for attractor) is a function of soil moisture holding capacity, MAP, MAT, and the underlying permeability. There is also a tendency for increased sensitivity to inputs as MAI decreases. Offsets in the mean annual cloud cover (MACC)[7] are assumed to be very weakly correlated to MAV offsets and essentially uncorrelated with other parameters.

The abstracted relationship describing the response of bare-soil MAI to the input parameters is

$$H = log_{10}\left(\frac{MAI}{MAP}\right) = \alpha_0 + F(1+\alpha_f H) + (\alpha_{s2} S + \alpha_{w2} W)H + [\alpha_1 + S(1+\alpha_s H) + W(1+\alpha_w H)]L_2(B_a) \quad (4\text{-}21)$$

The functional form of the shape function containing B_a allows increasing MAI with increasing soil thickness for shallow soils over low-permeability media. For a capillary attractor, B_a is defined by

$$B_a = \varepsilon_s b\left(\frac{k_f}{k_{fo}}\right)\frac{\exp(\mathrm{MAT/MAT_0})}{(\mathrm{MAP/MAP_0})} \quad (4\text{-}22)$$

where ε_s is soil porosity and *b* is soil thickness. Other evaporation-affecting parameters may also modify B_a, but additional simulations would be required to investigate this hypothesis.

---

[6] Infiltration Tabulator for Yucca Mountain is used frequently throughout this chapter; consequently, the abbreviation ITYM will be used.

[7] Mean annual cloud cover is used frequently through this chapter; consequently, the abbreviation MACC will be used.

Constants with specified values were estimated by inspection. Only the response to MAP and MAT was directly investigated via simulation; the constants for the remaining meteorological inputs were estimated by scaling the corresponding soil/capillary-barrier coefficients by the change in the MAT coefficients. The remaining constants in the response function were determined by nonlinear least-square minimization and are presented in Table 4-3. The objective function defined by Eq. (4-1) was 0.0111, using the results from 142 simulations that include soil over carbonate-filled and soil-filled fractures as well as soil over bedrock (using the soil-filled-fracture simulations for both the capillary-attractor and capillary-barrier regressions). Soil depths considered ranged from 10 through 150 cm [3.9 through 59 in]. Additional simulations with MAI less than 0.02 mm/yr [8×10^{-4} in/yr] were considered inaccurate for estimation in log space and discarded.

Table 4-3. Coefficients for Response of Bare-Soil Mean Annual Infiltration to Hydraulic and Meteorological Inputs for Soil Over a Carbonate or Soil-Filled Fracture Continuum or Unfractured Bedrock. The Objective Function Is 0.0111 Using 142 Values.

Parameter	Function	Reference Value	Coefficient	Exponent
α_0	—	—	14.629	—
α_1	—	—	−46.856	—
α_s	—	—	−70.430	—
α_f	—	—	−2.5189	—
α_w	—	—	−16.223	—
α_{s2}	—	—	28.729	—
α_{w2}	—	—	7.8008	—
B_a	L_2*	7.381 cm	—	0.2449 −0.1668
Soil Properties				
k_s	L_1†	2.151×10^{-9} cm^2	−0.0442	4.7369
m_s	$[(m_s - m_{s0})/m_{s0}]^2$	0.1993	0.2295‡	2§
P_{os}	L‖	2 kPa§	−0.7028	—
Fracture Properties				
k_f	L_1	3.768×10^{-11} cm^2	0.0734	37.422
m_f	P¶	0.4§	−0.1574	−2.8800
P_{of}	L	1 kPa§	0.6056	—
ε_f	L_1	0.0292	0.0184	45.851
Meteorological Inputs				
MAP (Mean annual precipitation)	L	162.8 mm/yr§	3.8634	—
MAT (Mean annual temperature)	P	290.31 K§	−41.348	1§
MAV (Mean annual vapor density)	P	4.84×10^{-6} g/cm^3§	0.7717‡	2§
MAR (Mean annual radiation)	L	483.3 W/m^2§	−0.7729#	—
MAW (Mean annual wind speed)	L	4.18 m/s§	−2.0061#	—

*L_2 = function defined by Eq. (4-3)
†L_1 = function defined by Eq. (4-4)
‡Use 0 for m outside the range 0.1 through 0.3
§Imposed by inspection
‖L = function defined by Eq. (4-3)
¶P = function defined by Eq. (4-4)
#Estimated by scaling the corresponding unfilled-fracture coefficients

Representative matches between simulation results and abstraction predictions are shown in Figure 4-2. Responses to changing soil and fracture hydraulic properties are shown in Figure 4-2 (a,b), while responses to changing meteorological inputs are shown in Figure 4-2(c). The simulated and abstracted estimates shown in Figure 4-2 match considerably better than the capillary-barrier results; the better visual fit is corroborated by the smaller objective function. The better fit may be due to enhanced representativeness, because more wetting pulses will pass the soil/bedrock interface for any given soil thickness in capillary attractor systems than in capillary barrier systems. The lower value of soil saturation necessary to trigger fracture flow in capillary attractors means that smaller, more frequent pulses can reach the necessary threshold.

As with the soil/capillary-barrier abstraction, the van Genuchten *m* parameter for the overlying soil is not used in ITYM, but the parameter is retained in the input data set.

4.5 Plant Uptake

Transpiration from vegetation is an important part of the hydrologic cycle that is not included in bare-soil simulations and abstractions. Evaporation and transpiration are competing processes, and under the present warm and dry climatic conditions, mean annual potential evapotranspiration is so much larger than MAP that bare-soil evaporation alone strongly limits MAI, particularly with shallow soils. As climatic conditions become cooler and wetter, however, potential evapotranspiration decreases relative to MAP and the neglect of transpiration may cause more significant errors.

ITYM is based on detailed simulations using just bare-soil evaporation, even though transpiration is an important part of the hydrologic cycle. Natural plant communities are exquisitely tuned to environmental conditions, adjusting on a minute-by-minute basis to changes in the environment. The detailed simulations did not consider transpiration because (i) the simulations necessarily would become much more complex and difficult to explain in order to accommodate plant dynamics, (ii) available uptake models were not developed to represent shallow fractured bedrock underlying the soil column, and (iii) it would be difficult to translate community-specific plant parameters into ITYM parameters that are valid for a variety of climatic conditions.

Despite the difficulties in considering plant uptake in detailed simulations, it is reasonable to expect that well-adapted plant communities use plant-available water within a relatively narrow efficiency band because water is a limiting resource for plants in arid and semiarid climates (except for areas with a high water table or nearby stream). Competition for the scarce resource results in a community of plant species and plant densities that dynamically varies over time, continually exploiting the soil water efficiently, subject to the constraints offered by the physical environment. Because water is expected to be a limiting resource for plants over the range of climatic conditions considered by ITYM, except perhaps for extremely cool or wet conditions, it is reasonable to expect that competition will maintain efficient exploitation of the soil water resource. This implies in turn that overall plant uptake efficiency would remain consistently large over the climatic conditions considered by ITYM.

With this rationale, ITYM uses a simple heuristic model developed specifically for ITYM to account for the effects of vegetative transpiration. The model interpolates between the two limiting conditions of zero and infinite water storage capacity. In the deep alluvial basins, which

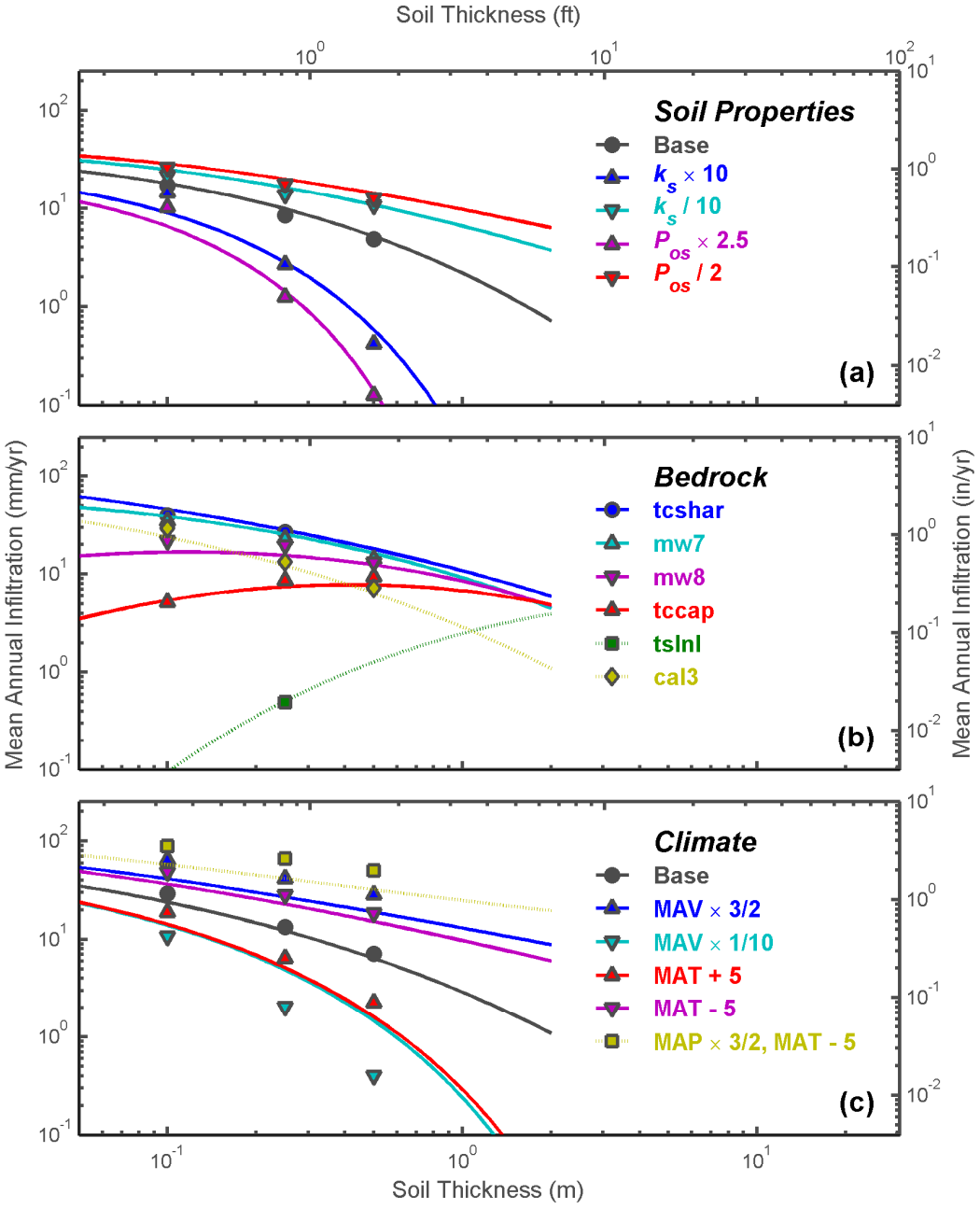

Figure 4-2. Abstraction for Mean Annual Infiltration Compared to Reference Bare-Soil Simulations for Soil Overlying Filled Fractures and Bedrock. Hydraulic Properties Are Varied for (a) Soil (Above Reference Carbonate-Filled Fractures), (b) Bedrock, and (c) Carbonate Fill. Lines Represent the Abstraction and Symbols Represent Simulation Results.

have large water storage capacities, distributed MAI is extremely small, thereby indicating that vegetation is efficient in scavenging water that would otherwise become MAI. Shallow and nonexistent soils provide the least water storage capacity, so that vegetation is relatively sparse and scavenging by plants is least. Scavenging becomes more effective as the soil thickness increases, eventually reaching the deep-soil effectiveness. The deep-soil depth depends on the rooting structure of the plants, which in turn depends on the climatic conditions.

The root-mass distribution of plants tends to decrease roughly exponentially with depth below the ground surface when the roots are not blocked. However, the effect of shallow fractured bedrock on root-mass distributions and uptake patterns is neither well characterized nor understood. Wetting pulses that reach bedrock are largely held within the soil column, providing additional water for plant transpiration. The model for plant scavenging used by ITYM simply assumes that the effect of plant scavenging increases exponentially with soil moisture capacity

$$f_{scav} = E_0 + \left[1 - \exp(-\alpha B)\right](E_1 - E_0) \tag{4-23}$$

where f_{scav} is the fraction of bare-soil MAI scavenged by plants, B is the soil moisture capacity (soil porosity times thickness), α is an uptake decay factor with soil moisture capacity, and E_0 and E_1 are the efficiencies with zero and infinite soil capacity, respectively. The f_{scav} parameter lies between 0 and 1. This model results in a correction factor for calculated MAI

$$\mathrm{MAI} = (1 - f_{scav})\,\mathrm{MAI}_{bare} \tag{4-24}$$

where MAI_{bare} is bare-soil MAI.

The E_1 parameter must be close to 1 to limit MAI in sandy alluvial flats; bare-soil simulations for deep soil suggest that recharge fractions (i.e., MAI/MAP) may be 15 percent or more without plant uptake, whereas field evidence in the Nevada Test Site suggests that recharge fractions are less than 2 percent (Tyler and Jacobson, 1990). Allison, et al. (1985) estimate recharge values of 13 mm/yr [0.51 in/yr] for Australian dunes with introduced pasture and 0.06 mm/yr [0.0024 in/yr] for dunes with native vegetation. Their use of the chloride mass balance technique suggests E_1 would be at least 0.995 for this situation.

The E_0 and α parameters are more uncertain than the E_1 parameter. Plant scavenging is likely to be substantially effective under present-day climate with less than 1 m [3.3 ft] of soil cover, which can store approximately 300–400 mm [12–16 in] of water, approximately 2 years of precipitation. Some scavenging occurs at a reduced efficiency with no soil cover, evidenced by the capability of plants to root into bare bedrock. Because there is little information available to select these parameters, E_0 and α are used as calibration parameters.

In general, E_0, E_1, and α are dependent on the vegetation type and density, which in turn is dependent on the climate. The simplest way to parameterize vegetation type and density is

through bare-soil MAI, which encapsulates all of the factors affecting plant-available moisture. As bare-soil MAI increases, plants become more numerous and larger (hence deeper rooted), implying that E_0 increases, E_1 decreases, and α decreases. In ITYM, all three of the parameters are assumed to be functions of MAI in the form

$$E_0(\mathrm{MAI}) = E_{00} + G_0 \log_{10}(\mathrm{MAI}_{bare}) \tag{4-25}$$

$$E_1(\mathrm{MAI}) = E_{10} + G_1 \log_{10}(\mathrm{MAI}_{\mathrm{bare}}) \quad (4\text{-}26)$$

$$\alpha(\mathrm{MAI}) = \alpha_0 + G_\alpha \log_{10}(\mathrm{MAI}_{\mathrm{bare}}) \quad (4\text{-}27)$$

The six constants are all sampled parameters in ITYM.

4.6 Overland Flow[8]

The abstractions for net infiltration developed in Sections 4.1 through 4.5 neglect the effect of run-on, but the one-dimensional BREATH model incorporates runoff by not allowing surface water to pond. The effect of runoff and run-on is incorporated into the net infiltration abstraction as equivalent extra precipitation provided to the infiltration abstraction.

A watershed model was used to quantify excess infiltration or the infiltration during a storm minus storm precipitation, for each grid element in the watershed model in order to estimate the effect of run-on. Averaging the runoff-producing events during a 9-year period provides a basis for approximating the effect of overland flow as a local effective increase in MAP. The abstraction is completed by characterizing local effective increase in MAP as a function of landscape position and local soil depth.

4.6.1 Watershed Model

Upper Split Wash is a representative eastward trending watershed for Yucca Mountain, coincidentally located above the Enhanced Characterization Repository Block Cross Drift (Figure 4-3). Surficial geology and topography were used to define cascading plane and channel elements (Figure 4-4) for the distributed surface water flow and a two-layer infiltration model called KINEROS2 (Smith, et al., 1995; Woolhiser, et al., 1990). In KINEROS2, surface water routing is based on kinematic flow equations, while infiltration is based on approximations for capillary and gravity-driven unsaturated flow. Woolhiser and Fedors (2000) and Woolhiser, et al. (2006) describe the Upper Split Wash model and hydrological parameter values.

Nine years of tipping-bucket data from stations at Yucca Mountain were used as input for the event-based KINEROS2 model. A KINEROS2 simulation runs from start of rain to cessation of overland flow. Twelve winter events were extracted from the tipping-bucket data, based on the potential for producing net infiltration, runoff, and run-on. No other events were considered large enough to affect net infiltration. MAI could be estimated for each plane and channel in the model using the 12 events. The effect of run-on on net infiltration was approximated by comparing the amount of infiltration with the amount of precipitation falling on any grid element. The term “excess infiltration” was derived for this comparison and is defined as follows. For the j^{th} storm in plane i, the excess infiltration, e_{ij}, is obtained by subtracting the depth of infiltration, f_{ij}, from the rainfall depth, P_{ij}.

[8]Randall Fedors and David Woolhiser, who authored Section 4.6, developed the overland flow module in ITYM.

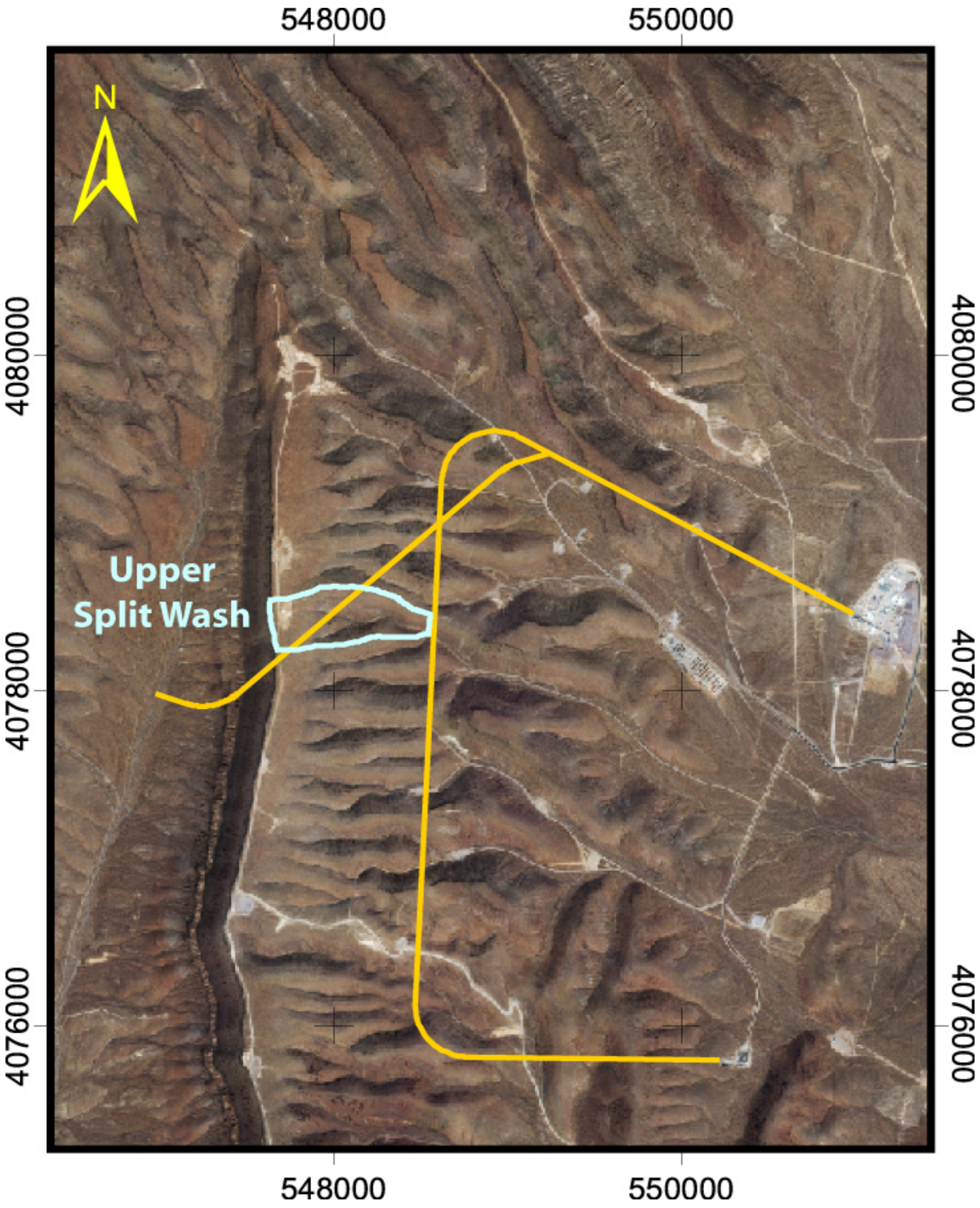

Figure 4-3. Location of Upper Split Wash on Yucca Mountain. Coordinates Are UTM Zone 11, NAD27 (m). [1 m = 3.281 ft]

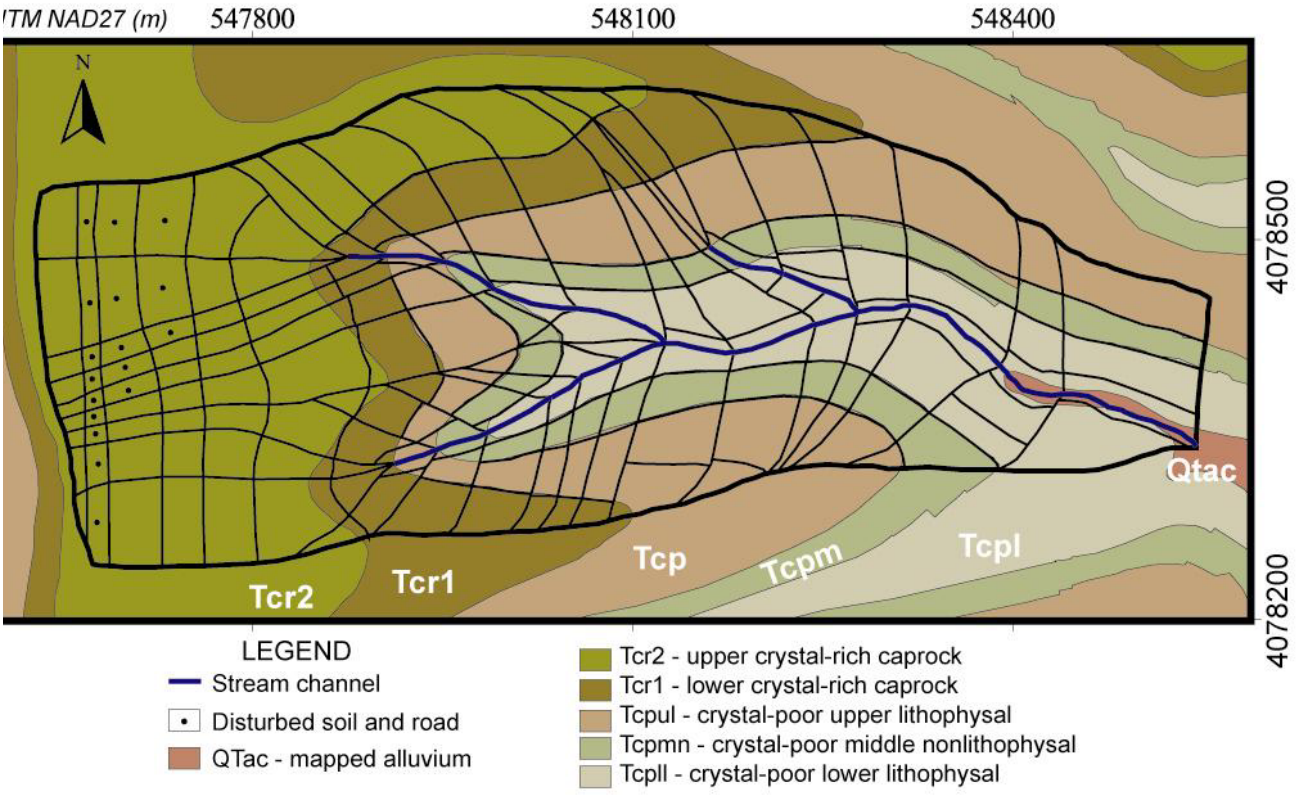

Figure 4-4. Geology and Grid Element Discretization for KINEROS2 Watershed Model [1 m = 3.281 ft]

$$e_{ij} = P_{ij} - f_{ij} \tag{4-28}$$

The total excess infiltration in plane *i* for *m* storms is then

$$E_i = \sum_{j=1}^{m} e_{ij} = \sum_{j=1}^{m} \left(P_{ij} - f_{ij}\right) = \sum_{j=1}^{m} P_{ij} - \sum_{j=1}^{m} f_{ij} \tag{4-29}$$

The average annual excess for plane *i* for *N* years is

$$\overline{E}_i = \frac{E_i}{N} \tag{4-30}$$

Positive values of excess infiltration indicate that run-on increased the amount of infiltration. Negative values of excess infiltration indicate that runoff from a grid element was greater than run-on. Annual average excess infiltration for each plane in the watershed grid is illustrated in Figure 4-5. Woolhiser, et al. (2006) suggest that the magnitude of excess infiltration could be related to geomorphic positions within the watershed. It appeared that the amount of excess

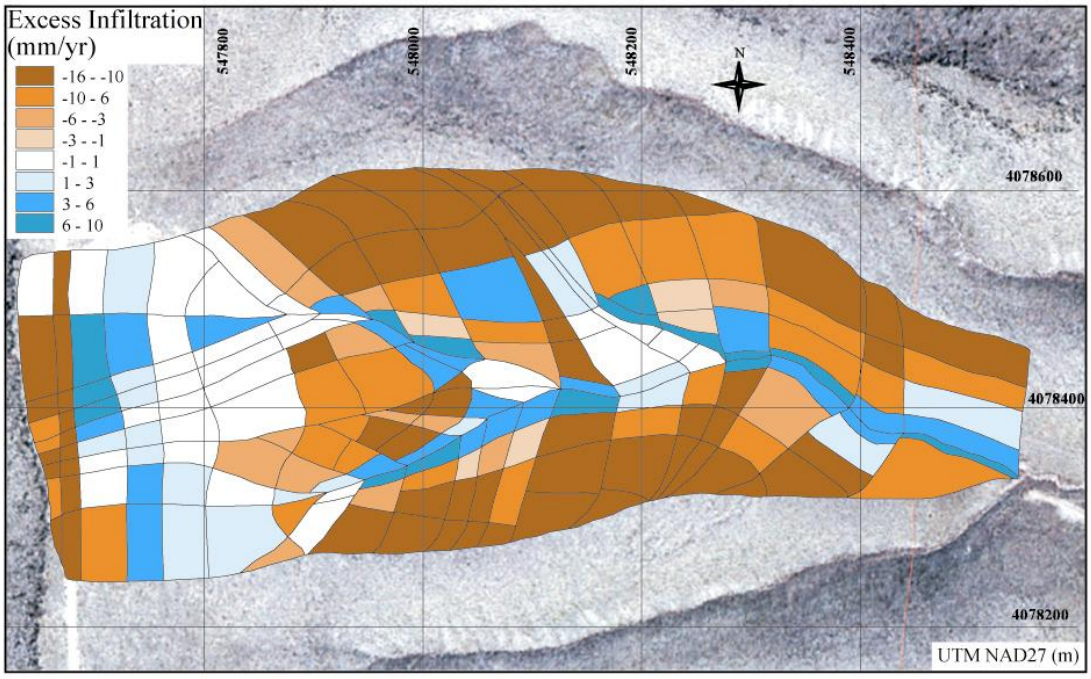

Figure 4-5. Spatial Distribution of Annual Average Excess Infiltration Across the Upper Split Wash Watershed Model [1 m = 3.281 ft; 100 mm = 3.94 in]

infiltration was correlated to topographic slope and soil depths, thus suggesting a method for abstracting the watershed modeling results for ITYM to use.

4.6.2 Run-on Abstraction

An abstracted relationship between excess infiltration, soil depth, and topographic characteristics was derived from Upper Split Wash watershed model results. The first step was to relate excess infiltration to geomorphic positions. Quantitative relations between soil and topographic characteristics were then developed using only the areas of the watershed where the simulator estimates excess infiltration, with other areas of the watershed excluded from the abstraction algorithm. The goal of the analysis was to provide an abstraction that could be used to estimate the amount of run-on entering each 30-m [98-ft] pixel in the grid used by the ITYM module. The ITYM module uses an abstraction based on MAP and MAT to estimate net infiltration. With the run-on abstraction, mean annual net infiltration is based on an effective MAP that includes both actual precipitation for a given climate and run-on. The run-on abstraction is developed for the present-day climate; wetter and cooler climates may cause larger run-on values.

The greatest negative excess infiltration (runoff) occurred in channels on bedrock or plane elements with shallow soils. The greatest infiltration excess was for plane elements with deep soils located downslope from elements with shallow or disturbed soils. Because rainfall intensities were low during this 9-year period, near-zero values occurred for elements with deep soils and no run-on. Using these generalizations, plane elements were classified as ridge, slope, or toe-of-slope according to their position on the hillslope. Areal percentages for Upper

Split Wash are ridge = 29.9 percent, slope = 59.6 percent, toe-of-slope = 9.8 percent, and channel = 0.7 percent. Virtually all of the ridge elements had net runoff, so the TPA abstraction sets run-on to zero for the ridge elements. Approximately 62 percent of the slope elements and 12 percent of the toe-of-slope elements have net runoff. Therefore, the TPA analysis was applied directly to approximately 68 percent of the area of watersheds similar to Upper Split Wash. Most of the run-on for undisturbed areas occurred during the four largest storms, so these storms were used in the regression analyses.

Cumulative distribution functions of average annual excess infiltration were calculated for each hillslope class and for the entire watershed. The amount of infiltration excess for individual storms is strongly dependent on total storm precipitation above a threshold value sufficient to generate saturation-induced runoff. Elements with the greatest infiltration excess shared the following important characteristics:

- Soil depth of the element greater than 40 cm [16 in]
- Upslope plane soil depths less than 40 cm [16 in]
- Elements with larger contributing area tended to have larger infiltration excess

Area and soil depth for each plane element were obtained from Upper Split Wash parameter files, and the following variables were calculated for each plane *i* by summing over the *n* planes upslope of plane *i*

$$A_{ri} = \frac{1}{A_i}\sum_{k=1}^{n} A_k = \frac{A_{ci}}{A_i} \tag{4-31}$$

$$h_{ci} = \frac{\sum_{k=1}^{n} A_k h_k}{\sum_{k=1}^{n} A_k} \tag{4-32}$$

where

A_i — area of plane *i*
A_{ci} — contributing area to plane *i*
A_{ri} — ratio of contributing area to plane area for plane *i*
h_k — soil depth in plane *i*
h_{ci} — area-weighted mean depth of the planes contributing to plane *i*
n — number of elements contributing to plane *i*

Area ratios and mean depths were calculated for 35 plane elements with positive MAI excess. The focused contribution of channels to areal infiltration rates was determined to be small for the Upper Split Wash watershed and thus was ignored in the development of the run-on

abstraction. Using data from the plane elements, multiple regressions resulted in the abstraction

$$E_i = 0.4097 + 0.3A_{ri} - 0.0104\bar{h}_i \quad (4\text{-}33)$$

where E_i is excess precipitation due to run-on. The specified coefficients require that E_i and h_{ci} are defined in units of millimeters. The abstraction is derived from plane elements with soil depths greater than 40 cm [16 in]. The A_{ri} and h_{ci} parameters are estimated by a preprocessor that uses the equivalent steady state water balance model described in Section 7 to determine flow routing. The A_{ri} value for a pixel is simply the volume of overland flow passing into the pixel divided by the volume of precipitation passing into the pixel. The h_{ci} value for a pixel is the flux-weighted average of h_{ci} in the pixels immediately upstream.

Figure 4-6 shows the contribution solely from run-on for the modern climate, illustrating the relative differences between neglecting and including the effect of run-on. The spatial pattern illustrates that the contribution of run-on is focused near the bottoms of hillslopes leading into channels. Excess infiltration from run-on is more than 10 mm/yr [0.39 in/yr] in only a small subset of grid cells, generally channels in deep alluvium. Because MAP is more than 150 mm/yr [5.9 in/yr] with the climatic abstractions described in Section 5, the abstracted effect of run-on on distributed infiltration is like an increase in MAP of less than 7 percent. The abstraction would likely differ somewhat if it considered a longer meteorologic record or additional washes with different hydrologic characteristics, but the uncertainty in estimated distributed MAI arising from uncertainty in run-on appears to be relatively small compared to uncertainty arising from other infiltration-affecting parameters.

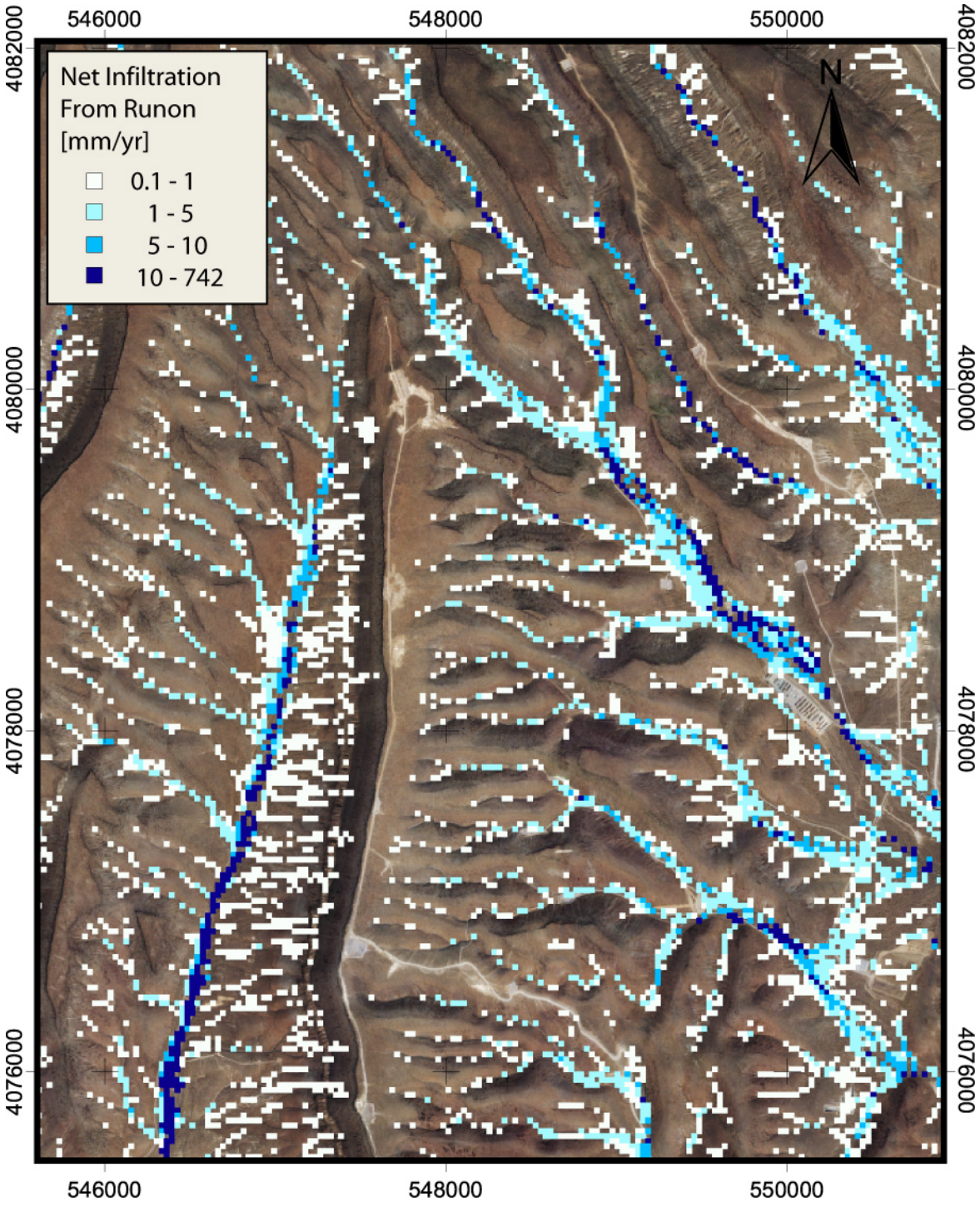

Figure 4-6. Estimates of Run-On for Modern Climate Near the Potential Repository Area. Coordinates Are UTM Zone 11, NAD27 (m). [1 m = 3.281 ft; 100 mm = 3.94 in]

5 SITE-SPECIFIC CLIMATIC PARAMETERS

The abstractions for mean annual infiltration (MAI)[1] described in Section 4 require site-specific climate estimates in each grid cell for each climatic condition considered. Infiltration Tabulator for Yucca Mountain (ITYM)[2] characterizes MAI for specific reference values of mean annual precipitation (MAP)[3] and mean annual temperature (MAT)[4] at a fixed intermediate elevation within the potential-repository footprint. Regional climate is related to local climate using these reference values in downstream analyses [e.g., using the Total-system Performance Assessment (TPA)[5] code or in the analyses by Stothoff and Walter (2007)].

ITYM can consider a single climatic state characterized by MAP, MAT, mean annual wind speed (MAW),[6] mean annual vapor density (MAV),[7] mean annual longwave radiation (MALW),[8] and mean annual shortwave radiation (MASW),[9] with all climatic parameters systematically varying across the domain and all climatic parameters considered uncertain. Or, as used for this report, ITYM can consider a suite of climatic states characterized by combinations of reference MAP and MAT values, using the same uncertain distribution of MAW, MAV, MALW, and MASW for all combinations of MAP and MAT. Present-day values are used in this report to approximate MAW, MAV, MALW, and MASW for each combination of MAP and MAT. Analyses presented in this section suggest that anticipated changes in MAW, MAV, MALW, and MASW under different climatic conditions induce a small change in MAI relative to changes induced by MAP and MAT.

Simple models are used to estimate the spatial distributions of meteorological factors where possible. For example, ITYM distributes MAP (Section 5.1), MAT (Section 5.2), and MAV (Section 5.3) based on elevation. ITYM distributes both MALW and MASW (Section 5.5) according to slope, aspect, and mean annual cloud cover (MACC).[10] Wind speed, however,

---

[1] Mean annual infiltration is used frequently throughout this chapter; consequently, the abbreviation MAI will be used.

[2] Infiltration Tabulator for Yucca Mountain is used frequently throughout this chapter; consequently, the abbreviation ITYM will be used.

[3] Mean annual precipitation is used frequently throughout this chapter; consequently, the abbreviation MAP will be used.

[4] Mean annual temperature is used frequently throughout this chapter; consequently, the abbreviation MAT will be used.

[5] Total-system performance assessment is used frequently throughout this chapter; consequently, the abbreviation TPA will be used.

[6] Mean annual wind speed is used frequently throughout this chapter; consequently, the abbreviation MAW will be used.

[7] Mean annual vapor density is used frequently throughout this chapter; consequently, the abbreviation MAV will be used.

[8] Mean annual longwave radiation is used frequently throughout this chapter; consequently, the abbreviation MALW will be used.

[9] Mean annual shortwave radiation is used frequently throughout this chapter; consequently, the abbreviation MASW will be used.

[10] Mean annual cloud cover is used frequently throughout this chapter; consequently, the abbreviation MACC will be used.

depends in a more complex way on the rugged topography of Yucca Mountain, which has a mosaic of exposed and sheltered locations, thus ITYM estimates MAW with a heuristic model that accounts for topographic effects (Section 5.4). The way that ITYM describes uncertainty in model parameters is discussed in Section 5.6.

5.1 Mean Annual Precipitation

Precipitation at Yucca Mountain is spatially variable, with systematic elevation-dependent trends and local variation. Typical precipitation characteristics can be illustrated using the network of nonrecording gages around Yucca Mountain. Nonrecording gages stored precipitation without recording precipitation rates; these gages were read episodically, allowing estimates of total precipitation over events. The 83 nonrecording gages at Yucca Mountain shown in Figure 5-1 all had a complete record for October 1, 1991, through September 30, 1992 (i.e., water year 1992) (Ambos, et al., 1995). The symbols are color-coded according to location, with the outline color representing relative north-south location (blue in the north grading to red in the south) and the fill color representing relative east-west location (green in the east grading to yellow in the west). The same color codes are used throughout this document to indicate relative position. The stations are also assigned shapes to indicate landscape position, with upward-pointing triangles indicating particularly exposed locations (ridges), downward-pointing triangles indicating especially sheltered locations (washes and channels), and circles indicating intermediate locations (sideslopes and flats).

Figure 5-1 indicates the Exploratory Studies Facility and the Enhanced Characterization of the Repository Block cross drift as red lines, providing spatial references for comparison of figures. Figure 5-1 also indicates for reference the Footprint Box defined by Stothoff and Walter (2007), which circumscribes the potential repository and which was used as the domain boundary for estimates of million-year-average MAI.

Figure 5-2 shows total precipitation for water year 1992 for the network of stations, using the same symbol-coding scheme used for Figure 5-1. There is a systematic trend toward increased precipitation with higher elevations, but gages on ridgetops and on Yucca Crest fall well below the trendline. Spatially variable wind patterns may provide a second systematic effect; higher winds typical of ridgetop and Yucca Crest locations may cause gages to under-record rain events, but it is possible that wind turbulence arising from the pattern of alternating ridges and washes may also systematically divert precipitation from the ridges into the washes.

Some scatter may be due to gage characteristics. Two gages located at USW UZ–N90 differ in measured precipitation for water year 1992 by approximately 8 percent. The difference also may be due to local differences in precipitation.

Some scatter is due to local effects during individual storms. For example, recorded precipitation totals ranged from 7.4 to 16 mm [0.29 to 0.63 in] for the frontal storm of December 28–30, 1992. Note that frontal storms tend to be much wider in extent than the convective storms typical of other times of the year; thus frontal storms provide more spatially uniform precipitation patterns. Interestingly, the gages with precipitation extremes in this storm are separated in elevation by less than 120 m [390 ft].

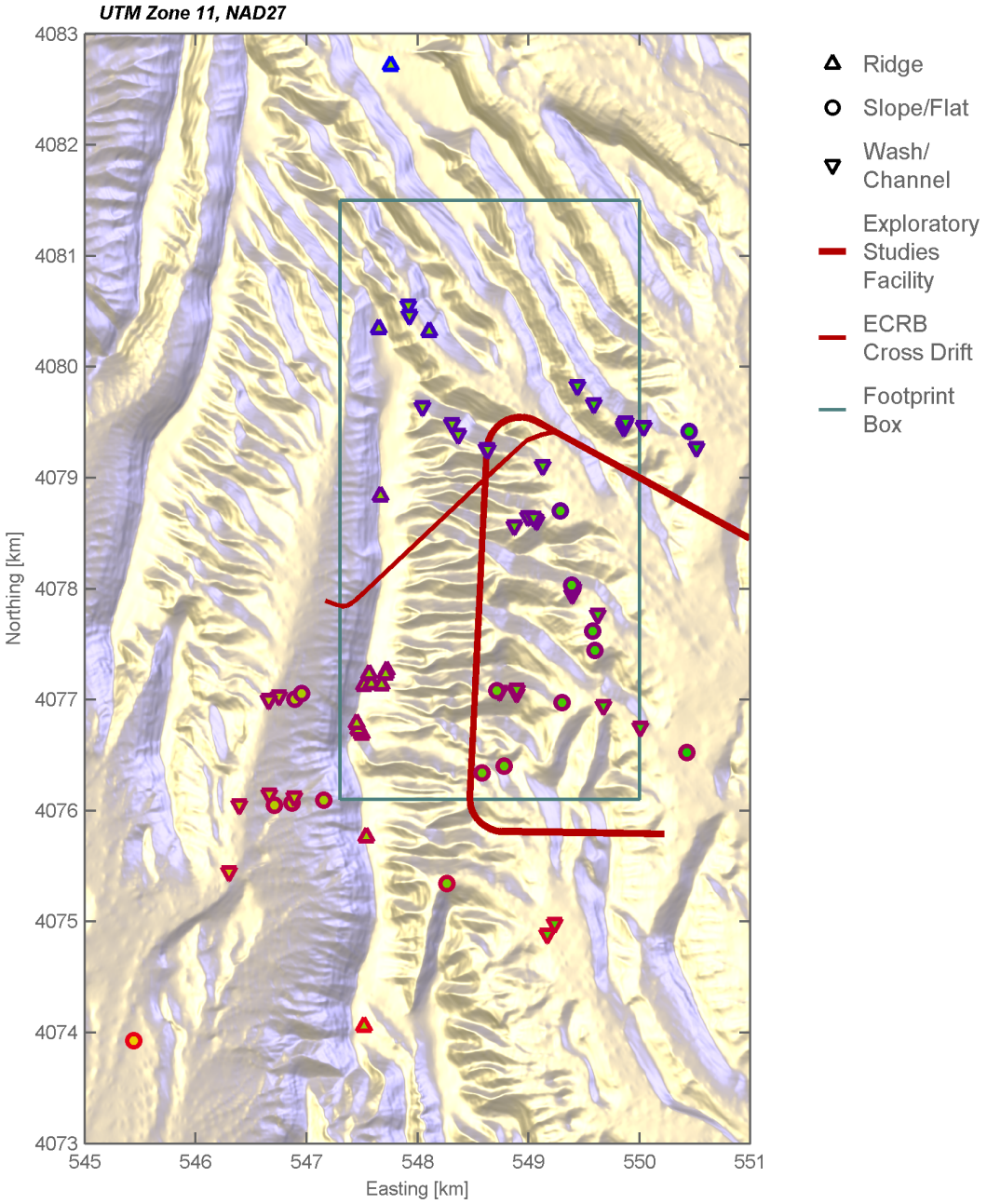

Figure 5-1. Location of Nonrecording Gages in the Yucca Mountain Vicinity Active Throughout Water Year 1992. The Projection Is Universal Transverse Mercator, Zone 11, 1927 North American Datum. Blue Lighting Is From the West-Southwest and Yellow Light Is From the East-Southeast.

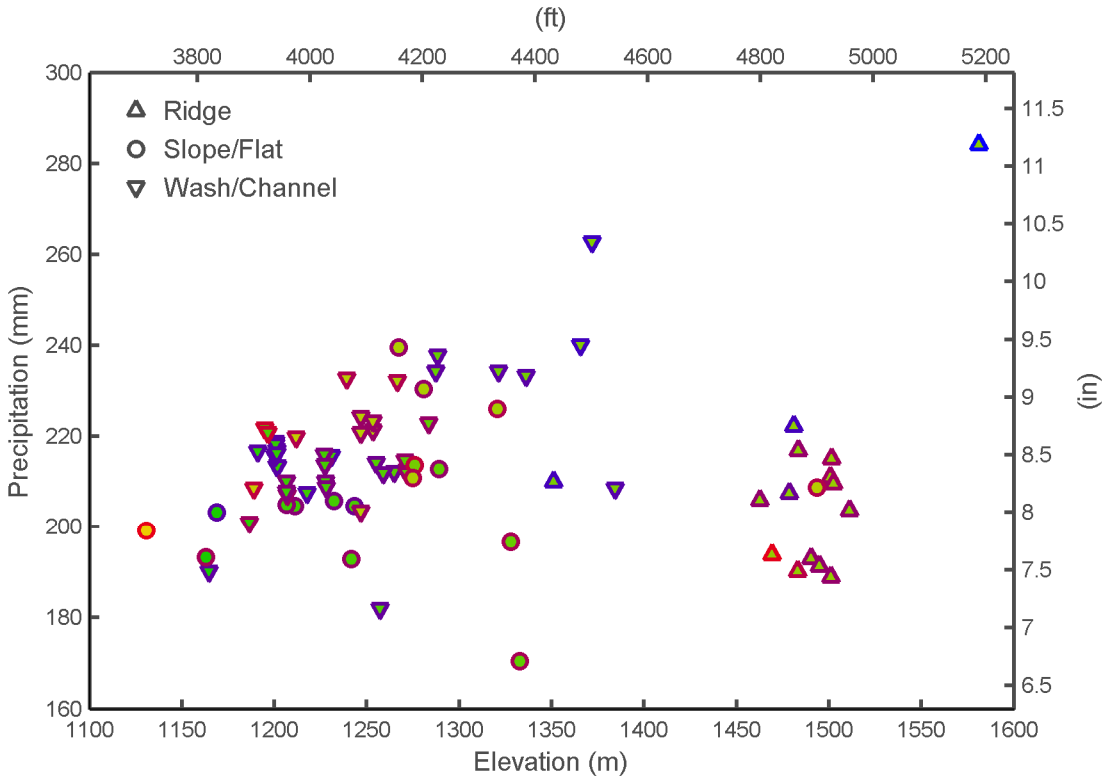

Figure 5-2. Water Year 1992 Precipitation in Nonrecording Gages in the Yucca Mountain Vicinity

Spatial variability may be dominated by local effects for short averaging periods (e.g., individual storms), but systematic trends become dominant for sufficiently long averaging periods. Stothoff and Walter (2007) found that temporal fluctuations in MAP estimated from an 8,000-year bristlecone pine record would increase long-term-average MAI by less than 6 percent, suggesting that temporal variability not captured by the climatic record used to develop the MAI abstractions in ITYM would not strongly affect MAI estimates.

Observations within the immediate Yucca Mountain area have a limited elevation range and duration, with sufficient scatter to make it difficult to estimate systematic variation in MAP. However, observations outside of the immediate Yucca Mountain area provide a basis for evaluating systematic elevation-dependent variation in MAP.

Daily precipitation and temperature-extreme records, from station inception through 1997, were obtained for the network of Cooperative Observer Program (COOP)[11] stations in Arizona, California, Nevada, and Utah. A reduced set of stations was obtained by including only those stations in more or less the same climatic regime as Yucca Mountain under present or

[11] Cooperative Observer Program is used frequently throughout this chapter; consequently, the abbreviation COOP will be used.

postulated potential future conditions, with stations occurring within at least a 2° radius of Yucca Mountain. The Sierra Nevada and San Gabriel ranges make natural boundaries, while the northern and eastern boundaries are more diffuse. The set of stations was further reduced by eliminating stations with record lengths less than a cutoff value. ITYM estimates are based on MAP cutoff values of 20 and 40 years; the corresponding MAT cutoff value is 5 years. The COOP stations used in the MAP and MAT analyses are shown in Figure 5-3.

ITYM estimates expected MAP given a reference MAP at an elevation of 1,400 m [4,600 ft] and systematic elevation-dependent variation in MAP using the relationship

$$\log_{10}(\text{MAP}) - \log_{10}(\text{MAP}_0) = 0.2755(z - z_0) \tag{5-1}$$

where MAP is in mm/yr, *z* is ground elevation in kilometers, and a 0 subscript denotes a reference value. This relationship is derived from all 171 stations with records at least 20 years long, using a 3-term cubic polynomial combination of normalized longitude and normalized incident shortwave radiation to represent spatial variation and subsequently localized to Yucca Mountain values. Shortwave radiation varies almost linearly with latitude in this region. The reference elevation is representative of the potential-repository footprint, intermediate between Yucca Crest {1,480 m [4,860 ft]} and Coyote Wash {1,280 m [4,200 ft]}. The gradient is considered uncertain with a standard deviation of 0.03.

Mean daily precipitation measures how much moisture is available for infiltration. Figure 5-4 shows seasonal variation of mean daily precipitation for the COOP stations. Mean daily precipitation for each Julian day of the year is obtained by averaging the precipitation for the same day in every year observations were made. As precipitation is episodic and infrequent, the statistics are quite noisy; accordingly, a moving average of 60 days is used to smooth the noise (each daily value is replaced by the average of the month before and after the day). It is apparent from Figure 5-4 that, within an area with similar storm tracks, mean daily precipitation increases approximately as a power of increasing elevation, implying that MAP also should increase approximately as a power of elevation.

Several schemes were investigated to predict $\log_{10}$(MAP), primarily involving polynomial interpolations based on elevation, latitude, longitude, and products of these factors. With sufficient high-order terms, more than 70 percent of the variability is explained. However, formulae using high-order polynomials are not transparent to analyze and it is computationally demanding to search the possible combinations. An alternative approach is adopted here that uses elevation, latitude, longitude, and a set of radial basis functions to predict $\log_{10}$(MAP). The basis functions provide local modification to the regional interpolation. The number of candidate basis functions was kept small to keep the number of undetermined coefficients much smaller than the number of observations.

The formula for interpolation using radial functions is written

$$\hat{Y} = a_0 + a_z N_z + a_g N_g + a_t N_t + \sum_i a_i P_i(N_g, N_t) \tag{5-2}$$

$$N_z = z/1000 \tag{5-3}$$

$$N_t = (L_t - 34)/(42 - 34) \tag{5-4}$$

$$N_g = (L_g - 113)/(120 - 113) \tag{5-5}$$

$$P_i = \left[(N_g - N_{gi})^2 + (N_t - N_{ti})^2\right]^{1/2} \tag{5-6}$$

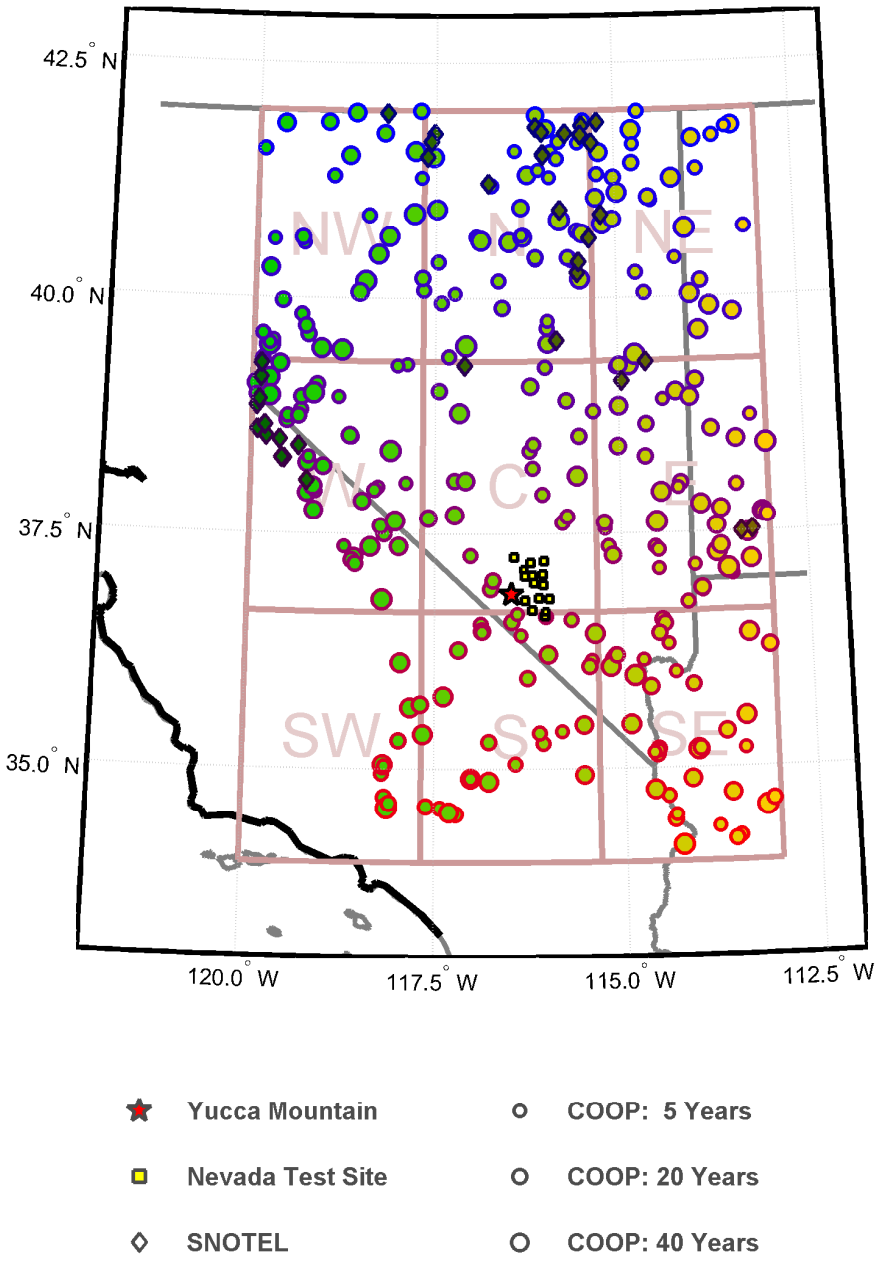

Figure 5-3. Location Map for Cooperative Observer Program Stations (Denoted by COOP) Used in Meteorological Analyses. Yucca Mountain, Nevada, Test Site and Snowpack Telemetry (Denoted by SNOTEL) Stations Are Shown for Reference. The Grid Defines the Nine Regions Used To Illustrate Systematic Patterns.

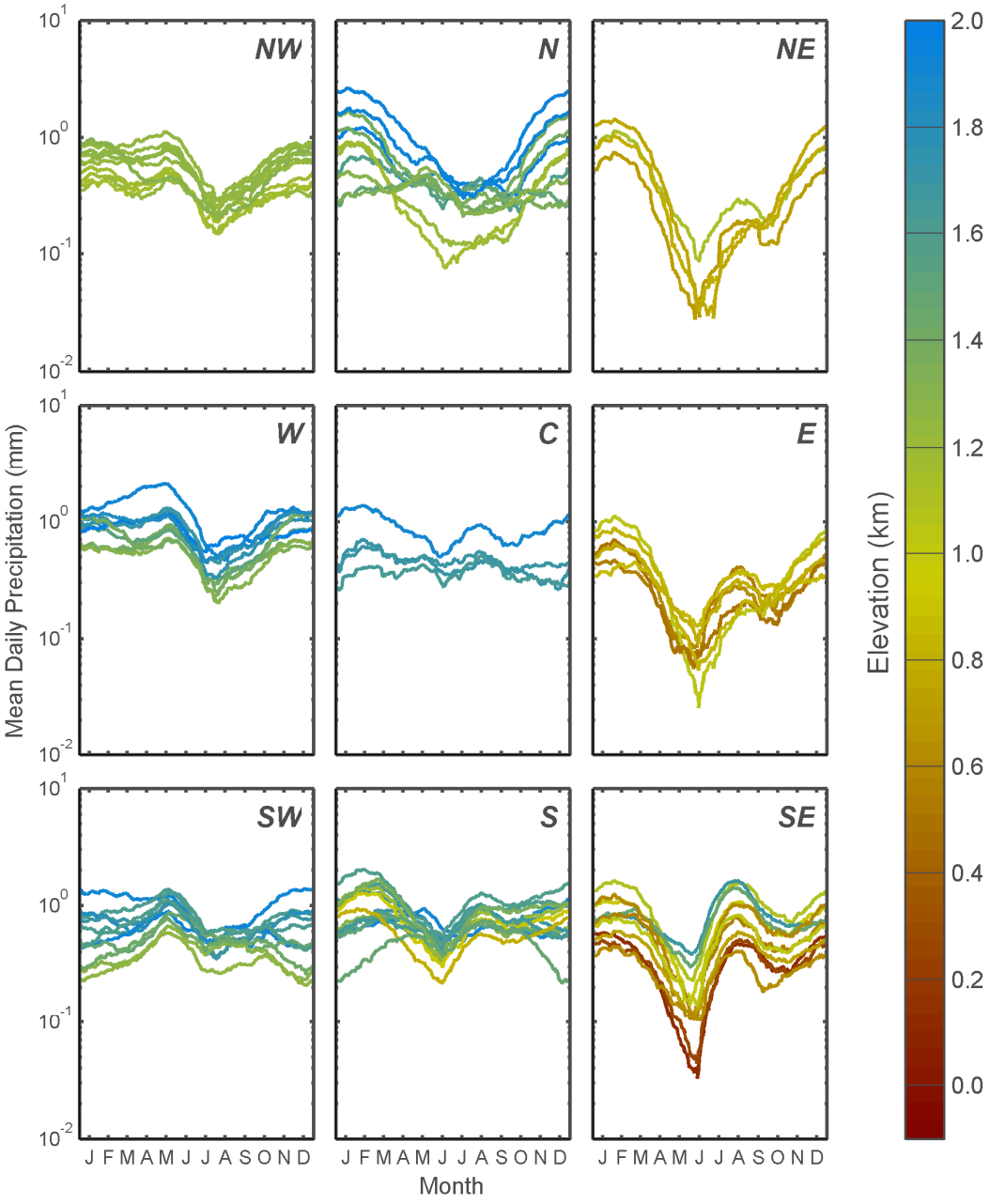

Figure 5-4. Mean Daily Precipitation for Each Cooperative Observer Program Station With a Record of at Least 40 Years Over the Station's Period of Record. Smoothing Used a 60-Day Window. Color Indicates Station Elevation. [100 mm = 3.94 in; 1 km = 3,281 ft]

where $\hat{Y}$ is predicted $\log_{10}$(MAP), L_t is north latitude in decimal degrees, L_g is west longitude in decimal degrees, z is elevation in meters, the i subscripts denote the location of interpolation poles, and the a parameters denote regression constants. Both radial and inverse-radial ($1 / P_i$) basis functions were examined. Radial functions performed slightly better than inverse-radial functions and are defined when a pole is located over a COOP station, so inverse-radial functions are not discussed further.

Two data sets are used in the regression results: all 171 COOP stations with at least a 20-year record length and the 86 of these stations having at least a 40-year record length. For both sets, 4 regressions are presented: (i) elevation only; (ii) elevation, latitude, and longitude; (iii) elevation, latitude, longitude, and 9 poles located at the corners and half points (N_g = 0, 1/2, and 1; N_t = 0, 1/2, and 1); and (iv) elevation, latitude, longitude, and 16 poles located at combinations of corners and 1/3 points (N_g = 0, 1/3, 2/3, and 1, N_t = 0, 1/3, 2/3, and 1).

Figures 5-5 and 5-6 display the results of the regressions. The COOP stations are represented by filled circles, with the size of the circle proportional to record length. The outline color grades from red in the south to blue in the north and the fill color grades from yellow in the west to green in the east; stations near Yucca Mountain are red with yellow-green centers. Regression equations are included in the figures, as are the values of R^2 (fraction of variability explained by the regression).

Additional stations shown in the plots were not used in the regression and provide an independent check. These stations include (i) U.S. Department of Energy (DOE) stations (Western Regional Climate Center, 1985–2004) from the Yucca Mountain area (stars), (ii) Special Operations and Research Division stations (Air Resources Laboratory/Special Operations and Research Division, 1959–2005) on the Nevada Test Site (squares), and (iii) high-altitude snowpack telemetry (SNOTEL)[12] sites (Natural Resources Conservation Service, 1979–2005) (diamonds) within the regression area in Nevada, California, and Utah. The locations of these stations are indicated in Figure 5-3. The precipitation values for the nine DOE stations in the Yucca Mountain area are for 1986 through December 31, 2004 (for five stations), or 1993 through December 31, 2004 (for four stations). Only Nevada Test Site locations with record periods of at least 40 years are shown. The displayed SNOTEL stations all have record lengths of at least 20 years and are color-coded using the same scheme as the COOP stations.

Figures 5-5 and 5-6 show increasingly good fits to the data as additional regression variables are added, as is expected. Using only elevation as a regression variable explains half of the variability in $\log_{10}$(MAP). With the maximum number of regression variables, almost 7/8 of the variability is explained.

The external data provides a useful check on the predictions. The SNOTEL data tend to be larger than the regression estimates, especially for Sierra Nevada stations, suggesting that the gradient with respect to elevation may be somewhat larger than estimated or the spatial variation may not be well represented at the western edge of the data set. Interestingly, the observations from the Nevada Test Site and DOE Yucca Mountain stations become increasingly larger than regression predictions as the number of regression variables increase, although the observations are within or on the edge of the scatter from the stations used for the regression.

---

[12] Snowpack telemetry is used frequently throughout this chapter; consequently, the abbreviation SNOTEL will be used.

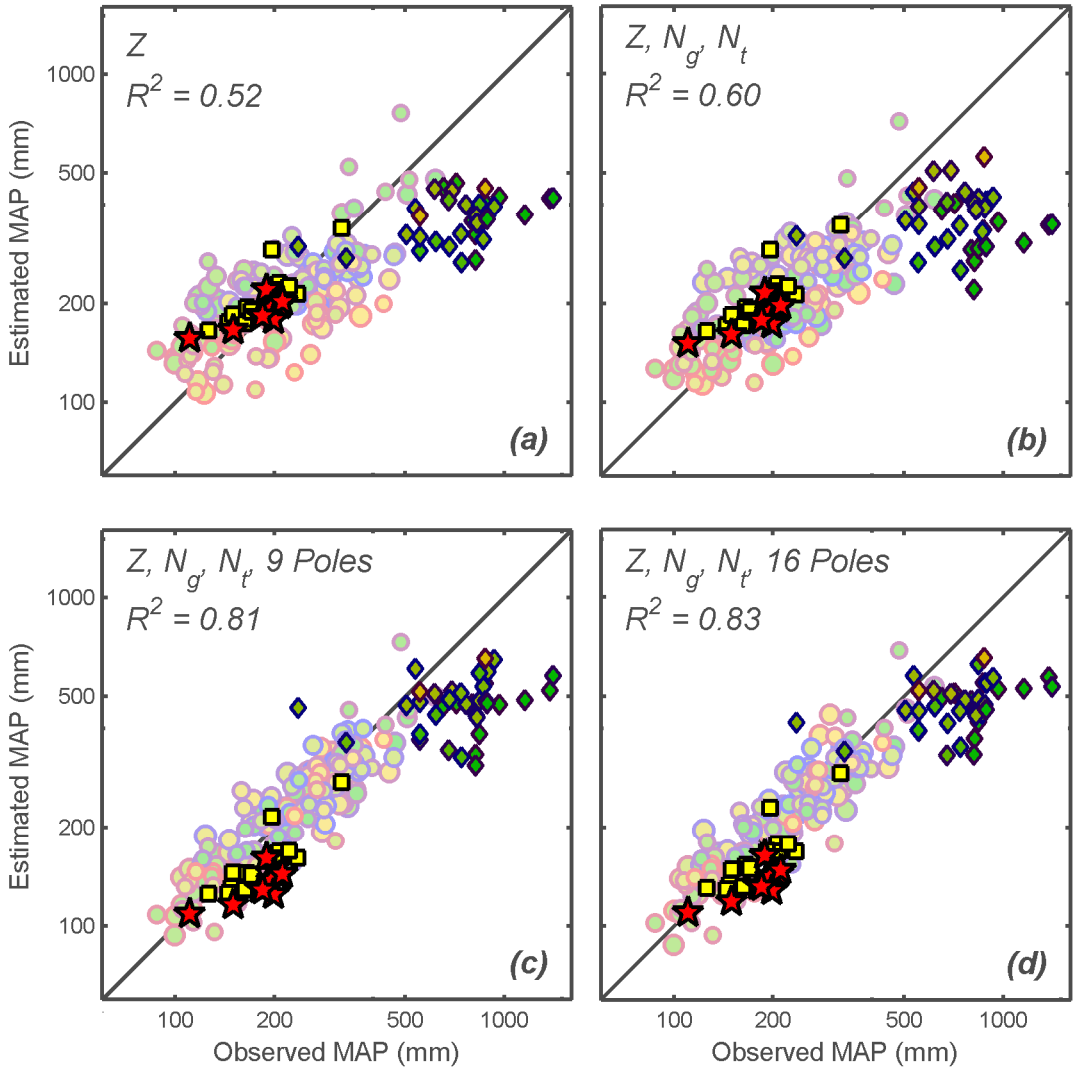

Figure 5-5. Estimated Versus Observed Log_{10}(MAP) for All 171 Stations With at Least 20 Years of Observations. The Regression Shown in (a) Only Uses Elevation. The Regressions Shown in (b), (c), and (d) Use Elevation, Latitude, and Longitude. In Addition, the Regressions Shown in (c) Use 9 Poles and in (d) Use 16 Poles. Symbols Are Defined in Figure 5-3.

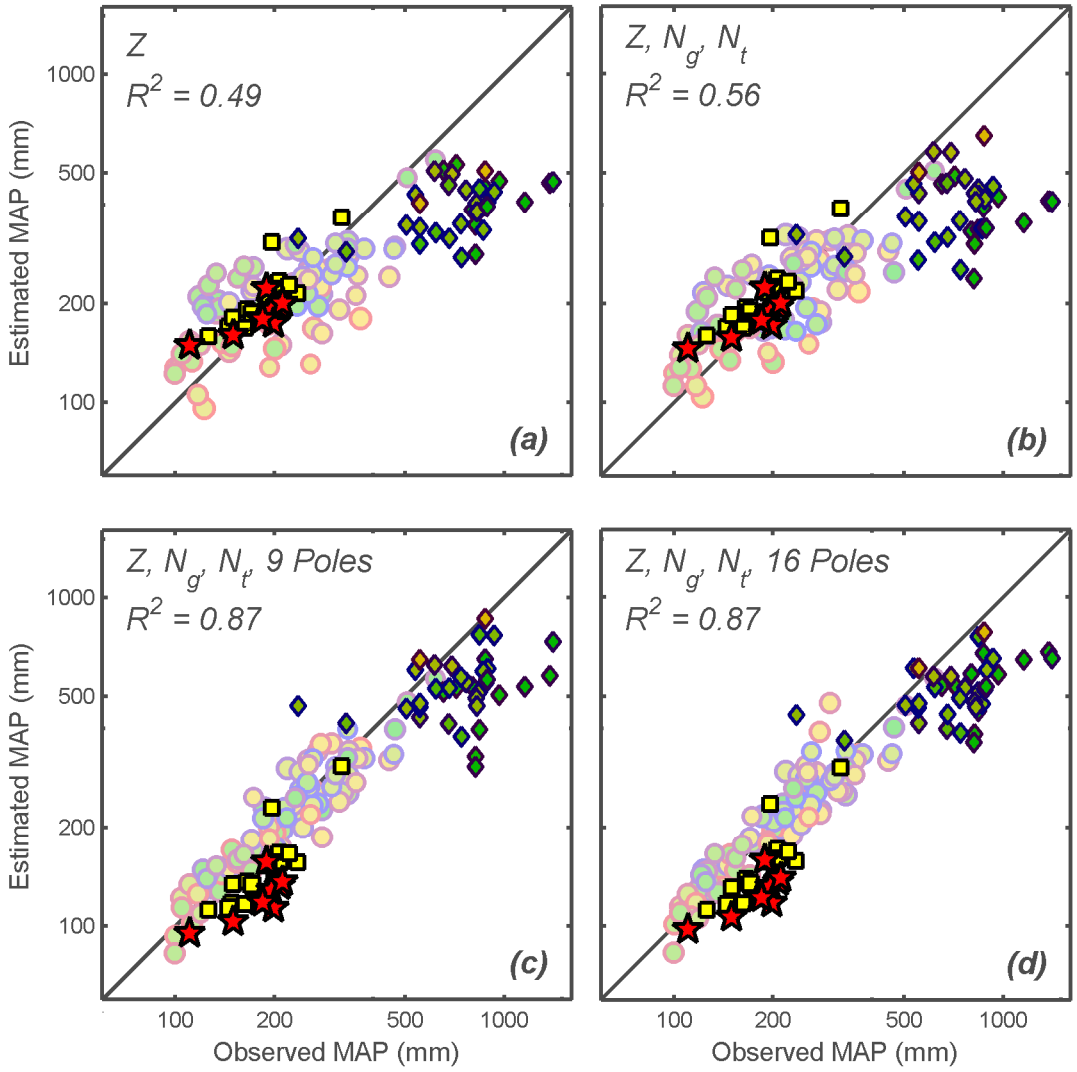

Figure 5-6. Estimated Versus Observed Log_{10}(MAP) for All 86 Stations With at Least 40 Years of Observations. The Regression Shown in (a) Only Uses Elevation. The Regressions Shown in (b), (c), and (d) Use Elevation, Latitude, and Longitude. In Addition, the Regressions Shown in (c) Use 9 Poles and in (d) Use 16 Poles. Symbols Are Defined in Figure 5-3.

Regressions using only stations with at least 40 years of data (Figure 5-6) tend to estimate slightly lower log_{10}(MAP) in the Yucca Mountain area than regressions using stations with at least 20 years of data (Figure 5-5). Accordingly, Nevada Test Site and Yucca Mountain observations agree slightly better with the 20-year regressions. Note that there are few COOP

stations with 40-year records near Yucca Mountain and the 20-year stations provide better spatial coverage.

The regression analysis equations can be reduced to a relationship solely dependent on elevation if the latitude and longitude are specified. Selecting a location centered on Yucca Mountain (36°50' N, 116°30' W), the various relationships predicting $\log_{10}$(MAP) are summarized in Table 5-1 and Figure 5-7. These are described in the form

$$\log_{10}(\text{MAP}) = A + Bz \tag{5-7}$$

where MAP is in mm/yr and z is ground elevation in kilometers. French (1986) and Hevesi, et al. (1992a,b) developed similar regressions relating MAP to elevation; these are also listed in Table 5-1 and are shown in Figure 5-7.

Table 5-1. Regression Equations for Mean Annual Precipitation Shown in Figure 5-7. All Equations Have the Form $\log_{10}$(MAP) = A + Bz, Where MAP Denotes Mean Annual Precipitation in mm/year and z Is Elevation in km. R and N Denote the Coefficient of Determination and the Number of Observations, Respectively.

A	B (1/km)	R^2	N	Source
1.872	0.228	0.48	63	Southern Nevada*
1.902	0.271	0.76	12	Nevada Test Site*
1.876	0.256	0.56	42	Yucca Mountain region†
1.850	0.281	0.79	1531	Cokriged grids‡
1.875	0.280			Yucca Mountain region§
1.999	0.233	0.52	171	20-year COOP‖ stations: z¶
1.947	0.270	0.49	86	40-year COOP stations: z
1.973	0.245	0.60	171	20-year COOP stations: $z/N_t/N_g$
1.917	0.293	0.56	86	40-year COOP stations: $z/N_t/N_g$
1.790	0.291	0.75	171	20-year COOP stations: $z/N_t/N_g$/4 poles
1.701	0.340	0.75	86	40-year COOP stations: $z/N_t/N_g$/4 poles
1.776	0.292	0.81	171	20-year COOP stations: $z/N_t/N_g$/9 poles
1.658	0.363	0.87	86	40-year COOP stations: $z/N_t/N_g$/9 poles
1.793	0.286	0.83	171	20-year COOP stations: $z/N_t/N_g$/16 poles
1.703	0.338	0.87	86	40-year COOP stations: $z/N_t/N_g$/16 poles
1.888	0.263			Averaged equation (OCCYM Middle)
1.824	0.276			ITYM

*French, R.H. "Daily, Seasonal, and Annual Precipitation at the Nevada Test Site, Nevada." Publication No. 45042. Reno, Nevada: Desert Research Institute. 1986.
†Hevesi, J.A., J.D. Istok, and A.L. Flint. "Precipitation Estimation in Mountainous Terrain Using Multivariate Geostatistics. Part I: Structural Analysis." *Journal of Applied Meteorology*. Vol. 31, No. 7. pp. 661–676. 1992a.
‡Hevesi, J.A., A.L. Flint, and J.D. Istok. "Precipitation Estimation in Mountainous Terrain Using Multivariate Geostatistics. Part II: Isohyetal Maps." *Journal of Applied Meteorology*. Vol. 31, No. 7. pp. 677–688. 1992.
§Bechtel SAIC Company, LLC. "Simulation of Net Infiltration for Present-Day and Potential Future Climates." MDL–NBS–HS–000023. Rev. 00. Las Vegas, Nevada. Bechtel SAIC Company, LLC. 2004.
‖Cooperative Observer Program
¶z = elevation [km]; N_t = normalized north latitude [$(L_t - 34)/(42 - 34)$, where L_t is north latitude]; N_g = normalized west longitude [$(L_g - 113)/(120 - 113)$, where L_g is west longitude]

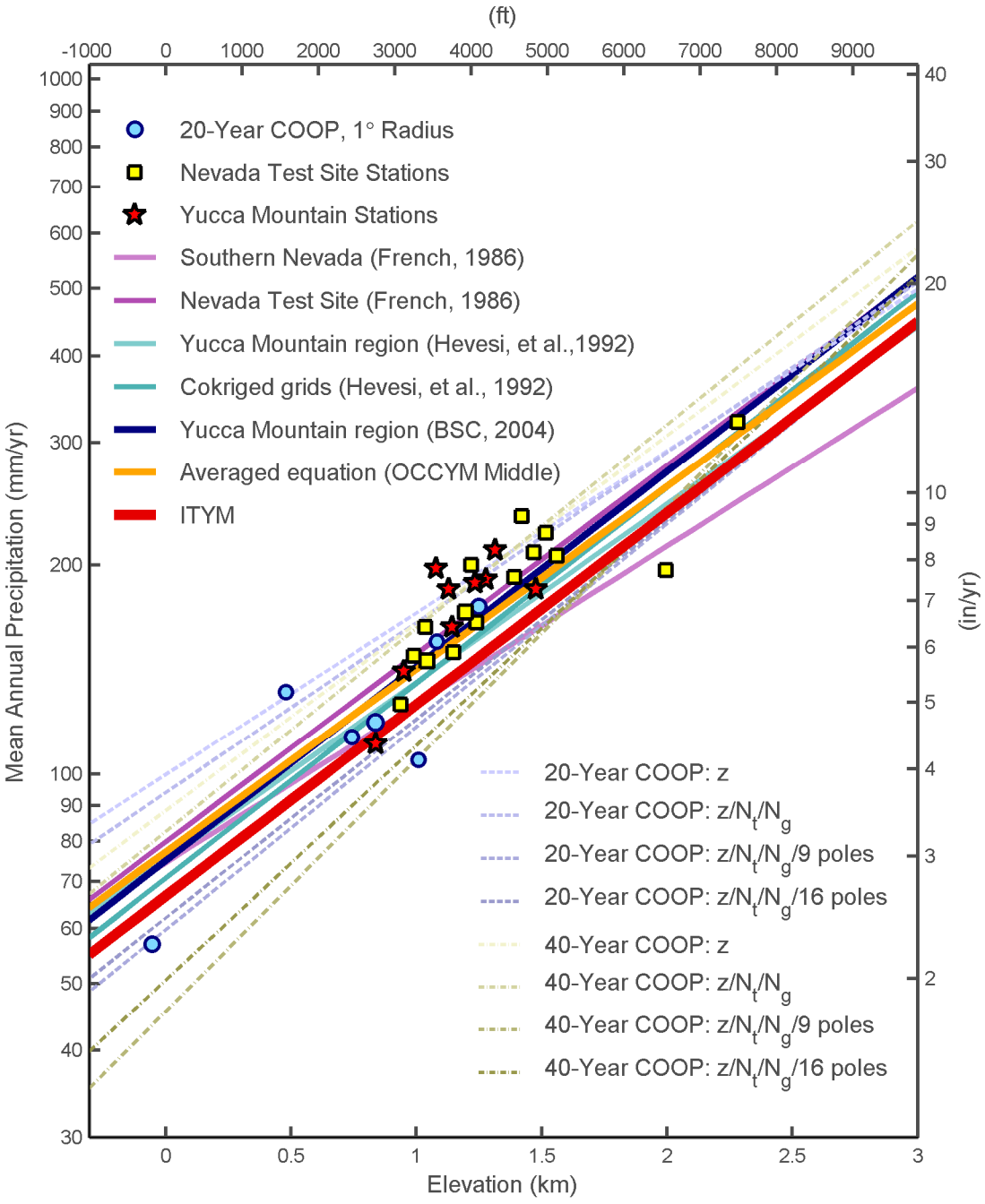

Figure 5-7. Regression Lines for the Elevation Dependence of Mean Annual Precipitation Near Yucca Mountain

The equations all have generally similar coefficients and tend to form a band of estimates. The scatter between the points illustrates the difficulty in estimating MAP near Yucca Mountain; factors that are not considered in the regressions clearly have a significant affect on MAP. Observed MAP may easily be 4/5 or 5/4 of estimated MAP.

Two 20-year regression curves provide reasonable bounds on MAP predictions, based on the comparison of site-specific observations with regression curves in Figure 5-7. The regional elevation-only curve suggests that conditions may be wetter than observed, while the nine-pole curve suggests that conditions may be drier than observed. Averaging the two equations provides a reasonable best guess for local MAP distributions and is very close to the formula used by Bechtel SAIC Company, LLC (2004a). The predictive equations are listed in Table 5-1 as "20-year COOP stations: z" and "20-year COOP stations: $z/N_t/N_g$/9 poles," and the average of the two equations is listed as "Averaged equation (OCCYM Middle)." At the reference elevation of 1,400 m [4,600 ft], the 3 equations estimate 211, 153, and 180 mm/yr [8.3, 6.0, and 7.1 in/yr], respectively. At the same elevation, the relationship used by Bechtel SAIC Company, LLC (2004a) estimates 185 mm/yr [7.3 in/yr] for MAP.

To place the regression results in context, the range of 0.23 to 0.36 km^{-1} in estimated values for B yields estimates for MAP at Yucca Crest that are between 1.18 and 1.11 times larger than MAP in Coyote Wash, implying that MAP has relatively little variation across the potential-repository footprint due to systematic elevation-dependent relationships. The ITYM strategy of using a reference value for MAP at an intermediate elevation would yield similar estimates of MAP across the potential-repository footprint were the constant in Eq. (5-1) set to any of the B coefficients in Table 5-1.

5.2 Mean Annual Temperature

ITYM uses an equation for the gradient of MAT with respect to elevation that is based on a network of 262 COOP stations with record lengths of at least 5 years. A shorter averaging period was used to estimate MAT than MAP because the same general patterns repeat from year to year and interannual variability in temperature is much smaller than interannual variability in precipitation.

Maximum and minimum daily temperature is recorded at each COOP station. The average of the daily maximum and minimum temperature was used to estimate the mean daily temperature, with seasonal trends for the COOP stations shown in Figure 5-8. Unlike the analogous precipitation patterns shown in Figure 5-4, the temperature curves are not smoothed. Seasonal patterns in mean daily temperature are quite consistent across the region, with elevation providing the primary difference within a region.

Annual-average values for all three measures of daily temperature are well predicted with two variables: elevation and either latitude or mean annual solar flux on a horizontal plane external to the atmosphere at the latitude of the station. The relationship based on latitude is

$$\mathrm{MAT} = A + Bz + CN_t \tag{5-8}$$

Eq. (5-8) explains 95 percent of variability in regional MAT, 97 percent of variability in maximum daily temperature, and 84 percent of variability in minimum daily temperature (Figure 5-9). The

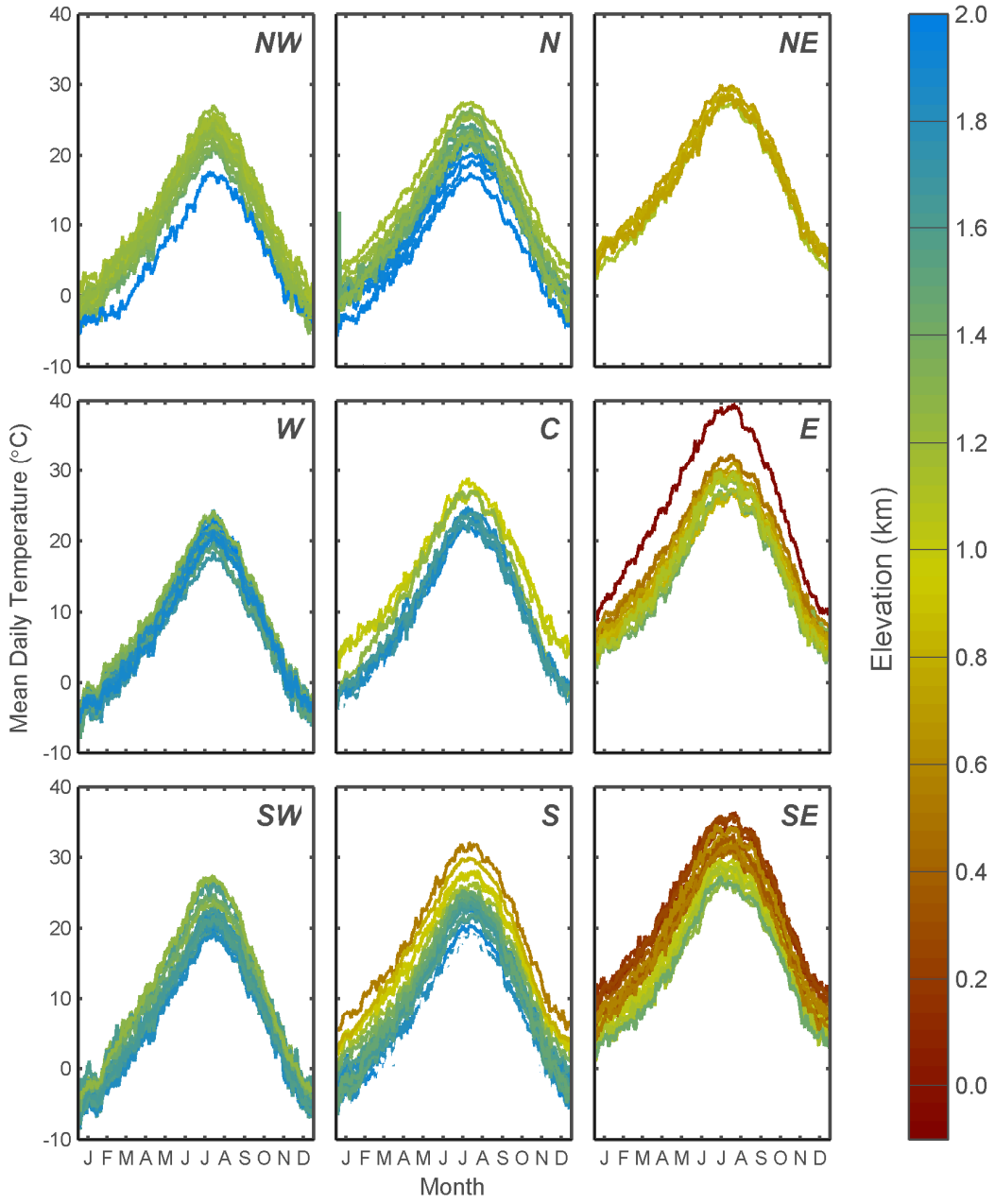

Figure 5-8. Mean Daily Temperature for Each Cooperative Observer Program Station With a Record of at Least 40 Years Over the Station's Period of Record. No Smoothing Is Used. Color Indicates Station Elevation. [°F = (9/5)°C + 32; 1 km = 3,281 ft]

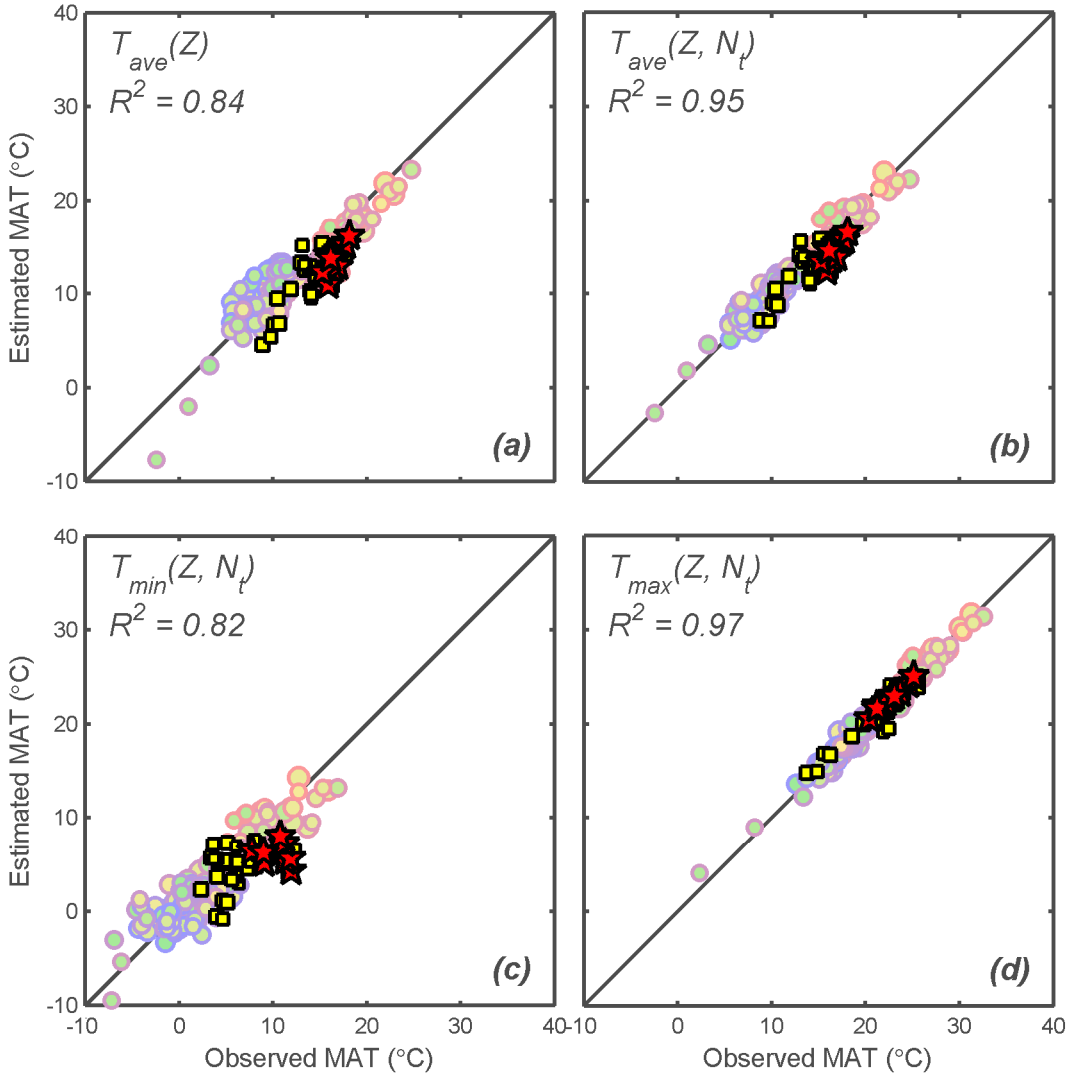

Figure 5-9. Estimated Versus Observed Annual Temperatures for All 262 Stations With at Least 5 Years of Observations. Mean Daily Temperature(T_{ave}) Is Estimated Using (a) Only Elevation, and (b) Elevation and Normalized Latitude. Daily (c) Minimum (T_{min}) and (d) Maximum (T_{max}) Temperature Are Estimated Using Elevation and Normalized Latitude. Symbols Are Defined in Figure 5-3.

difference between maximum and minimum daily temperature is not noticeably dependent on elevation, latitude, or longitude. ITYM uses the *B* coefficient for MAT labeled "Regional daily temperature localized to Yucca Mountain" in Table 5-2 to describe systematic, elevation-dependent variation of MAT.

Figure 5-10 displays the regional relationships and relatively short-term site observations from the Nevada Test Site (Air Resources Laboratory/Special Operations and Research Division, 1981–2001) and Yucca Mountain (Western Regional Climate Center, 1985–2004). The site observations provide limited confirmation that the regional trends represent Yucca Mountain. Temperature measurements at the nine Radiological and Environmental Programs Department meteorological monitoring stations (Western Regional Climate Center, 1985–2004) maintained by DOE on and near Yucca Mountain were used to estimate the gradient of MAT with elevation, labeled "9-Stations mean daily temperature" in Table 5-2. The regional and 9-stations equations estimate MAT of 13 and 15.6 °C [55.4 and 60.1 °F], respectively, at the reference elevation of 1,400 m [4,600 ft], with an estimated difference in MAT from Yucca Crest to Coyote Wash of 1.27 and 0.8 °C [2.3 and 1.4 °F], respectively. These correspond to lapse rates between 6.4 and 4.0 °C/km [18 and 12 °F/mi]. Observed values for MAT are reasonably close to the regional trend, although the local Yucca Mountain observations suggest somewhat less sensitivity to elevation. Given the same reference MAT at the reference elevation, the two lapse rates yield MAT estimates that agree to within less than 0.25 °C [0.45 °F] within the repository footprint. The difference between lapse rates is too small to materially influence MAI estimates using the abstractions developed in Section 4. The difference between Yucca Crest and Coyote Wash ranges from 0.8 to 1.3 °C [1.4 to 2.3°F]

Table 5-2. Regression Equations for Mean Annual Daily Maximum and Minimum Temperature. All Equations Have the Form $Y = A + Bz + CN_t$, Where Y Is Mean Annual Temperature in °C, z Is Elevation in km, and N_t Is Latitude Normalized Between 34° N and 42° N. R Denotes the Coefficient of Determination.

A	B (1/km)	C	R^2	Description
23.18	−8.315	0	0.86	Regional daily temperature (z only)
31.98	−8.543	0	0.91	Regional daily maximum temperature (z only)
14.38	−8.096	0	0.73	Regional daily minimum temperature (z only)
24.30	−6.340	−6.861	0.95	Regional daily temperature (with N_t)
32.93	−6.856	−5.828	0.97	Regional daily maximum temperature (with N_t)
15.67	−5.824	−7.895	0.84	Regional daily minimum temperature (with N_t)
21.87	−6.340	0	0.95	Regional daily temperature localized to Yucca Mountain
30.87	−6.856	0	0.95	Regional daily maximum temperature localized to Yucca Mountain
12.87	−5.824	0	0.84	Regional daily minimum temperature localized to Yucca Mountain
21.20	−4.000	0	0.60	9-Stations mean daily temperature
33.71	−9.506	0	0.93	9-Stations mean daily maximum temperature
7.60	2.310	0	0.05	9-Stations mean daily minimum temperature
17.3	−9.8	0		DOE mean daily temperature*

*Bechtel SAIC Company, LLC. "Simulation of Net Infiltration for Present-Day and Potential Future Climates." MDL–NBS–HS–000023. Rev. 00. Las Vegas, Nevada: Bechtel SAIC Company, LLC. 2004.

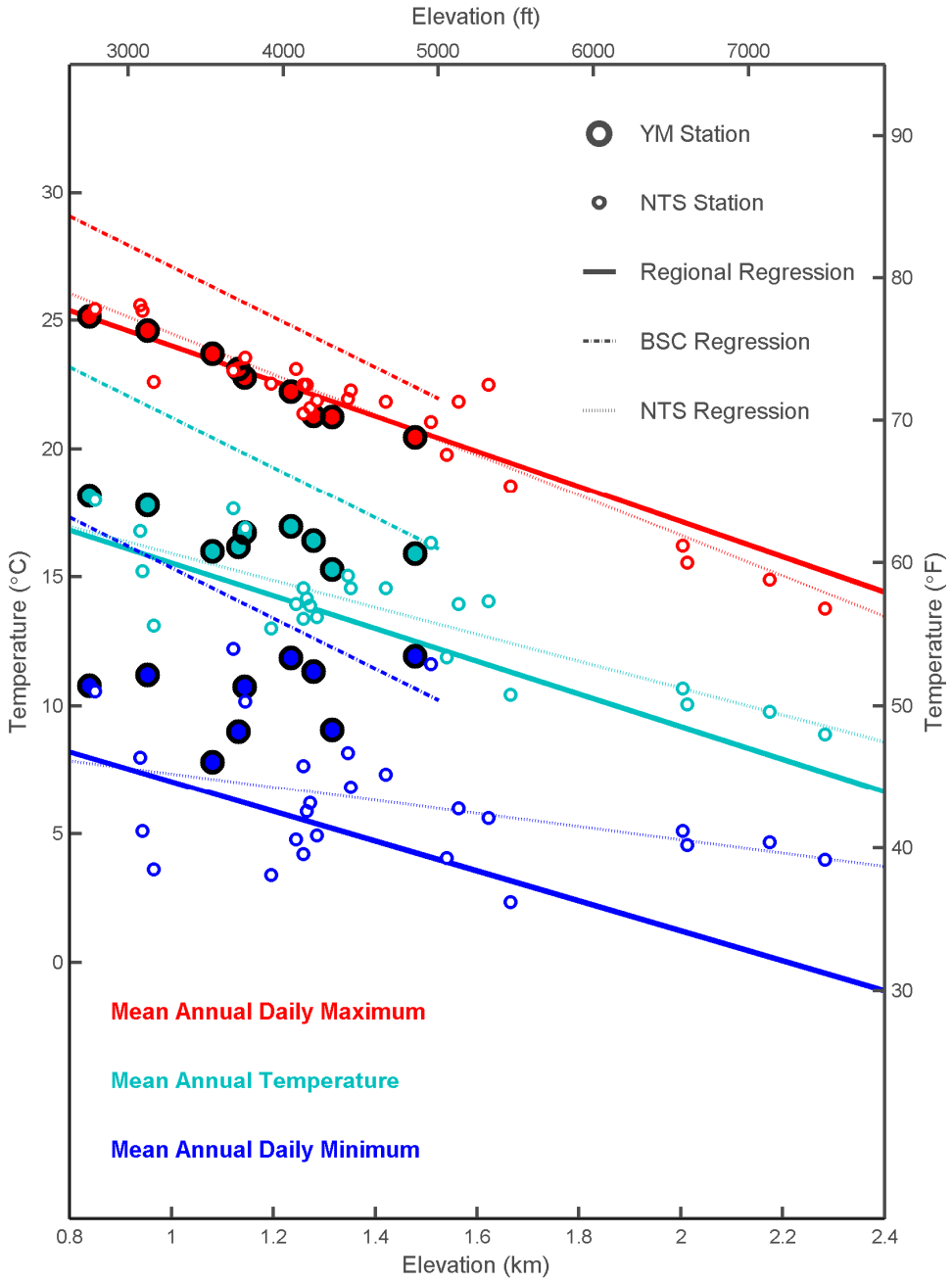

Figure 5-10. Regression Equations for the Elevation Dependence of Mean Annual Temperature in the Yucca Mountain Vicinity. Mean Annual Daily Minimum and Maximum Temperatures Are Shown for Reference. "BSC Regression" Indicates the Regression Used by Bechtel SAIC Company, LLC (2004a). "NTS Regression" Indicates a Regression on Just the Nevada Test Site Stations.

Bechtel SAIC Company, LLC (2004a) uses the gradient of −9.8 °C/km [−28 °F/mi] to distribute MAT across Yucca Mountain, which yields an estimated difference of 2.0 °C [3.6 °F] between Yucca Crest and Coyote Wash. The Bechtel SAIC, LLC (2004a) relationship induces a small difference in estimated MAI using the abstractions developed in Section 4.

Figure 5-10 also indicates maximum and minimum daily temperature observations at Yucca Mountain. Maximum daily temperatures are reasonably well estimated using the regional relationship, but minimum daily temperatures differ from the regional trend by up to 8 °C [14 °F]. Note that the minimum daily temperature at Yucca Mountain appears to increase with elevation, contrary to the regional relationships. Yucca Mountain washes exhibit drainage of cool night air, causing temperature inversions. Drainage is coincident with peak wind speeds within the washes, while peak wind speeds occur during the day for crests and alluvial valleys. Anomalous temperatures may also be due to advection from the nearby warm flats to the ridges.

Stothoff (1997) found that bare-soil MAI estimates from simulations using hourly observations of evaporation-affecting meteorological parameters differed little from MAI estimates using a monthly moving average for days not within 1 day of a precipitation event. Retaining hourly meteorological variation near precipitation days during simulations allows the systematic pattern of above-average relative humidity following precipitation to be captured. Not considering this systematic relative humidity pattern artificially increases evaporation rates and decreases MAI. The observation that calculated MAI is almost the same for simulations considering hourly and monthly temperature patterns suggests that diurnal temperature patterns have little effect on MAI. The abstractions used in ITYM do not consider daily temperature extremes. Thus, although diurnal temperature patterns at Yucca Mountain appear to differ somewhat from regional patterns, available information suggests that such differences may not influence MAI estimates significantly.

5.3 Mean Annual Vapor Density

Precipitation and temperature are the climatic parameters that change MAI estimates most significantly between climate states that are comparable to different stages of a glacial cycle. Precipitation regulates the amount of moisture potentially available for net infiltration; temperature and the remaining climatic parameters modify evapotranspiration rates that return the water to the atmosphere.

MAI is more sensitive to MAV than most climatic parameters (see Figure 3-5) because evapotranspiration rates are proportional to the difference between atmospheric vapor density (characterized by MAV) and the vapor density near the ground (i.e., at the soil surface and within plant stomata). Most climatic parameters affect vapor density at the soil, but evaporation is also mediated by the hydraulic characteristics of the soil unless the soil surface is almost saturated. Wind speed directly affects the proportionality constant between flux and density difference, but evapotranspiration is relatively less sensitive to MAW in windy environments because evapotranspiration becomes limited by the capability of the soil and vegetation to supply water vapor.

The set of simulations showing the greatest sensitivity to MAV out of all simulations used to derive the ITYM abstractions has an 11-fold increase in MAI for a 2.25-fold increase in MAV. The sensitivity is asymmetric for large changes in MAV; reducing MAV reduces MAI to a smaller extent than the same increase in MAV increases MAI.

The vertical distribution of MAV was originally estimated for use in ITYM using the Desert Rock, Nevada, meteorological station and one of the stations reported by McKinley and Oliver (1994) in the Kawich and Toiyabe Ranges, east and north of Tonopah, Nevada. In preparing this report, it was found that the coefficient in the relationship that describes the rate of change of MAV with respect to elevation was apparently mistyped when creating the ITYM input file for TPA Version 4.0, resulting in a distribution for MAV that decreases with elevation approximately an order of magnitude too quickly. The result is MAV values that are approximately an order of magnitude too small, or atmospheric conditions that are far more arid than actually exist at Yucca Mountain. As a result, evaporation is over-estimated. This mistyped value affects simulations for TPA Versions 4.0 through 5.1 and the simulations considered by Stothoff and Walter (2007).

Relative humidity is the ratio between actual vapor density and saturated vapor density. Relative humidity changes according to season, but the effect of the mistyped MAV value on MAI can be qualitatively assessed using annual-average relative humidity. The largest possible evaporation rate for a given wind condition arises when the soil has a relative humidity of 1 (i.e., the vapor density is at its maximum value—always the case within the soil column) and the atmosphere has a relative humidity of 0 (i.e., vapor density is zero). The meteorological stations at Yucca Mountain recorded an average relative humidity between 0.29 and 0.34 from 1993 through 2004, implying that on average the evaporation rate was approximately 66 to 71 percent of the maximum possible rate. Decreasing MAV (and relative humidity) by a factor of 10 (inadvertently, because of the typographical error) increases the evaporation rate to approximately 97 percent of the maximum rate, implying that evaporation rates would increase by approximately 37 to 46 percent.

As it turns out, the typographical error has a minimal effect on overall MAI estimates because the model is calibrated by adjusting transpiration rates with the plant-scavenging factors described in Section 4.5. The effect of the mistyped value for MAV was unwittingly compensated for with a relatively small calibration adjustment to reduce the plant scavenging effect, and Stothoff and Walter (2007) demonstrated that the resulting MAI values are consistent with site and regional observations. When the mistyped value is corrected, the plant scavenging factors may be adjusted as well.

Regression equations based on regionally distributed sites with observed values of MAV (shown in Figure 5-11) can be used to estimate the spatial distribution of MAV at Yucca Mountain. Hourly values of vapor density were calculated from hourly temperature and relative humidity readings from 1961 through 1990 for a subset of the Solar and Meteorological Surface Observation Network (SAMSON) stations and the meteorological station used for the BREATH simulations located at Desert Rock, Nevada; the hourly readings were averaged to yield MAV for each station. Observations of minimum and maximum daily temperature and daily relative humidity from the nine Radiological and Environmental Programs Department meteorological monitoring stations maintained by DOE in the Yucca Mountain area were used to estimate MAV, using the records from station onset through December 31, 2004. Two estimates of vapor density were made for each day: (i) assuming that minimum temperature corresponds to maximum relative humidity (nighttime estimate) and (ii) assuming maximum temperature corresponds to minimum relative humidity (daytime estimate). Several additional high-altitude vapor densities were estimated using 6 years of temperature and relative humidity observations for the four stations reported by McKinley and Oliver (1994) in the Kawich and Toiyabe Ranges, east and north of Tonopah, Nevada.

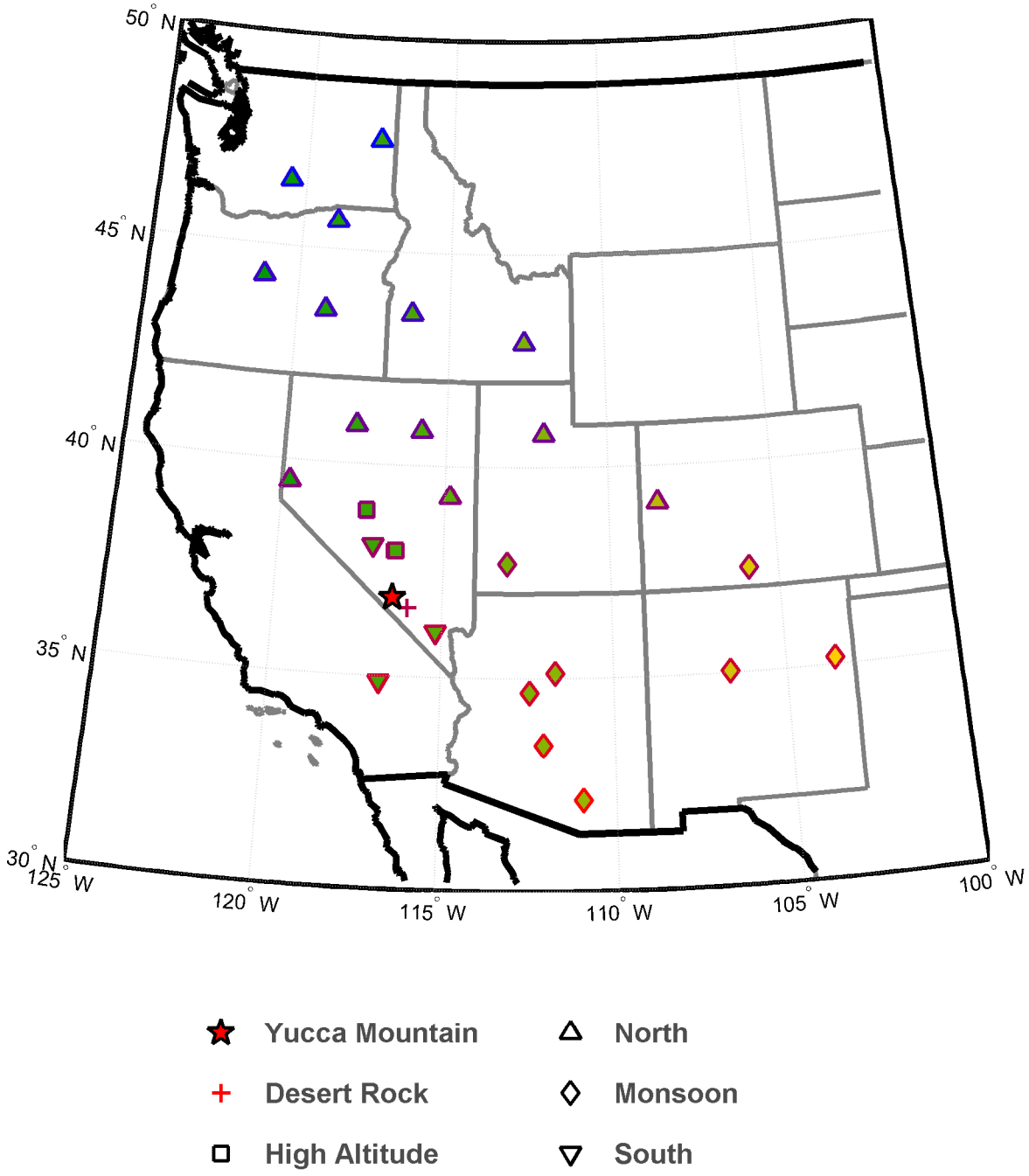

Figure 5-11. Location of Stations Used To Estimate Mean Annual Vapor Density

The data sets were partitioned into three groups. The monsoon group includes sites with a significant monsoon component (Arizona; New Mexico; Alamosa, Colorado; and Cedar City, Utah). The nonmonsoon group includes all other Solar and Meteorological Surface Observation Network sites and Desert Rock, Nevada. The Yucca Mountain group consists of the nine DOE meteorological stations. The high-altitude sites are not included in any regression.

Regressions for MAV were performed for each group in the form of

$$\log_{10}(\text{MAV}) = A + Bz \qquad (5\text{-}9)$$

where MAV is in the units of g/m^3, z is elevation [km], and A and B are regression coefficients (B has units of km^{-1}). Regressions for MAV and $\log_{10}$(MAV) yielded essentially identical values of R^2, with R^2 differing by less than 0.006 for each group.

Figure 5-12 shows observed MAV values and regression relationships. The monsoon group has the steepest gradient of $\log_{10}$(MAV) with respect to elevation, and the Yucca Mountain group using the daytime estimate has the shallowest gradient. The estimated MAV values for

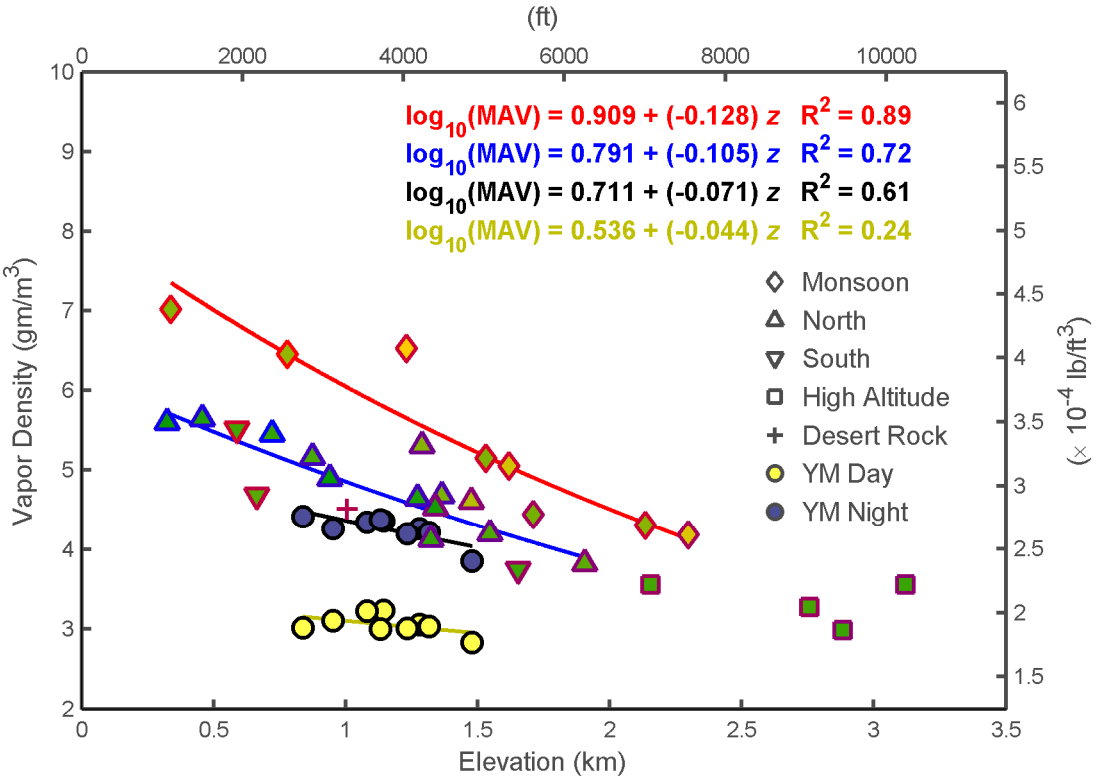

Figure 5-12. Regional Dependence of Mean Annual Vapor Density (Denoted by MAV) on Elevation. Symbols Are Defined in Figure 5-11. Circles Indicate Yucca Mountain Meteorological Stations. The Desert Rock Station Was Used for BREATH Simulations. The Red Regression Uses Monsoon Sites, the Blue Regression Uses Nonmonsoon Sites, and the Black and Yellow Regressions Only Use Yucca Mountain Stations. All Regressions Use MAV in g/cm^3 and z in km.

the Yucca Mountain stations using the nighttime estimate are consistent with the Desert Rock, Tonopah, and Las Vegas estimates that are based on hourly values. All of these are in the dry side of the nonmonsoon estimates. The Yucca Mountain estimates using the daytime observations are approximately 30 percent smaller than the estimates using the nighttime observations. The hourly Desert Rock observations indicate that vapor density systematically varies during the day, lagging diurnal temperature changes by an hour or two, which may partially explain the discrepancy between the two Yucca Mountain estimates.

The regression originally intended for use in ITYM, based on the Desert Rock station and the high-altitude stations, would be consistent with the information shown in Figure 5-12. Note that there is approximately a 6 percent change in MAV between Yucca Crest and Coyote Wash for the steepest regression, so that spatial variability of MAV should only minimally influence MAI estimates.

ITYM uses a single relationship for MAV regardless of climatic conditions. There is little information regarding changes in MAV under previous climatic conditions, but it is reasonable to expect that wetter conditions may tend to produce larger values of MAV.

A change to monsoon conditions at Yucca Mountain would increase MAV by approximately 30 percent, comparing the monsoon and daytime Yucca Mountain relationships, but monsoon conditions are expected to be relatively infrequent at Yucca Mountain over glacial cycles (Stothoff and Walter, 2007). Note that elevated values of MAV for the monsoon stations arise from summer precipitation. Stothoff and Walter (2007) discuss recharge seasonality, finding that winter precipitation is far more efficient at causing recharge than summer precipitation. This in turn implies that atmospheric vapor density during cool seasons may be the dominant influence on MAI, rather than vapor density averaged over the entire year. The rationale that cool-period vapor density is critical for MAI implies that the MAV values used in ITYM would likely be more representative of monsoon periods of a glacial cycle than implied by Figure 5-12.

A shift to conditions representative of the stations in Washington, Oregon, and Idaho, which may be analogous to glacial conditions at Yucca Mountain, would increase MAV by less than 10 percent, based on the nonmonsoon and daytime Yucca Mountain relationships. This lack of a strong spatial trend in present-day MAV suggests that MAV may have been only slightly greater than under present-day conditions during past glacial maxima.

These comparisons suggest that the MAV values used for ITYM estimates are expected to be quite similar to present-day values; thus the unchanged MAV approximation used for ITYM is not expected to strongly affect MAI estimates for climatic conditions representing other glacial states.

5.4 Mean Annual Wind Speed

Wind affects the ease with which water vapor can move from the ground surface to the atmosphere, with faster wind increasing evapotranspiration rates and thereby reducing MAI. The simulations used to derive the abstractions for MAI that are used in ITYM considered the effect of MAW for a few representative cases. These simulations suggest that MAI is not particularly sensitive to MAW; estimated MAI was at most 2.4 times larger for a fourfold reduction in MAW. Illustrative responses of MAI to MAW are presented in Figure 3-5.

As explained in the Yucca Mountain Site Description (TRW Environmental Safety Systems, Inc., 1998), wind near Yucca Mountain tends to be funneled to the north and south by the generally

north-south trending ranges in the Great Basin. The least windy months are January and December, and the windiest are April and May. Winds tend to respond to solar heating and thus are strongest during the day and calmer at night. The washes above the potential-repository footprint are protected from the prevailing winds, however, and in this sheltered area the strongest winds are generally associated with nighttime drainage of cool air. For example, the four most exposed sites of the nine Radiological and Environmental Programs Department meteorological monitoring sites have an annual average wind speed between 4.2 and 4.4 m/s [13.8 to 14.4 ft/s], while the most sheltered station (in Coyote Wash) has an annual average wind speed of 2.5 m/s [8.2 ft/s].

ITYM considers systematic spatial variation of MAW based on ground topography to account for the influence of MAW on MAI, but it is expected that MAW has relatively little effect on MAI. Using the largest sensitivity of MAI to MAW estimated from the simulations, MAI in Coyote Wash would be approximately 1.5 times larger than MAI in exposed locations. Note that this sensitivity is for a small value of MAI, and MAI becomes less sensitive to MAW as MAI increases. Systematic spatial variation is accounted for using a separate MAW coverage that is used for all climatic conditions. Uncertainty in MAW is accounted for by multiplying all values of MAW in the coverage by a single sampled parameter.

The MAW coverage is generated using a heuristic relation to generate a function indicating the relative strength of "wash" (sheltered) and "open" (exposed) characteristics for each pixel. The heuristic relation increases the wash strength for areas with strong upward curvatures or steep north-south slopes. The open strength is increased for areas with strong downward curvatures or relatively horizontal slopes. The wind speed gradually increases with elevation for open areas and is significantly reduced in wash areas, reflecting the tendency for Yucca Crest wind speeds to be larger than in the flats and for east-west trending washes above the repository to be sheltered.

The index function is built up in steps. First, a set of index values is created for each pixel to describe slope (I_1), north-south slope (I_2), east-west slope (I_3), and north-south curvature (I_4)

$$I_1 = \text{norm}(s) \tag{5-10}$$

$$I_2 = \text{norm}\left(\left|\partial z/\partial y\right|\right) \tag{5-11}$$

$$I_3 = \text{norm}\left(\left|\partial z/\partial x\right|\right) \tag{5-12}$$

$$I_4 = \text{norm}\left(-\partial^2 z/\partial^2 y\right) \tag{5-13}$$

$$\text{norm}(u) = \frac{u - \min(u)}{\max(u) - \min(u)} \tag{5-14}$$

where s is the ground slope, x and y are east-west and north-south coordinates, z is elevation (all in the same units), and u is a generic variable. These pixel index values are reset at threshold values to match wash characteristics. In the typical case developed here, I_2 is set to 1 if greater than 0.05 (significant ground slope) and I_3 and I_4 are set to 1 if greater than 0.6. Index values are then created for each pixel to describe wash intensity (I_w) and openness intensity (I_o)

$$I_w = \text{norm}\{\text{smooth}[\max(I_2, I_4)(1 - I_1)]\} \tag{5-15}$$

$$I_o = \text{norm}\{\text{smooth}[1 + \text{norm}(I_1 + I_3) - I_w]/2\} \quad (5\text{-}16)$$

where smooth (u) indicates the average of u in adjacent cells.

Surface elevation-dependent MAW is created for the open areas while accounting for a certain amount of protection in alluvial valleys near Yucca Mountain

$$W_o = W_1 + \frac{z - z_1}{z_2 - z_1}(W_2 - W_1) \quad (5\text{-}17)$$

where W_o is the alluvial valley MAW variation with elevation; z_1 and z_2 are reference elevations of 1,000 and 1,500 m [3,280 and 4,920 ft], respectively; and W_1 and W_2 are reference MAW values obtained from the Radiological and Environmental Programs Department meteorological monitoring sites. Values for MAW from NTS–60 (Site 1) and Alice Hill (Site 4) are used to estimate W_1 and W_2. The Alice Hill site has the maximum average wind speed out of all sites (2 percent larger than Site 2, located on Yucca Crest). Finally, the index values are combined with the MAW values to yield

$$W = W_o I_o + W_w (1 - I_o) \quad (5\text{-}18)$$

where W_w is the wash MAW value, using Coyote Wash (Site 3) to provide a reference value. The reference values for W_w, W_1, and W_2 are 2.5, 3.4, and 4.4 m/s [8.2, 11, and 14 ft/s], respectively, using values provided by TRW Environmental Safety Systems, Inc. (1998).

Figure 5-13 shows the distribution of present-day MAW using the index approach. Ridgetops in the footprint have significantly higher MAW than washes, in accordance with observation.

5.5 Mean Annual Incident Radiation

Radiation can be partitioned into shortwave and longwave radiation. Shortwave radiation is the radiation received from the sun, while longwave radiation is emitted from the ground and sky. ITYM uses separate relationships for shortwave and longwave radiation, adding the contributions to obtain total incident radiation. Both relationships are affected by cloud cover. All parameters other than the common factor of cloud cover are held constant, with all uncertainties regarding incident radiation represented by uncertainty in cloud cover.

5.5.1 Shortwave Radiation

Shortwave radiation can be reliably estimated outside the atmosphere, but the atmosphere reduces the amount of shortwave radiation striking the ground surface. The primary reduction is through reflection from clouds and absorption by atmospheric dust. Brutsaert (1982) presents several relationships that account for the attenuation of shortwave radiation through the atmosphere. ITYM uses the Kimball (1928) relationship between shortwave radiation striking

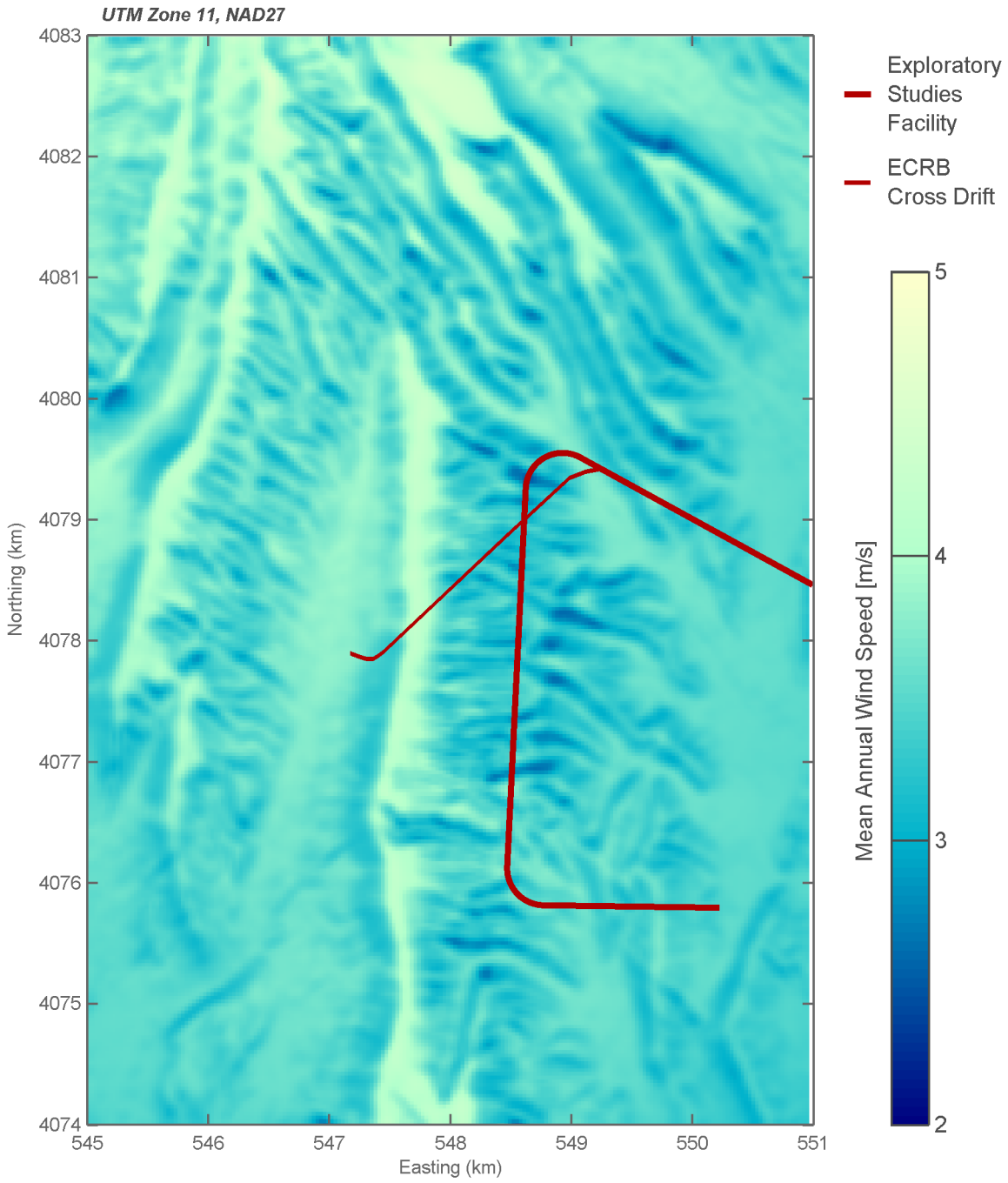

Figure 5-13. Estimated Mean Annual Wind Speed in the Yucca Mountain Vicinity [1 m/s = 2.24 mph; 1.6 km = 1 mi]

the ground surface (R_s), mean cloud cover (C_c) as a fraction, and shortwave radiation at the outside of the atmosphere (R_{sc})

$$R_s = R_{sc}(1 - aC_c) \tag{5-19}$$

where *a* is approximately 0.71 (Brutsaert, 1982).

The net radiation absorbed by the ground surface is also affected by the surface albedo, with high-albedo surfaces (e.g., snow) reflecting most of the incident radiation and low-albedo surfaces (e.g., open water) absorbing most of the incident radiation. Brutsaert (1982) collected albedo values for several types of natural surfaces, reproduced in Table 5-3. The Yucca Mountain dusts are fairly light, but rock fragments and exposed bedrock are darker. Albedo would be expected to become smaller under wetter and cooler climatic conditions, primarily due to additional plant cover. An albedo of 0.25 is used for ITYM calculations. Thus, the formula used in ITYM to estimate net MASW from MACC and shortwave radiation is

$$\text{MASW} = 0.25R_{\text{masc}}(1 - 0.7\text{MACC}) \tag{5-20}$$

where R_{masc} is the MASW on a plane external to the atmosphere at the latitude of Yucca Mountain and MACC is a fraction. Under present-day conditions, MACC is approximately 0.3 at Desert Rock, Nevada.

The angle of the ground surface affects the incident shortwave radiation by affecting R_{masc}. ITYM uses a table of R_{masc}, shown in Figure 5-14, to account for ground-surface orientation by interpolating using the actual orientation of the ground surface for each grid cell. The blocking effect of ridges is not considered. Figure 5-15 shows the spatial distribution of MASW for ITYM with MACC = 0.3: the mean value used for ITYM simulations. Sideslopes in washes facing

Table 5-3. Approximate Mean Albedo Values for Various Natural Surfaces*

Nature of Surface	Albedo
Deep water	0.04–0.08
Moist dark soils; plowed fields	0.05–0.15
Gray soils; bare-fields	0.15–0.25
Dry soils; desert	0.20–0.35
White sand; lime	0.30–0.40
Green grass and other short vegetation (e.g., alfalfa, potatoes, beets)	0.15–0.25
Dry grass; stubble	0.20–0.30
Dry prairie and savannah	0.10–0.15
Coniferous forest	0.15–0.25
Deciduous forest	0.20–0.30
Forest with melting snow	0.35–0.65
Old and dirty snow cover	0.60–0.75
Fresh dry snow	0.80–0.90

*Brutsaert, W. *Evaporation Into the Atmosphere: Theory, History, and Applications*. Dordrecht, The Netherlands: Kluwer Academic Publishers. 1982.

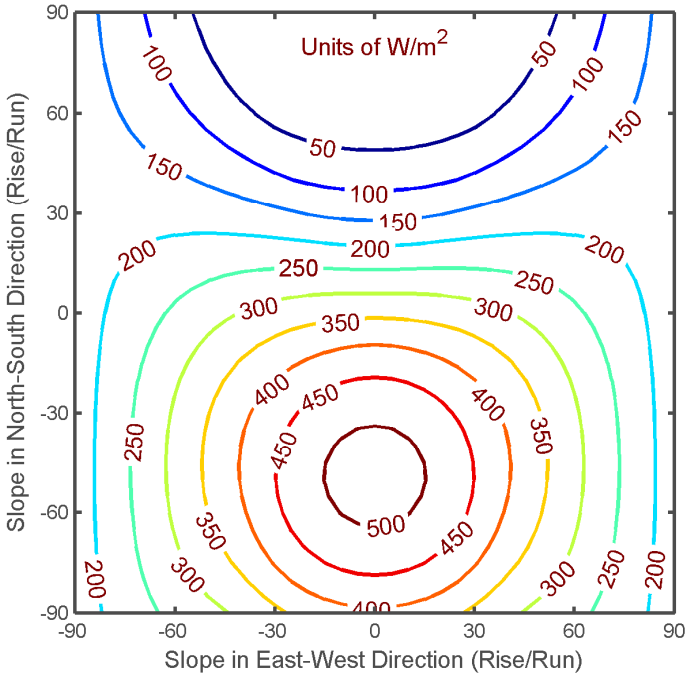

Figure 5-14. Mean Annual Extraterrestrial Solar Radiation Flux on a Flat Plate at the Latitude of Yucca Mountain as a Function of Orientation. Positive and Negative Slopes to the North Represent North- and South-Facing Slopes, Respectively. Similarly, Positive and Negative Slopes to the East Represent East- and West-Facing Slopes. [1 W/m^2 = 0.317 BTU/hr/ft^2]

north receive significantly less shortwave radiation over the course of a year than do the corresponding south-facing slopes. Some of the simulations used to develop the abstraction for MAI used in ITYM varied the shortwave radiation load to represent different ground orientations, holding all other properties fixed. Estimated MAI for north-facing slopes was as much as 2.5 times MAI for the corresponding south-facing slope.

5.5.2 Longwave Radiation

Downward longwave radiation is also affected by cloud cover. Brutsaert (1982) presents several relationships that estimate downward longwave radiation. ITYM uses a simple relationship

$$R_{ld} = R_{ldc}\left(1 + aC_c^2\right) \tag{5-21}$$

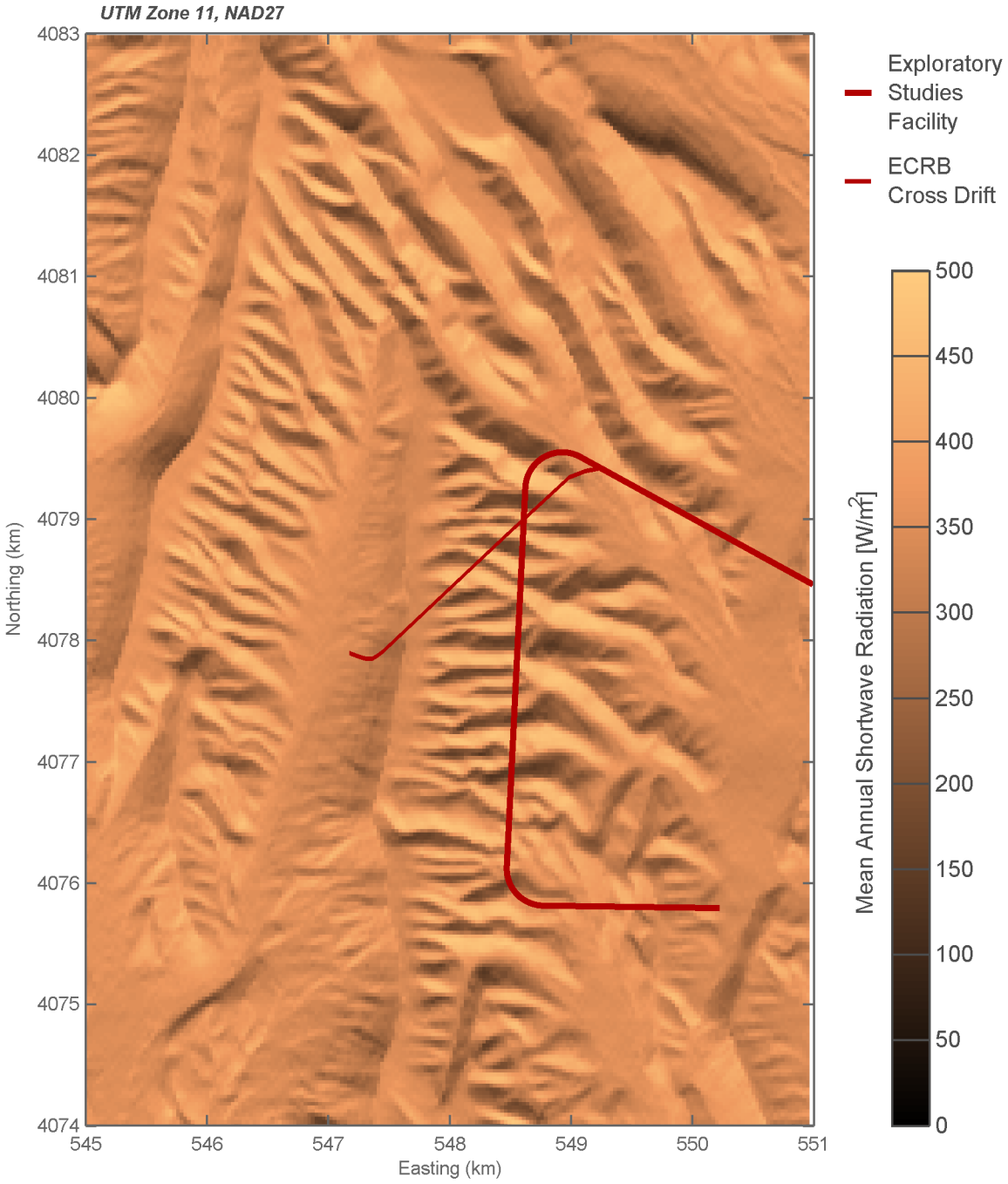

Figure 5-15. Estimated Mean Annual Solar Radiation Flux (Without Atmospheric Absorption) in the Yucca Mountain Vicinity [1 W/m^2 = 0.317 BTU/hr/ft^2]

where R_{ld} is the adjusted longwave radiation, R_{ldc} is clear-sky longwave radiation, and a is a constant depending on cloud type (taken to be 0.2 in ITYM). A typical equation to estimate R_{ldc} is of the form

$$R_{ldc} = \varepsilon_{ac} \sigma T_a^4 \tag{5-22}$$

where ε_{ac} is the effective atmospheric emissivity, σ is the Stefan-Boltzmann constant (5.67×10^{-8} W m^{-2} K^{-4} or 4.76×10^{-13} BTU s^{-1} ft^{-2} R^{-4}), and T_a is the air temperature near the ground [K]. Note that ε_{ac} is typically on the order of 0.7 to 0.8.

The BREATH simulations that defined the abstractions accounted for atmospheric vapor to provide estimates of ε_{ac} on the short time scales that are relevant to infiltration. ITYM uses a simpler representation

$$\varepsilon_{ac} = 0.92 \times 10^{-5} T_a^2 \tag{5-23}$$

Brutsaert (1982) notes that this empirical formula can be reconciled with more theoretical relationships. ITYM estimates total downward longwave radiation emitted by the atmosphere using the combined formula

$$R_{ldc} = 0.92 \times 10^{-5} \sigma \mathrm{MAT}^6 \left(1 + 0.2 \mathrm{MACC}^2\right) \tag{5-24}$$

where R_{ldc} is in W cm^{-2} K^{-4}, σ is in W cm^{-2} K^{-4}, MAT is in K, and MACC is a fraction (0 to 1).

Incoming longwave radiation is only approximately captured for most Yucca Mountain pixels because ridges block some of the sky in many pixels and ITYM does not consider ridge blocking. Ridges also emit longwave radiation. The effect of the blocking can be estimated using a simple weighted average of atmospheric and ground radiation

$$R_l = \sigma \mathrm{MAT}^4 \left[0.92 \times 10^{-5} \mathrm{MAT}^2 f \left(1 + 0.2 \mathrm{MACC}^2\right) + (1 - f) \varepsilon_s \left(\overline{T}_s / \mathrm{MAT}\right)^4\right] \tag{5-25}$$

where ε_s is the emissivity of the ground (typically 0.95 to 0.97), $\overline{T}_s$ is mean annual ground surface temperature, and f is the fraction of the hemisphere above the pixel that is occupied by sky. The mean annual effective atmospheric emissivity [i.e., $0.92 \times 10^{-5} \mathrm{MAT}^2 (1 + 0.2 \mathrm{MACC}^2)$] ranges from 0.7 to 0.8 as MAT ranges from 0 to 20 °C [32 to 68 °F] with present-day cloud cover (i.e., MACC = 0.3), implying that the bottom of a wash may have more incoming longwave radiation than fully exposed locations. For a reasonably extreme location where one-third of the sky is blocked, Eq. (5-25) estimates 14 and 3 percent more incoming longwave radiation than Eq. (5-24) for MAT values of 0 and 20 °C [32 to 68 °F], respectively, assuming MACC = 0.3 and $\varepsilon_s (\overline{T}_s / \mathrm{MAT})^4$ = 1 (i.e., $\overline{T}_s$ is a few degrees warmer than MAT). Such a small increase in radiation would only slightly reduce MAI in the abstractions developed in Section 4.

5.5.3 Climatic Parameter Uncertainty

ITYM describes climate using climatic parameters of MAP, MAT, MAV, MAW, MASW, and MALW. ITYM calculates realizations of MAI for a set of representative climate states at a reference elevation, using combinations of MAP and MAT to represent the climate states. Each

climate state uses the same representation for MAV, MAW, MASW, and MALW, and the same systematic elevation dependence for MAP and MAT, with all of these climatic parameters approximated based on present-day conditions. The climatic parameters used by ITYM are inherently uncertain, because (i) the period with meteorological observations is short relative to the performance period, (ii) climatic conditions during other stages of past glacial cycles are imperfectly known, and (iii) past climatic conditions may not be a perfect analog for future climatic conditions. Present-day distributions of climatic parameters have associated uncertainties, as described throughout Section 5; even greater uncertainties occur under other climatic states. Climatic parameters are also spatially variable across the site, with residual variability existing after systematic spatial patterns are accounted for (see Figures 5-7 and 5-10, for example). The uncertainty parameters listed in Tables 5-4 and 5-5 are used to account for these factors.

These uncertainties are considered by sampling the deviation from the mean for each climatic parameter in each realization, then applying the sampled offset to all cells. This sampling strategy assumes that residual offsets in adjacent grid cells are strongly correlated, which is true for uncertainty about regional changes in atmospheric conditions. Uncertainty about the representation of local spatial patterns uses the same sampling strategy, with the rationale that unconsidered local heterogeneity in climatic parameters (i.e., at the hillslope and wash scale) is unlikely to be sufficiently large to have a systematic effect on MAI.

Table 5-4. Description of Variability and Uncertainty for Climatic Parameters. Uncertainty Is Expressed as the Standard Deviation of the Statistical Parameter.

Parameter	Mean Value at z_0*	Standard Deviation	Mean Gradient	Uncertainty in Mean Value	Uncertainty in Standard Deviation	Uncertainty in Mean Gradient
$\log_{10}$ {mean annual precipitation (MAP) [mm/yr]}	2.21	0.05	0.2755	0.1	0.05	0.03
MAT {mean annual temperature [˚C]}	17	0.5	−6.5	0.1	0.1	0.01
$\log_{10}$ {mean annual vapor (MAV) density [g/cm^3]}	−5.35	0.1	−1	0.1	0.01	0.01
MACC {mean annual cloud cover [fraction]}	0.3	0.1	0	0.1	0.005	0
W†	1	0.1	0	0.1	0.05	0

*z_0 = reference Elevation of 1.4 km [4,600 ft]
†W = multiplier of the Values in the Spatially Distributed Mean Annual Wind Speed

Table 5-5. Correlation Matrix Between Climatic Parameters

Parameter	$\log_{10}$(MAP)	MAT	$\log_{10}$(MAV)	MACC	W*
$\log_{10}$ {Mean annual precipitation (MAP) [mm/yr]}	1	−0.8	0.1	0.1	0
MAT {Mean annual temperature [˚C]}	−0.8	1	−0.1	−0.01	0
$\log_{10}$ {Mean annual vapor density (MAV) [g/cm^3]}	0.1	−0.1	1	0.3	0
MACC {Mean annual cloud cover [fraction]}	0.1	−0.01	0.3	1	0
W	0	0	0	0	1

*W = multiplier for the spatially distributed mean annual wind speed values

MAP and MAT are both distributed across the landscape according to the difference in elevation between each grid cell and a reference elevation, with the relationship considered uncertain and with a residual offset to account for local effects other than elevation and to account for uncertainty in how well the regional relationship applies to Yucca Mountain. Offsets in MAP and MAT were considered until TPA Version 5.1, to account for decadal-to-millennial scale variability, and were assumed to be strongly negatively correlated based on an expert elicitation on climate (DeWispelare, et al., 1993). The input for TPA Version 5.1 assumes that MAP and MAT are known at the reference elevation (i.e., offsets in MAP and MAT are zero), because Stothoff and Walter (2007) inferred that millennial-scale climatic variability had minimal effect on MAI, but uncertainty in the systematic change in MAP and MAT with elevation is retained.

MAV is distributed across the landscape using the same scheme as MAP uses, except that the same elevation-dependent relationship is used for every climatic state. ITYM uses the base-10 logarithm of both MAP and MAV to sample and distribute climatic parameters. MAV offsets are assumed to be almost uncorrelated with MAP and MAT. Figure 5-12 suggests that MAV patterns are fairly consistent across the American west, across a range of MAP and MAT values, supporting this assumption.

MAW is provided as a distributed input file with a separate MAW value for grid cell. Uncertainty in MAW is accounted for by sampling a single multiplier that is applied to every grid cell. MAW is assumed to have a relatively small uncertainty (i.e., wind patterns are considered to be similar to present under other climatic states) and deviations from the systematic patterns are assumed to be uncorrelated to deviations in other climatic parameters.

MASW and MALW are assumed to be deterministic except for the effects of MACC. Each grid cell has a separate value for MASW, determined from ground orientation, and all grid cells have the same value for MALW. All uncertainty in MASW and MALW is described using a sampled parameter for MACC, with the implication that MASW and MALW are perfectly correlated. Offsets in MACC are assumed to be very weakly correlated to MAV offsets and essentially uncorrelated with other parameters.

Uncertainty in climatic parameters has a secondary effect on ITYM estimates relative to uncertainty in hydraulic parameters, because the magnitude of potential climate change within a climatic state is not large enough to strongly affect MAI in the ITYM abstractions. Section 6 will demonstrate much larger effects on MAI arising from uncertainties in hydraulic properties than are seen with climatic perturbations. This conclusion is further illustrated by Stothoff and Walter (2007), who used ITYM to consider changes in estimated MAI under climatic change representative of glacial cycles. Stothoff and Walter (2007) identified uncertainty in hydraulic properties as the dominant uncertainty in determining million-year-average MAI, even with the large changes in climate state that occur over glacial cycles.

6 SITE-SPECIFIC HYDRAULIC PROPERTIES

The abstractions for mean annual infiltration (MAI)[1] described in Section 4 consider a thick vertically uniform soil layer and a shallow vertically uniform soil layer overlying a vertically uniform bedrock continuum. The abstractions require site-specific hydraulic properties for the soil and bedrock in each grid cell. Soil and bedrock are both described as overlapping continua by the Infiltration Tabulator for Yucca Mountain (ITYM),[2] with soil composed of rock fragments embedded in a fine matrix and bedrock composed of a rock matrix with embedded unfilled, soil-filled, and carbonate-filled fractures. Hydraulic properties required for each continuum include intrinsic permeability, retention parameters, and porosity. The volume fraction of each continuum type is also considered a hydraulic property. Soil thickness is treated like a hydraulic property for the purposes of the abstractions presented in Section 4; calculations to estimate soil thickness distributions are described in Chapter 7.

Flint, et al. (1996a) developed estimates of soil and bedrock hydraulic conductivity for mapped soil and bedrock units. U.S. Geological Survey (2001) used a more detailed map of geologic units in the central block of Yucca Mountain to revise the properties used for the bedrock. These units and hydraulic properties were used for U.S. Department of Energy (DOE) infiltration modeling through at least 2004 (Bechtel SAIC Company, LLC, 2004a).

As described in this section, the ITYM analyses use a framework based on the soil and bedrock maps and derived properties that is consistent with the work by U.S. Geological Survey (2001). Some of the site-specific hydraulic properties developed by Flint, et al. (1996a) and U.S. Geological Survey (2001) are also used in ITYM analyses. Additional analyses were performed to verify that these properties reasonably describe the observations, with supplemental information used to modify some of the property values and to provide values for properties that were not considered by Flint, et al. (1996a).

Section 6.1 describes the spatial distribution of soil units across Yucca Mountain and their representation in the ITYM model. Section 6.2 describes the spatial distribution of bedrock units across Yucca Mountain and the modeled hydraulic properties for both the bedrock matrix and the fracture system in each unit. Section 6.3 describes the model implementation describing uncertainty in bedrock and fracture hydraulic properties. Finally, Section 6.4 summarizes the ITYM model implementation of site-specific hydraulic properties.

6.1 Soil Units

Flint, et al. (1996a) consider soil properties in terms of their effect on MAI. Flint, et al. (1996a) used the soil maps developed by Lundstrom, et al. (1996, 1995, 1994) and Lundstrom and Taylor (1995) to develop aggregated soil types, with aggregation primarily based on texture. Descriptions of the mapped units consistently indicate that the soils are mixtures of a fine soil component and rock fragments, with sand dominating the fine component of the soil. The fine soil is described as eolian in some units, and an eolian soil component is identified in other

[1] Mean annual infiltration is used frequently throughout this chapter; consequently, the abbreviation MAI will be used.

[2] Infiltration Tabulator for Yucca Mountain is used frequently throughout this chapter; consequently, the abbreviation ITYM will be used.

units. Rock fragments are sparse in some units; in other units, the fine component may be below the top of the rock clasts by tens of centimeters.

Lundstrom, et al. (1994) describes soil texture, identifiable soil horizons, carbonate and silicate deposition stage, and estimated deposition age for their mapped soil types. Mapped units are generally less than 3 m [10 ft] thick and are underlain by older unmapped units in areas with deep alluvial fill. Clay, carbonate, or silicate layers coating a bedrock surface are not described; personal field observations suggest that such layers may exist locally on hillslopes and ridgetops within the potential repository footprint.

Figure 6-1 indicates soil age for the soil units, estimated as the median value for the age range provided by Lundstrom, et al. (1994). The light gray areas in Figure 6-1 represent the cu unit, described as Quaternary undifferentiated colluvium, generally less than 1 m [3.3 ft] thick, with a fine-grained matrix inferred to be mostly of eolian origin. The medium gray areas in Figure 6-1 represent the cs unit, described as Pleistocene surface-clast-supported colluvium (lacking a fine-grained matrix at the surface) with a fine-grained matrix increasing at a depth that is inferred to be mostly of eolian origin. The dark gray areas in Figure 6-1 represent the rc unit, described as Quaternary to Tertiary residuum: a fine-grained matrix that is inferred to be mostly of eolian origin with an increased clay content through weathering and pedogenesis. Descriptions of the cu, cs, and rc units do not mention any internal low permeability soil horizons that would restrict wetting pulses like a bedrock layer. Figure 6-1 uses cyan to indicate disturbed ground and purple to indicate small areas with extensive exposed bedrock.

Most of the area considered by ITYM features (i) surficial deposits with an unaltered or mildly altered eolian-derived fine matrix with various proportions of embedded clasts or (ii) alluvial/colluvial deposits that are interpreted to have been deposited subsequent to the last glacial maximum. Older deposits are limited to areas with deep soil and are generally not found within the potential repository footprint. Note that early to middle Pleistocene soils are located at the foot of the west flank of Yucca Mountain, updip (west) of the potential repository.

Figure 6-2 describes soil alteration stage, estimated as the mean Lundstrom, et al. (1994) stage among all soil horizons described for a mapped soil unit. The color scale ranges from 0 (unaltered) through 2 (stage II carbonate or silicate morphology). The light gray areas represent units with an unaltered fine matrix. The blue areas represent units with at least stage III carbonate development in which carbonate forms an essentially continuous medium. These units are only mapped in areas with deep fill and are rare within the potential repository footprint. The degree of alteration is estimated from the soil unit descriptions; units mapped as a mixture of more than one soil unit are assigned the average alteration among the contributing units. Soil age correlates well with the degree of soil alteration.

Figure 6-3 displays bulk saturated hydraulic conductivity values for surficial deposits in the ITYM domain, based on estimates by Flint, et al. (1996a, Table 4). Bulk saturated hydraulic conductivity is obtained by multiplying saturated hydraulic conductivity values by the soil volume fraction using the properties estimated by Flint, et al. (1996a). Bulk saturated hydraulic conductivity accounts for the reduction in overall permeability arising from essentially impermeable embedded rock fragments. Bulk saturated hydraulic conductivity ranges from 1.7 to 3.8 cm/hr [0.67 to 1.5 in/hr] across most of the ITYM domain, with active channels in deep fill exhibiting values of approximately 11 cm/hr [4.3 in/hr].

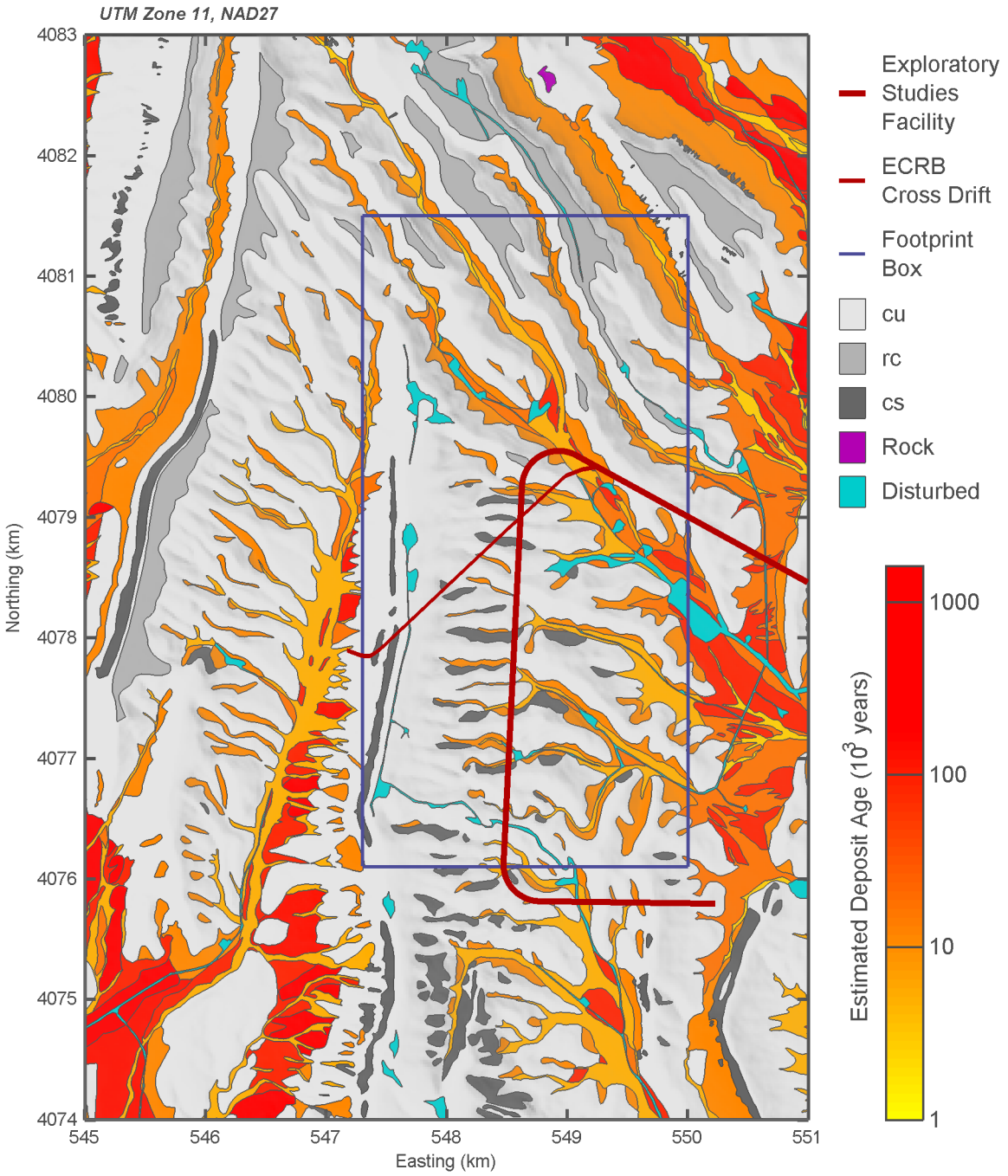

Figure 6-1. Estimated Median Age for Surficial Deposits in the Yucca Mountain Vicinity. Shadows Are Cast From the West Southwest.

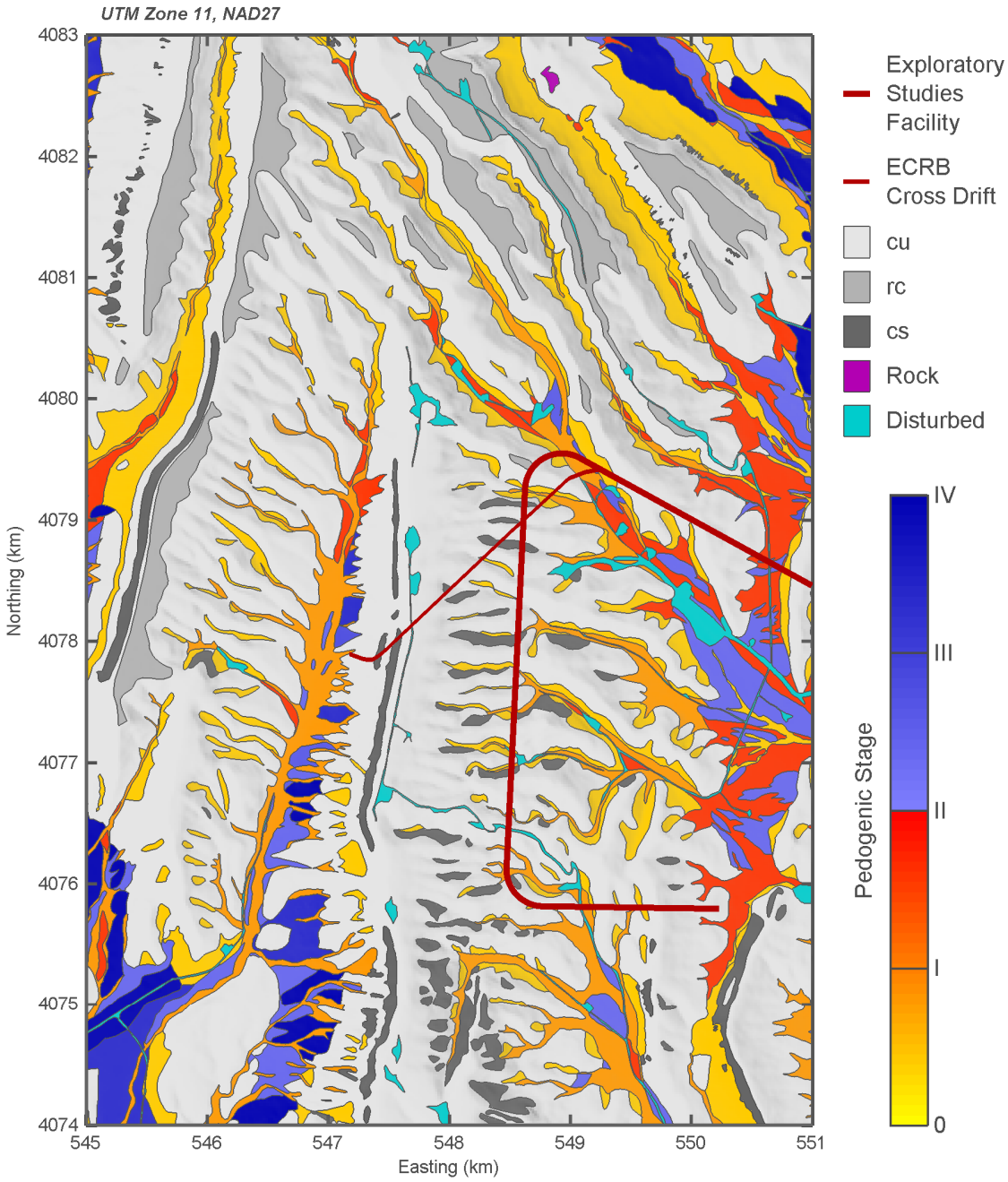

Figure 6-2. Estimated Pedogenic Stage for Surficial Deposits in the Yucca Mountain Vicinity. Stages III and IV Have Complete Matrix Plugging. Gray Shades Indicate That the Fine Matrix Component Is Unaltered and Has an Eolian Source. Shadows Are Cast From the West Southwest.

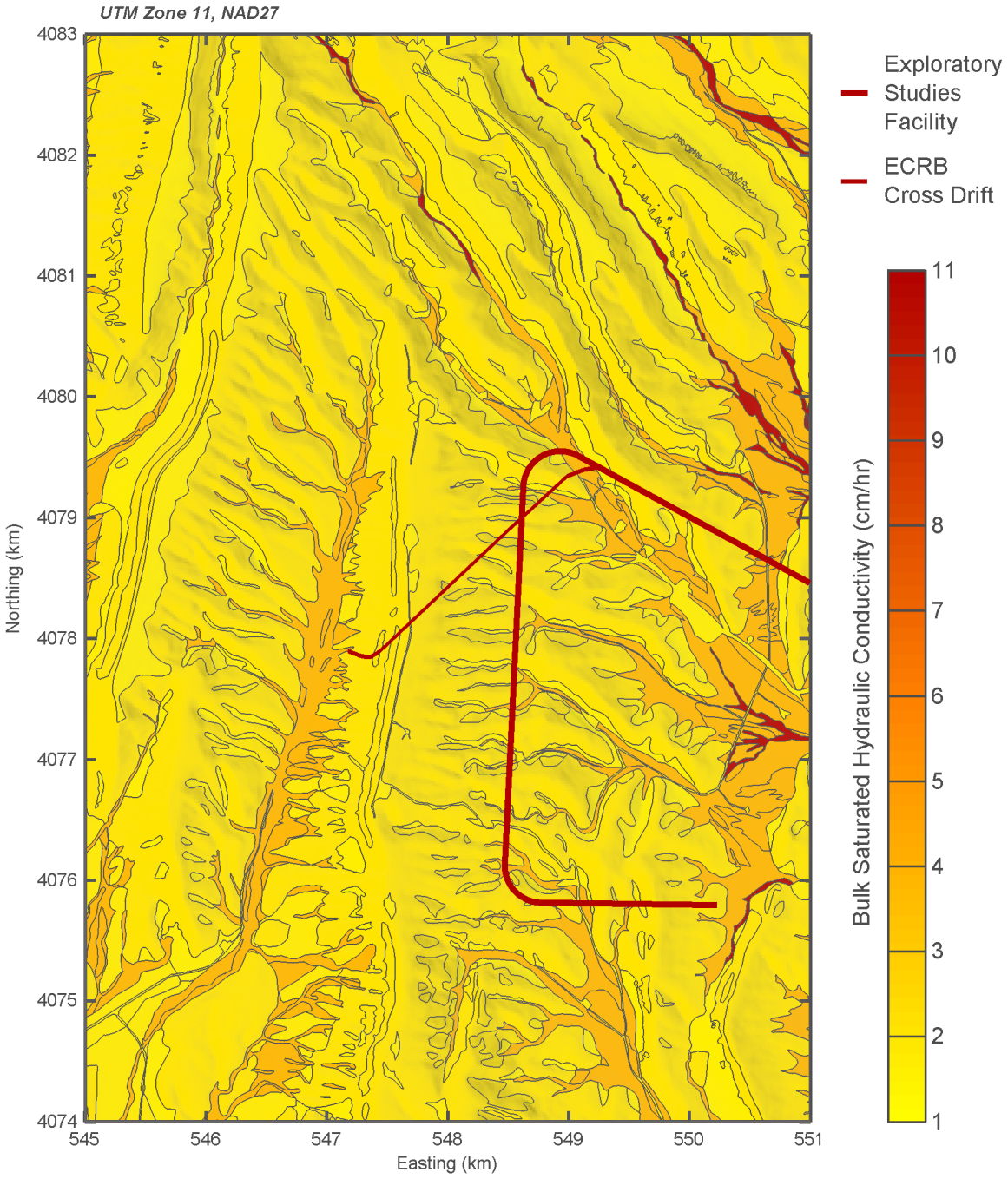

Figure 6-3. Estimated Median Bulk Saturated Hydraulic Conductivity for Surficial Deposits in the Yucca Mountain Vicinity [1 cm/hr = 0.39 in/hr]. Shadows Are Cast From the West Southwest.

Limited independent field observations (Stothoff, 2008) suggest that (i) shallow soil texture is dominated by the sand fraction and (ii) essentially uniform sand, silt, and clay fractions may be found across the potential repository footprint. These observations are consistent with the hypothesis that shallow soil is predominantly derived from eolian deposition. Permeability measurements using a double-ring infiltrometer at three ridgetop and upper hillslope locations within the footprint all provided estimates for saturated hydraulic conductivity of approximately 2 cm/hr [0.8 in/hr] (Stothoff, 2008), consistent with the estimates by Flint, et al. (1996a) that were derived from textural analysis and infiltrometer tests in deep alluvium. Measurements using a Guelph permeameter in the Solitario Canyon channel and overbank areas (Stothoff, 2008) yielded estimates for saturated hydraulic conductivity between 7 and 360 cm/hr [3 and 140 in/hr], with a median of 70 cm/hr [28 in/hr]. Note that the higher measured values may only be representative of active channels, which are a relatively small fraction of the area with deep alluvium.

The soil age map in Figure 6-1 and the soil alteration map in Figure 6-2 suggest that, in areas with shallow soil, the fine matrix of surficial deposits within the ITYM domain generally does not include low permeability subsurface horizons within the soil column. This conclusion is supported by personal observation from several field excursions, which suggested that hillslope and ridgetop soil columns are relatively unaltered. The field excursions suggested that some locations may feature a carbonate layer atop the bedrock in areas where the bedrock is relatively impermeable, particularly on south facing hillslopes where insolation drives relatively rapid evaporation. The NRG–5a drillpad exposes an extensive carbonate layer atop the bedrock. The cleared pavement at the Ghost Dance Fault and several trenches within the potential repository footprint also revealed a thin carbonate layer at the bedrock surface. Note that all of these locations are within densely welded horizons of the Tiva Canyon tuff, typically in lithophysal units, with essentially impermeable matrix and fractures that are relatively sparse or with narrow apertures. Field excursions also identified three areas where a thin buried clay-rich soil horizon exists (Fedors, 1998, pp. 70–73; 2007), possibly a relic soil of Pleistocene age. All three areas are sheltered from erosion in downslope (eastern) portions of the relatively flat-lying caprock of Yucca Mountain near Upper Split Wash, with soil thicknesses of between 24 and 60 cm [9.4 and 24 in]; the buried soil horizon was not found in other caprock locations. These thin features atop the bedrock are not described in the surficial deposit map documentation by Lundstrom and coworkers (Lundstrom, et al., 1996, 1995, 1994; Lundstrom and Taylor, 1995), and the area covered by such features is unknown.

The soil maps suggest that low permeability horizons exist in some areas with deep soils, especially as these areas may include unmapped, older buried soils that are more prone to alteration, whereas the soil permeability estimates indicated in Figure 6-3 suggest that deeper soils may be slightly more permeable than shallow soils. Soil permeability is likely to decrease significantly with depth below the ground surface in the early to middle Pleistocene soils mapped in Figure 6-2 because of horizons with stage III and IV carbonate and silica morphology, so the vertical average soil permeability may be less than estimated by Flint, et al. (1996a). Within valley-fill areas, young soils may have been deposited with a somewhat coarser texture than the shallow soil eolian deposits and thus may be more permeable even if somewhat altered.

The deep soil simulations and abstractions for MAI suggest that bare-soil MAI would be large in areas with deep soil that has the hydraulic characteristics described by Flint, et al. (1996a).

These abstractions do not consider the presence of low permeability layers, such as described in the soil maps, which would tend to reduce MAI. However, the presence of native vegetation

is understood to scavenge essentially all infiltrating water in the arid southwest, regardless of soil texture, except in active channels. This concept is borne out by studies using boreholes in alluvial flats on the Nevada Test Site (Tyler and Jacobson, 1990). The ITYM scavenging model reduces MAI in deep soils to a small value relative to peak values of MAI, regardless of the soil hydraulic properties; therefore, the ITYM model is not sensitive to soil properties in areas with deep soil. Within the potential repository footprint, in particular, estimates of areal-average MAI are relatively unaffected by deep-soil hydraulic properties.

The shallow soil simulations and abstractions for MAI presented in Sections 3 and 4 are relatively insensitive to most soil hydraulic properties for permeable sandy soils (aside from the van Genuchten capillary pressure, P_o, which helps determine the hydraulic conditions necessary to admit water to the bedrock). The shallow soil MAI abstractions suggest that MAI is more affected by the volume of pore space in the fine fraction of the soil (i.e., volumetric water storage) and bedrock hydraulic properties than by the remaining soil hydraulic properties. This observation makes intuitive sense, because the soil provides a primary control on MAI by determining whether precipitation is stored within the soil column or runs off. Hortonian runoff occurs if the soil is insufficiently permeable to accept rainfall at the rates occurring during storms, and saturation-induced runoff occurs if the soil becomes saturated and the bedrock cannot accept fluxes at the rainfall rates. Sandy soils tend to be sufficiently permeable to accept rainfall events typical of the Yucca Mountain region; thus volumetric water storage in the soil column is likely to be the primary soil control on MAI at Yucca Mountain. Note that the effect of shallow soil hydraulic properties on abstracted MAI is further discussed in Section 6.2.2.

Soil texture at Yucca Mountain may be modified by *in-situ* weathering and by precipitation of carbonates and silicates within the soil. Weathering tends to reduce soil permeability by increasing the clay content in the soil; infiltrating water pulses may subsequently displace clay particles to depth, ultimately creating a distinct clay-rich horizon. Carbonate and silicate precipitation occurs as infiltrating water moves to depth and evaporates within the soil column, leaving behind carbonate and silicates that were dissolved in the meteoric water. These processes ultimately create low permeability horizons at approximately the penetration depth of typical wetting pulses after tens or hundreds of thousands of years in arid environments. Low permeability soil horizons, where present, restrict downward movement of wetting pulses. ITYM assumes that the soil layer is vertically uniform (i.e., it does not consider such soil horizons), but does consider the related effect of redistribution into the bedrock fracture system.

In summary, ITYM uses the soil taxonomy aggregation and soil hydraulic properties estimated by Flint, et al. (1996a) without modification, because (i) personal observation does not contradict the estimates for shallow soils, particularly within the potential repository footprint and (ii) ITYM estimates for MAI are relatively insensitive to most soil hydraulic properties in deep soils, which have strong plant control on MAI. Nevertheless, the soil hydraulic properties are considered uncertain in the ITYM simulations.

6.2 Bedrock Units

U.S. Geological Survey (2001) used the bedrock maps developed by Day, et al. (1998), Scott and Bonk (1984), and Sawyer, et al. (1995) to determine bedrock units. The Day, et al. (1998) coverage describes the central block of Yucca Mountain, including the repository footprint. The Scott and Bonk (1984) and Sawyer, et al. (1995) coverages describe successively larger areas not covered by smaller maps, and U.S. Geological Survey (2001) used these coverages to supplement the smaller Day, et al. (1998) map.

The ITYM grid is more restricted in area than the U.S. Geological Survey (2001) grid; thus only the Day, et al. (1998) map is used for ITYM analyses. As shown in Figure 6-4, the Day, et al. (1998) map covers the primary area of interest (the area within and near the potential repository footprint) but a strip approximately 1 km [0.6 mi] wide is not covered along the western and southern edges of the ITYM model domain. MAI estimates within these boundary strips are not used in U.S. Nuclear Regulatory Commission (NRC) performance assessment calculations, nor were they used by Stothoff and Walter (2007), because these strips are outside the potential-repository footprint. These strips are assumed to be underlain by the TCW aggregated hydraulic unit discussed in Section 6.2.1, describing welded units of the Tiva Canyon formation, and estimates within these strips are only provided for illustration.

ITYM considers both bedrock and fracture pathways for water infiltrating into the bedrock units. ITYM calculates the effective saturated hydraulic conductivity (K_{sat}) for each pathway by multiplying K_{sat} for the medium forming the pathway by the pathway volume fraction. For example, if a fracture system is partially filled with soil that has a K_{sat} value of 2 cm/hr [0.78 in/hr], but the fracture system has a volume fraction of 1 percent and soil fills 50 percent of the fracture system, the bedrock pathway for soil-filled fractures has an effective K_{sat} of 0.01 cm/hr [0.0039 in/hr]. The bedrock matrix pathway has a volume fraction of 99 percent, and the carbonate-filled and unfilled fracture pathways must have a total volume fraction of 0.5 percent in this example. The volume fraction of a medium and K_{sat} for the medium are independent parameters.

Section 6.2.1 describes ITYM inputs for the bedrock matrix pathway. Section 6.2.2 describes the fracture volume fraction parameters ITYM uses, and Section 6.2.3 describes the soil-filled, carbonate-filled, and unfilled media properties used to characterize the fracture pathways. Section 6.2.4 provides confirmation analyses for effective bulk K_{sat} for the fracture system in selected bedrock units that are extensively exposed above the potential repository, using field tests, bedrock pavement maps, and fracture maps from the Exploratory Studies Facility (ESF).[3]

6.2.1 Bedrock Matrix Hydraulic Properties

Infiltrating water may proceed to depth in either the bedrock matrix or the fracture system. Hydraulic properties of the bedrock matrix are better established than hydraulic properties of the fracture system, because measurements of hydraulic properties have been performed on numerous core samples obtained from the bedrock matrix, but relatively few observations of fracture properties have been obtained.

ITYM simulations use values for the bedrock hydraulic properties that are taken from the Flint, et al. (1996a) model. Bedrock matrix properties are used without modification to provide the median estimate in the uncertainty analyses. These properties are based on laboratory measurements performed on core samples (Flint, 1998). The ITYM simulations use the Day, et al. (1998) map and nomenclature to provide the spatial distribution of the properties, rather than the coarser Scott and Bonk (1984) map used by Flint, et al. (1996a). The Day, et al. (1998) units shown in Figure 6-4 are assigned the aggregated hydraulic units used in the Flint, et al. (1996a) model using the mapping described by Flint (1998). The Flint, et al. (1996a) aggregated hydraulic units are indicated in uppercase (e.g., TCW, CUC, CW, etc.).

[3]Exploratory Studies Facility is used frequently throughout this chapter; consequently, the abbreviation ESF will be used.

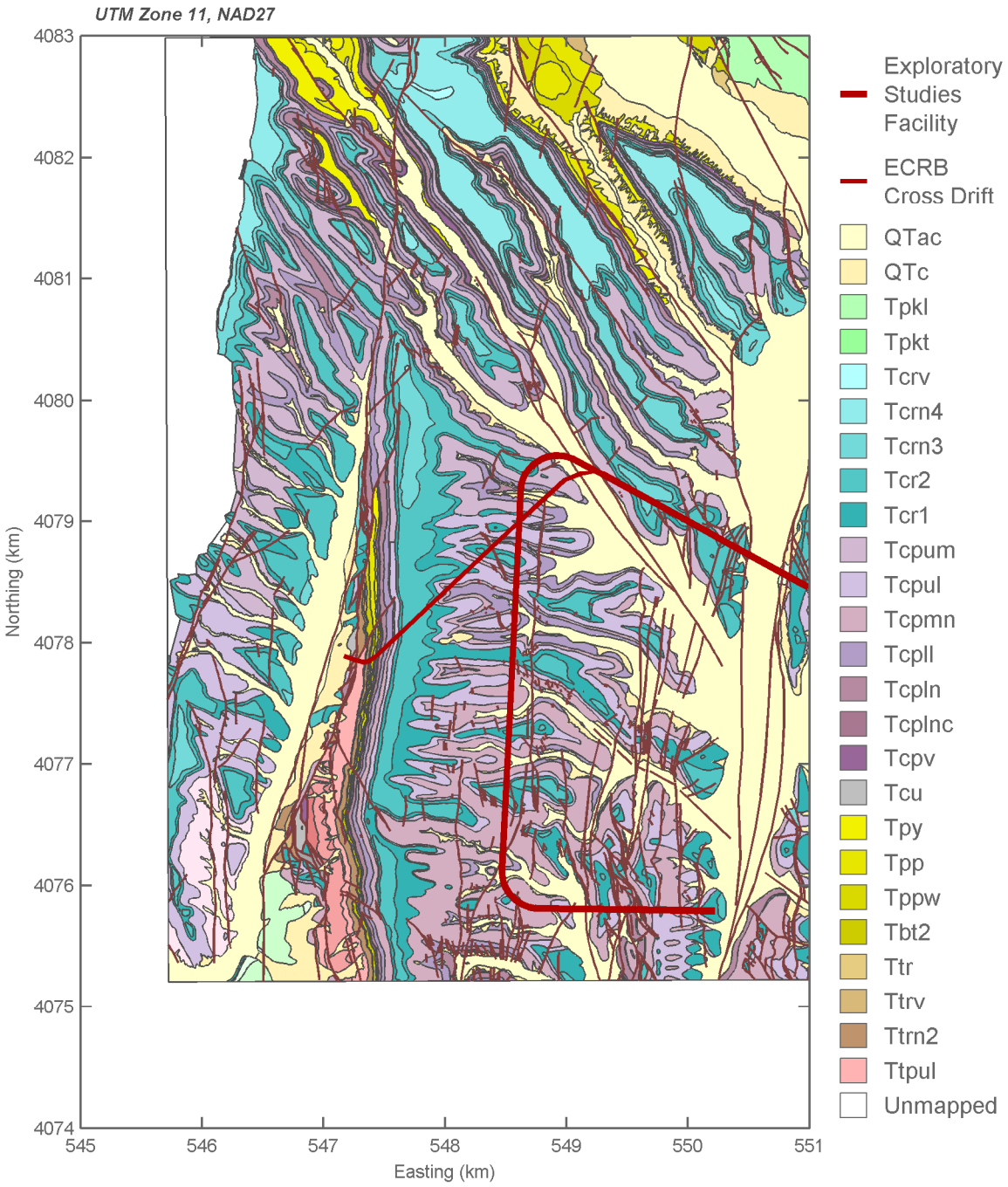

Figure 6-4. Bedrock Geologic Map of the Central Block Area as Mapped by Day, et al. (1998). Unit Nomenclature Follows Day, et al. (1998). Tiva Canyon Caprock Units Are Indicated by Shades of Teal.

The ITYM distribution of bedrock-matrix saturated hydraulic conductivity (K_{sat}) is shown in Figure 6-5. Conductivity is expressed in millimeters per day to illustrate the relationship between K_{sat} and infiltration into the bedrock. Three color ranges are used to indicate how bedrock K_{sat} influences MAI. The blue and red ranges indicate estimated K_{sat} values of <0.1 and >10 mm/d [<0.0039 and >0.39 in/d], respectively, and the yellow range indicates values intermediate between the extremes. MAI is only sensitive to bedrock K_{sat} in the yellow range.

The abstractions shown in Section 4 suggest that shallow-soil MAI is insensitive to bedrock matrix K_{sat} when K_{sat} is less than 0.1 mm/d [0.004 in/d], because bare-soil MAI is always <1 mm/yr [<0.04 in/yr] (i.e., matrix K_{sat} limits MAI). Movement of water into the bedrock primarily occurs when the soil is essentially saturated at the bedrock interface, and infiltrating water pulses only reach the bedrock interface episodically in the semiarid Yucca Mountain climate. Such episodes may only occur for a period of weeks and may only occur in particularly wet years. Not all water passing into the bedrock becomes net infiltration; evapotranspiration demand dries the soil column, which drives retrieval of some of the bedrock water. The bedrock matrix K_{sat} value of 0.1 mm/d [0.004 in/d] indicating the upper end of the blue range makes intuitive sense with the limited period available for infiltration under present-day climatic conditions.

Matrix K_{sat} does not limit infiltration in the red range, because MAI is determined by other factors such as climate, soil properties, and plant uptake. A lower bound of 10 mm/d [0.4 in/d] for the red range of matrix K_{sat} also makes intuitive sense, because this value is sufficiently large that most rainfall events can be accepted into the bedrock within a few days. Note that the soil K_{sat} is only slightly larger than this transition value.

Two alternative distributions of bedrock matrix K_{sat} suggest that the estimates of MAI within the potential repository footprint would be little affected by different estimates of bedrock matrix properties. The first distribution uses updated properties derived from Flint (1998) estimates, which are used by U.S. Geological Survey (2001) and Bechtel SAIC Company, LLC (2004a). The second distribution uses an independent NRC analysis of the Flint (1998) observations. The bedrock–matrix K_{sat} distribution using the Flint (1998) estimates (not shown) is similar to that shown in Figure 6-5 except for two differences: Flint (1998) (i) estimates much lower values for K_{sat} for the Ttpmn unit (the middle nonlithophysal unit of the Topopah Spring formation) and (ii) classifies the Tcr1 unit (the lowest crystal-rich unit of the Tiva Canyon formation) as the CW aggregated hydraulic unit rather than the CUC aggregated hydraulic unit.

The CW aggregated hydraulic unit is typically used to describe densely welded tuff, whereas the CUC aggregated hydraulic unit is typically used to describe moderately welded caprock. The first difference shows up as a switch from pink to blue in units on the west flank of Yucca Mountain near the mouth of Solitario Canyon (outside the southwest corner of the potential repository footprint). The second difference shows up as a switch from yellow to blue in a thin unit at the base of the caprock throughout the model domain. Both differences would tend to reduce MAI estimates; only the second difference would affect ITYM estimates within the potential-repository footprint.

Figure 6-6 displays K_{sat} estimates that NRC independently derived through least squares regression from the core sample measurements described by Flint (1998). The independently derived estimate for the Ttpmn unit also moves to the blue range—much lower than the ITYM value. A unit below the caprock [in this case, the Tcpul unit of the Tiva Canyon (the unit below the Tcr1 unit)] also drops from the yellow to the blue range by being assigned to a different

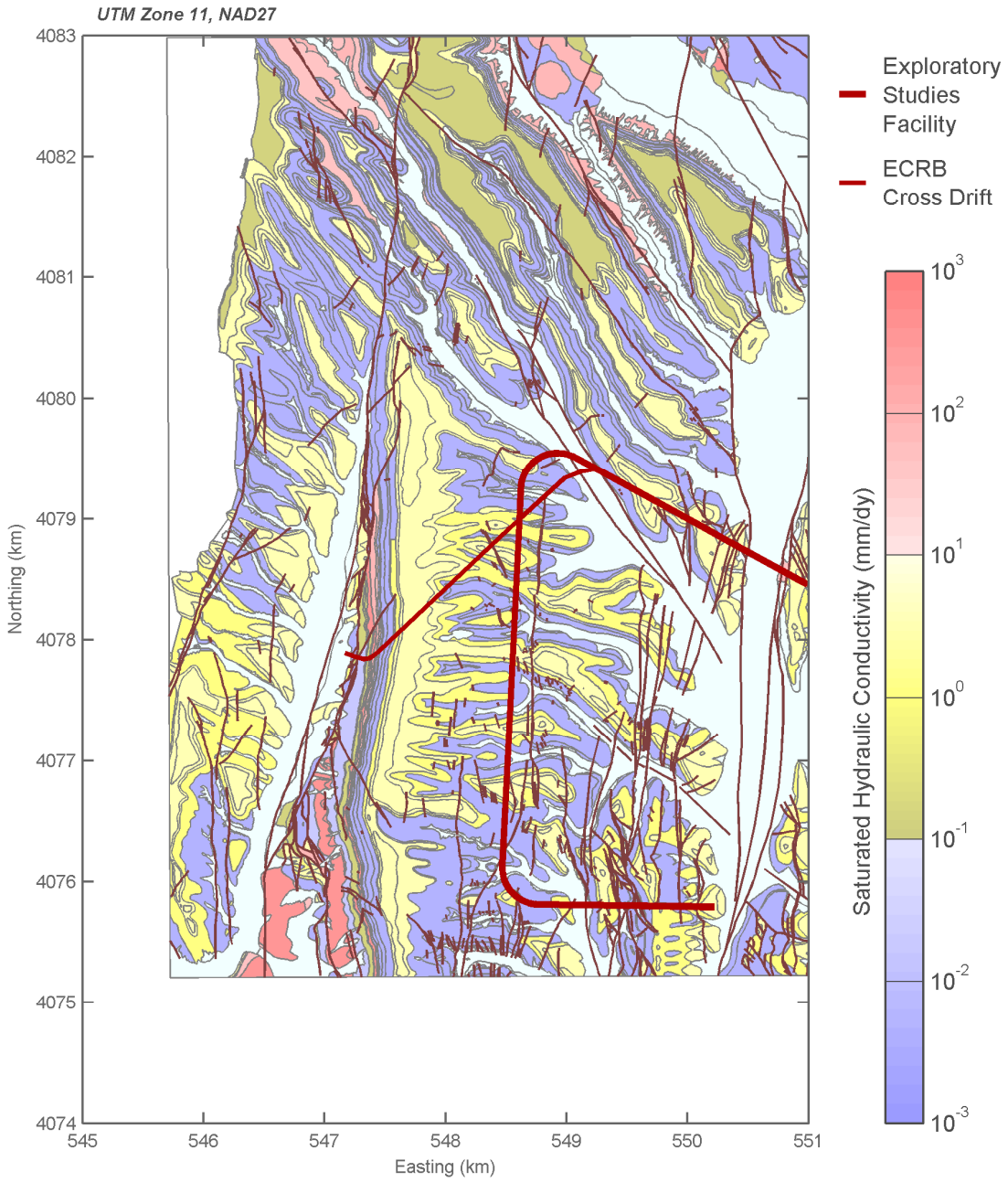

Figure 6-5. Median Bedrock Saturated Hydraulic Conductivity Used by Infiltration Tabulator for Yucca Mountain. Areas in Gray Use the Deep Soil Abstraction. [100 mm/day = 3.94 in/day]